Dissertation

submitted to the
Combined Faculties for the Natural Sciences and for Mathematics
of the Ruperto-Carola University of Heidelberg, Germany
for the degree of
Doctor of Natural Sciences

Put forward by
Galina Khachaturyan, M.Sc.
born in Yerevan, Armenia

Oral examination: January 25th, 2019

The role of Protein Kinase D signaling and the thermal microenvironment on single cell migration

Referees

Prof. Dr. Joachim P. Spatz
Institute for Physical Chemistry
University of Heidelberg
Max Planck Institute for Medical Research, Heidelberg

Prof. Dr. Reiner Dahint
Institute for Physical Chemistry
University of Heidelberg

"There's as many atoms in a single molecule of your
DNA as there are stars in the typical galaxy.
We are, each of us, a little universe"

Neil deGrasse Tyson

Contents

Contents i

Abstract v

Zusammenfassung vii

Abbreviations ix

I Introduction 1

1 Cell migration 3
1.1 Cell migration modes 3
1.2 Quantitative characterization of single cell migration 5

2 Temperature effects and neutrophils 9
2.1 Role of temperature in cell physiology 9
2.2 Neutrophils and differentiated HL-60 cell line 10

3 Pancreatic Cancer 13
3.1 Progression of pancreatic ductal adenocarcinoma 13
3.2 Carcinogenesis and cancer metastasis 14
3.3 Cancer cell invasion and motility 17
3.4 Importance of protein kinases in cancer and Protein Kinase D family 19
3.5 Protein Kinase D isoforms in cancer 20
3.6 Role of PKD isoforms in pancreatic cancer progression and pancreatic ductal adenocarcinoma 21

4 Objectives 23

II Materials and Methods 25

5 Materials and Methods 27
5.1 Fabrication of migration assays 27
5.1.1 Temperature gradient chamber fabrication for 2D and 3D experiments 27

5.1.2 PDMS-based microgrooved substrate and invasion chip fabrication and functionalization . . . 28
5.2 Cell biology methods . . . 30
5.2.1 Cell Culture . . . 30
5.2.1.1 HL-60 cell culture and differentiation . . . 30
5.2.1.2 3-D cell culture for temperature gradient studies . . . 31
5.2.1.3 Neutrophil isolation . . . 31
5.2.1.4 Pancreatic cancer cell culture . . . 31
5.2.2 Immunocytochemistry . . . 31
5.2.2.1 Giemsa-Wright staining of differentiated and non-differentiated HL-60 cells . . . 31
5.2.2.2 Pancreatic cancer cells . . . 32
5.2.3 Cell seeding, cell imaging and image analysis: Differentiated HL-60 cells . . . 33
5.2.3.1 2D glass surfaces . . . 33
5.2.3.2 Temperature gradient studies . . . 34
5.2.3.3 Shear flow assay . . . 35
5.2.4 Cell seeding, cell imaging and image analysis: Blood neutrophils . 35
5.2.5 Cell seeding, cell imaging and image analysis: Pancreatic cancer cells 36
5.2.5.1 2D glass surfaces . . . 36
5.2.5.2 PDMS-based microgrooved substrates . . . 37
5.2.5.3 PDMS-based microchannel invasion assay . . . 38
5.3 3-D optical stretching of pancreatic cancer cells . . . 39
5.4 Statistics . . . 41

III Temperature-sensitive migration dynamics in neutrophil differentiated HL-60 cells 43

6 Results 45
6.1 HL-60 cell differentiation . . . 45
6.2 Heat induced formation of motile cell fragments . . . 46
6.3 Temperature-dependent attachment and migration speed in differentiated HL-60 cells. . . . 48
6.4 Temperature-dependent effects on differentiated HL-60 cell directionality . . 51
6.5 Thermotaxis in differentiated HL-60 cells on 2D surfaces . . . 53
6.6 Differentiated HL-60 cell migration under shear flow . . . 55
6.7 Thermotaxis in differentiated HL-60 cells in 3D collagen gels . . . 57

7 Discussions 59
7.1 CKP formation was not possible in neutrophil differentiated HL-60 cells due to the reduced cell adherence at elevated temperatures . . . 60
7.2 Temperature-dependent increase in cell speed and reduction in cell persistence time lead to equal persistence length in migrating neutrophil-differentiated HL-60 cells . . . 60

7.3 Differentiated HL-60 cells exhibited “positive” and “negative” thermotaxis in 2D 63

IV *In vitro* studies of Protein Kinase D isoform dependent pancereatic cancer cell invasion related motility 65

8 Results 67
8.1 PKD-isoform dependent Panc1 cell attachment, proliferation and morphology 67
8.2 PKD isoform dependent cell motility in 2D 70
8.3 Changes in F-actin arrangement and focal adhesion morphology in response to PKD isoform specific protein deletion in Panc1 cell line 73
8.4 PKD-isoform dependent Panc1 cell contact guidance on microgrooved substrates 74
8.5 PKD isoform-specific knockout Panc1 single cell invasion studies 79
8.6 PKD1 isoform knockout induces changes in pancreatic cancer cell mechanical properties 84

9 Discussions 85
9.1 Loss of PKD1 leads to a more invasive pancreatic cancer phenotype 86
9.2 PKD2 knockout reverses EMT but enhances cell proliferation 88
9.3 PKD3 regulates cell motility 89

V Summary and Outlook 91

10 Summary 93

11 Outlook 95

Appendix 97

List of Figures 99

List of Tables 101

List of Publications 123

Acknowledgement 125

Abstract

Cell migration plays an essential role in development and homeostasis. This extraordinarily complex process, which is dynamically regulated by a coordinated interplay between the extracellular environment and intracellular signaling pathways, can also cause the emergence of disease states when dysregulated. A prominent example is cancer metastasis, which is the leading cause of cancer-related mortality. Despite an increasing body of literature focused on cell migration, many aspects remain unclear. In the current work, two complementary systematic *in vitro* cell migration studies were performed to gain insights into both healthy immune cell migration and pathological cancer cell migration.

Temperature-dependent neutrophil migration was analyzed using differentiated HL-60 cells as a model cell line. Neutrophils are the first cells to be activated during inflammation and subsequently migrate toward an injured tissue or infection site. This response is dependent on both biochemical signaling and the extracellular environment, one aspect of which includes increased temperature in the tissues surrounding the inflammation site. The results of this study reveal a positive correlation between the average speed of randomly migrating cells and temperatures from 30 °C to 42 °C. Higher temperatures also induce a concomitant increase in cell detachment. Further analysis of the migration data showed that persistence time is higher at low temperatures, while migration persistence length remains constant throughout the temperature range. Coupled with the increased speed observed at elevated temperatures, the obtained results indicate the ability of neutrophils to adapt their migration characteristics to the temperature in order to maintain relatively constant persistence length. As temperature gradients exist on both cellular and tissue scales, the ability of the HL-60 cells to sense and react to the presence of temperature gradients, a process known as thermotaxis, was also investigated. Towards this aim, a two-dimensional temperature gradient chamber was developed. In a gradient with the range of 27-43 °C both positive and negative thermotaxis was observed with cells migrating both to the high and the low temperature sources. To date, thermotaxis in neutrophil differentiated HL-60 cells has never been reported.

Next, an in-depth *in vitro* migration study was carried out on Panc1 pancreatic cancer cells to elucidate the role of Protein Kinase D (PKD) in cancer cell migration. CRISPR-mediated

knockouts of PKD1, 2, and 3 in Panc1 cells were used to investigate isoform-specific effects on cancer cell invasion-related motility. The data presented in this project reveals that absence of each PKD isoform plays a significant role in cell speed and migration persistence. To investigate the pancreatic cancer PKD isoform-dependent contact guidance, a panel of more complex PDMS-based substrates containing microgrooves of different heights and widths was utilized. These experiments further demonstrate pancreatic cancer cell shape, speed, and contact guidance dependence on the presence of different PKD isoforms. Based on these findings, in combination with previous works showing that contact guidance is affected by cell viscoelasticity, mechanical properties of each PKD isoform knockout cell line were also measured using a laser-based optical cell stretcher. These experiments showed a significant increase in Panc1 cell deformability in the absence of PKD1, demonstrating for the first time PKD involvement in regulation of cellular mechanical properties. Finally, these basic mechanical properties were correlated to MMP - independent confined migration, which is required for cells to metastasize *in vivo*.

Zusammenfassung

Die Migration von Zellen spielt eine zentrale Rolle bei der Entwicklung und Homöostase von Geweben, Organen und Organsimen. Der komplexe Prozess der Zellmigration, der durch ein koordiniertes Zusammenspiel aus Signalen zwischen der extrazellulären Umgebung und den intrazellulären Signalwegen dynamisch reguliert wird, kann bei verschiedenen Erkrankungen auch fehlreguliert sein. Ein prominentes Beispiel hierfür ist die Metastasierung von Krebs, ein Prozess, der die Hauptursache der krebsbedingte Mortalität darstellt. Trotz der zunehmenden Anzahl an Literatur, die sich thematisch auf die Tumorzellmigration konzentriert, sind viele Aspekte der Zellmigration noch unklar. In der Arbeit zu dieser Dissertation wurden zwei komplementäre systematische Zellmigrationsstudien durchgeführt, um Einblicke in die Immunzellmigration und die pathologische Krebszellmigration zu erhalten.

Die temperaturabhängige Migration von Neutrophilen Granulozyten wurde unter Verwendung differenzierter HL-60-Zellen als Modellzelllinie analysiert. Periphere Neutrophile im Blut sind die ersten Zellen, die während einer Entzündung aktiviert werden und anschließend in Richtung eines verletzten Gewebes oder einer Infektionsstelle wandern, ebenso reichern sie sich in Tumoren an. Diese gerichtete Migration hängt sowohl von biochemischen Signalen, als auch von physikalischen Eigenschaften und Signalen der extrazellulären Umgebung ab. Interessanterweise zeigen Geweben um Entzündungsstelle herum eine erhöhte Temperatur und haben somit zum umliegenden Gewebe auch einen Temperaturgradienten. Allerdings ist wenig über die Migration von Zellen, insbesondere Granulozyten bei erhöhter Temperatur oder in solchen Temperaturgradienten bekannt. Die hier beschriebene in vitro Untersuchung zeigt, dass die Migrationsgeschwindigkeit positiv mit der Erhöhung der Temperatur zwischen 30 °C und 42 °C, korreliert. Die Persistenz-Zeit der Migration war bei niedrigen Temperaturen höher als bei hohen Temperaturen, während das Produkt aus mittlerer Geschwindigkeit und Persistenz-Zeit, also ein Maß für die Persistenzlänge, im gesamten Temperaturbereich etwa konstant blieb. Da Temperaturgradienten sowohl auf Zell- als auch auf Gewebeebene existieren, wurde darüber hinaus die Fähigkeit der Zellen untersucht, auf Temperaturgradienten zu reagieren. Unter Verwendung einer zweidimensionalen Temperatur-Gradientenkammer mit

einer Temperaturdifferenz von 27–43 °C wurde sowohl positive als auch negative Thermotaxis bei den HL-60 Zellen beobachtet.

Des Weiteren wurde eine detaillierte biophysikalische *in-vitro*-Migrationsstudie mit Panc1-Bauchspeicheldrüsenkrebszellen durchgeführt, um die Rolle verschiedener Isoformen der Protein Kinase D (PKD) bei der Migration besser zu verstehen. Dazu wurden CRISPR-vermittelte Knockouts von PKD1, 2 und 3 in Panc1-Zellen verwendet, um isoform-spezifischer Effekte auf das invasive Verhalten der Zellen zu untersuchen. Der spezifische knock-down jeder einzelnen PKD-Isoform hatte Einfluss auf die Migrationsgeschwindigkeit und die Zellmorphologie, sowie auf die Fähigkeit der Zellen, durch enge Mikrokanäle (Confinement) zu wandern. Ebenso konnte gezeigt werden, dass die Zellmorphologie, die Migrationsgeschwindigkeit und die sogenannte Contact Guidance, die Migration und Orientierung entlang von Mikrotopographien von der Präsenz der verschiedenen PKD-Isoformen beeinflusst wird. Da frühere Arbeiten zeigen, dass das Contact Guidance Verhalten durch die Viskoelastizität der Zellen beeinflusst wird, wurden die mechanischen Eigenschaften der PKD-Isoform-Knockout-Zellen mit einem lasergestützten optischen Zellstrecker bestimmt. Die Ergebnisse zeigen eine signifikante Zunahme der Verformbarkeit von Panc1-Zellen in Abwesenheit von PKD1, jedoch weitaus geringere Veränderungen beim Knock-Down der beiden anderen Isoformen. Somit scheint PDK1 in Panc1-Zellen singulär zellmechanische Eigenschaften zu verändern, die für die Migration wichtig sind.

Abbreviations

2D	two-dimensional
3D	three-dimensional
ADM	acinar-to-ductal-metaplasia
ANOVA	analysis of variance
AR	aspect ratio
ATP	adenosine triphosphate
bFN	bovine fibronectin
BM	basement membrane
BSA	bovine serum albumin
CAF	cancer associated fibroblasts
CAMK	calcium/calmodulin-dependent kinase
CKP	cytokineplasts
CI	confidence interval
DAG	diacylglycerol
DA	direction autocorrelation
DMEM	Dulbecco's modified Eagle medium
DMSO	dimethyl sulfoxide
DNA	deoxyribonucleic acid
DPBS	Dulbecco's phosphate-buffered saline
ECM	extracellular matrix
EMT	epithelial-to-mesenchymal transition
F-actin	filamentous actin

FA	focal adhesion
FBS	fetal bovine serum
FDA	US Food and Drug Administration
IF	intermediate filament
KRAS	Ki-ras2 Kirsten RAt Sarcoma viral oncogene homolog
K	Keratin
MET	mesenchymal-to-epithelial transition
MMP	matrix metalloproteinase
mRNA	messenger ribonucleic acid
MSD	mean square displacement
NET	neutrophil extracellular trap
PanIN	pancreatic intraepithelial neoplasia
PDAC	pancreatic ductal adenocarcinoma
PDMS	polydimethylsiloxane
PFA	parafomaldehyde
PKC	protein kinase C
PKD KO	protein kinase D knockout
PKD	protein kinase D
PMN	polymorphonuclear cells
PRW	persistent random walk
RPMI	roswell park memorial institute medium
S.E.M.	standard error of the mean
Snail1	zinc finger protein SNAI1
SPC	sphingosylphosphorylcholine
SSH1L	slingshot protein phosphatase 1
UV	ultra violet
WLL	white light laser

Part I

Introduction

Chapter 1

Cell migration

Migration is imperative for life. It occurs on a wide range of spatio-temporal scales, starting with cellular locomotion necessary for development and maintenance of a living organism and reaching to animal migration in search for food. Cell migration is a highly complex process essential for embryonic development, immune response, tissue genesis and repair [1–6]. It requires a dynamic interplay between the intracellular signaling pathways and the extracellular environment. Although the biological and physical mechanisms of basic cell migration have been extensively studied, many questions still remain unanswered. A detailed understanding of this processes in cell migration is especially important, as the main cause of cancer-related death is cancer metastasis, i.e. relocation of cancer cells into distant organs and new tumor formation. The complexity of the underlying mechanisms of cell migration arises from the vast number of cell types and tissues that motile cells have to navigate and the presence of different migrational phenotypes. For example, individually migrating epithelial cells adapt mesenchymal migration mode which is characterized by strong attachment to the surrounding matrix and high cell contractility, whereas leukocytes, which need to migrate in diverse environments, largely engage in so called amoeboid migration, which does not involve cell-matrix anchorage [7].

1.1 Cell migration modes

There are two major categories of cell migration: single and collective (Fig. 1.1) [7]. Single cell locomotion can be further divided into two modes known as amoeboid and mesenchymal migration. Fast cells, such as leukocytes, fish keratinocytes and *Dictyostelium discoideum*, all undergo amoeboid movement [8, 9]. One common characteristic of cells migrating in amoeboid fashion is continuous change in cell morphology driven by rapid protrusion and retraction of cell extension either by plasma membrane blebbing or pseudopod formation [7], [10]. Cells moving in this fashion do not adhere strongly to the surface and depend on active filamentous

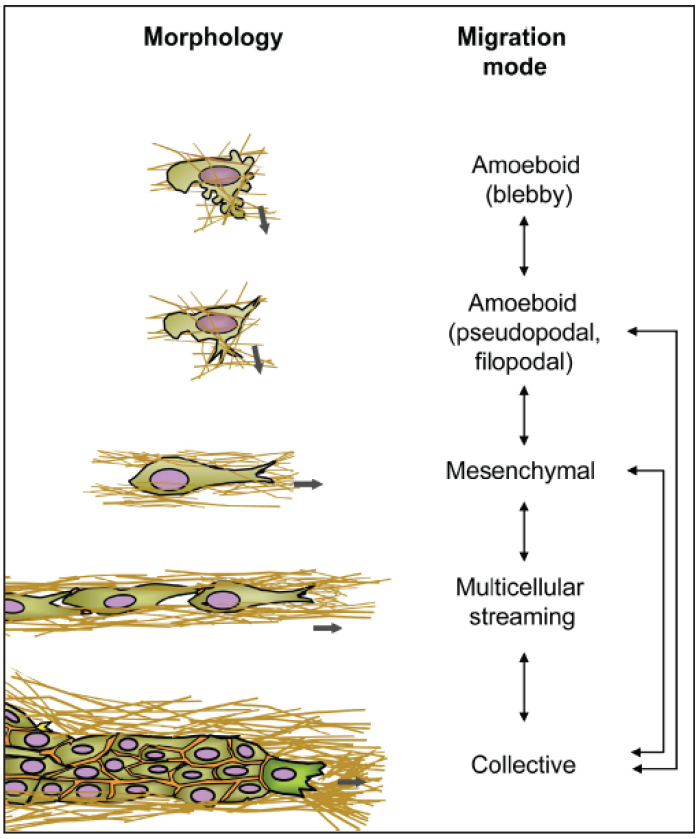

Figure 1.1: Cells can move in single (amoeboid and mesenchymal) and collective fashion (multicellular streaming and epithelial cell sheet migration). Migration modes depend on cell type and extracellular environment (extracellular matrix (ECM) composition, structure and gap size). As cells exhibit high degree of plasticity they can alternate between different migration modes (shown by the arrows). Adapted from Friedl *et al.* [7].

actin (F-actin) polymerization (pseudopodal migration) and actomyosin contraction (amoeboid blebbing) [10–12]. Mesenchymal single cell locomotion can be described by a multi-step cycle: F-actin polymerization at the leading edge creates an organelle-free membrane protrusion, which subsequently, through integrin-mediated attachment (focal adhesions), becomes anchored to the substrate. Consecutive, actomyosin contractility and cell detachment at the rear end results in forward cell movement. Mesenchymal migrating cells usually have spindle-shaped elongated morphology [7].

Interestingly, cells can also adapt to molecular and environmental changes by altering their migration mechanisms [9]. The most prominent example is epithelial-to-mesenchymal and mesenchymal-to-epithelial transitions (EMT and MET, respectively) observed in metastatic cancer cells [13, 14].

Collective cell migration occurs when group of cells migrate in a coordinated fashion by retaining their cell-cell contacts (Fig. 1.1). It is comparable to individual mesenchymal cell migration, with similar front-rear polarity and traction forces generated at the front of the collective [15]. The major difference is that cell-cell junctions play mechanosensitive signal and force transmission role from the leader cells towards the rear [16, 17]. This ensures a well-coordinated grouped forward movement with the posterior cells following the leader cells. Epithelial collective migration is characterized by tightly connected cell sheets with strong cell-cell junctions [17]. It is an important part of wound healing and morphogenesis, but is also common in pathological processes such as cancer metastasis [14]. Mesenchymal collective migration, also known as multicellular streaming, is characterized by looser arrangements and transient adherence junctions between cells [17]. This kind of behavior is observed, for example, in neural crest cells, key participants of vertebrate embryogenesis [3]. As in epithelial collective migration, cell streaming is also common in malignant invasion and metastasis [14].

Independent of migration mechanism, cell polarization, F-actin polymerization and myosin II-driven contractility are the dominant mediators of cell migration [18, 19]. This is strongly collaborated by the studies of blood polymorphonuclear cells (PMN) and fish keratinocytes in which the authors produced motile cytoplasmic fragments from the leading front of the migrating cells, lacking nuclei, microtubules and rest of the organelles [20–22].

1.2 Quantitative characterization of single cell migration

There are many models and theories describing cell migration phenomenologically and based on the underlying molecular mechanisms [23]. Cell migration is quantitatively characterized by a number of parameters, including speed, velocity and directional persistence [24]. Cell speed and velocity are easy enough to calculate by tracking cell displacement over sufficient amount of time. However, these two parameters are not sufficient to fully represent cell migration. Moving cells have varying degrees of intrinsic persistence even in the absence of extracellular guiding signals [24, 25]. It is becoming more and more clear that cells utilize non-Brownian migration patterns in order to efficiently search for their targets [26–28]. For example, in T cells which explore tissues through Lévy walk (alternating numerous short steps with longer straight steps in-between), a type of migration mechanism also observed in many animals when hunting for food [26, 27, 29]. *Dictyostelium discoideum*, a model single cell organism, also exhibit non-diffusive forward motion and migrate in a zigzag fashion by “remembering” their last turn direction [28]. Many quantitative parameters have been developed to characterize cell persistence, such as mean square displacement (MSD) and

direction autocorrelation (Fig. 1.2). The common assumption of these two methods is that the persistency with which the cells migrate is high at short time periods and decays exponentially over long time intervals. Thus, persistence time is the time period in which the cells exhibit correlated migration in one direction.

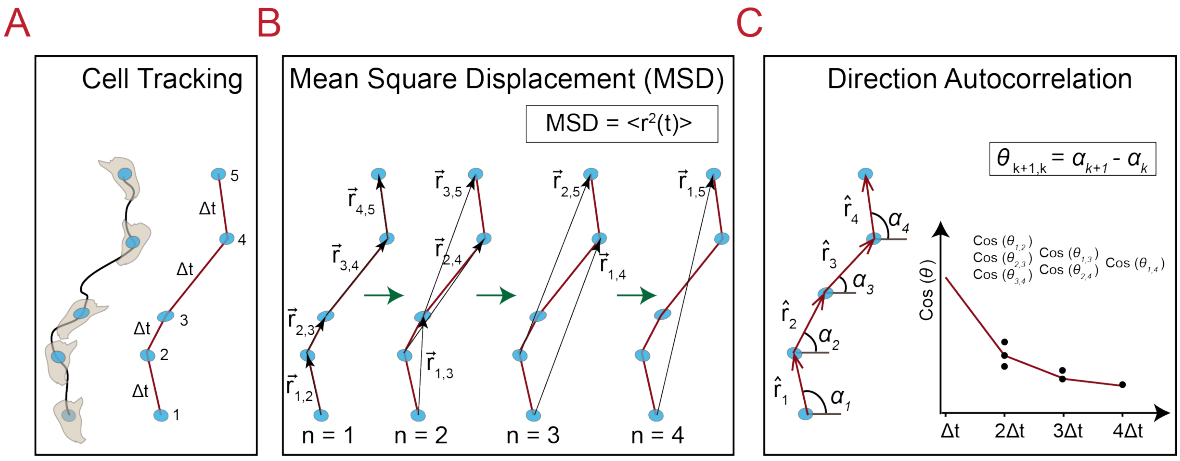

Figure 1.2: Cell tracking, mean square displacement (MSD) and directional autocorrelation analysis. **A.** Actual (left) and tracked (right) cell migration paths. Blue dots, representing cell nucleus, are tracked positions of the cells (1 to 5 in this example) with a set of (x,y) coordinates. Δt is the minimal time interval between two consecutive tracked positions (usually kept constant). **B.** At any given time interval t, with t = nΔt, overlapping squared displacement is calculated and averaged over all cells tracked and all possible displacement combinations for that specific t interval (see Equation 1.1). **C.** Direction autocorrelation represents correlation between the angles that the normalised displacement vectors ($\hat{r}$) form over increasing time intervals Equation 1.2. Autocorrelation values are given by , where cos (ϑ) is the angle difference between two vector angles (α). As with MSD analysis, the autocorrelation at time interval t is averaged over all cells tracked. Figure C was partially adapted from Gorelik *et al.* [24].

There are two types for MSD analysis based on overlapping and non-overlapping intervals between frames. Overlapping MSD method is the mostly one used as it provides more data sets for the averaging process (Fig. 1.2 B) [24, 30]. In 2D, for any time interval t (t = nΔt) MSD is given by [31]:

$$\langle r^2(t)\rangle = \frac{1}{N-n+1}\sum_{i=0}^{N-n}\left[(x_{(i+n)t}-x_{it})^2+(y_{(i+n)t}-y_{it})^2\right], \tag{1.1}$$

where N is the total number of steps tracked and n is the step size (Fig. 1.1B). The square brackets denote averaging for each time point over all tracked cell number. The average MSD is then plotted versus the time interval as shown in Figure 1.3.

Mean square displacement has a time interval dependence that follows a power law MSD $\propto t^{\beta}$, with $0 < \beta < 2$. The linear dependence is associated with Brownian motion, i.e. diffusive

random walk. Deviation from the linear behavior denotes subdiffusive, constraint (e.g. 3D migration with $0 \leq \beta \leq 1$) or superdiffusive (e.g. Lévy walk with $1 \leq \beta \leq 2$) migration modes. As mentioned above, in the absence of an extracellular guiding signal, cells migrate in a correlated manner in shorter time intervals and at longer observation periods they lose the persistency ($\beta \sim 1$). To quantify time dependent changes in $\beta(t)$, the logarithmic derivative of MSD ($\beta(t)$) over time is used (see Materials and Methods, Equation 5.5) [32]. In order to extract the persistence time, MSD curves are usually fitted with persistent random walk model (PRW) (see Materials and Methods, Equation 5.4). It is worth mentioning here that it is customary to use only 1/3 of the MSD data for fitting purposes, as with increasing time intervals less data points are available hence increasing the margin of error [24, 32].

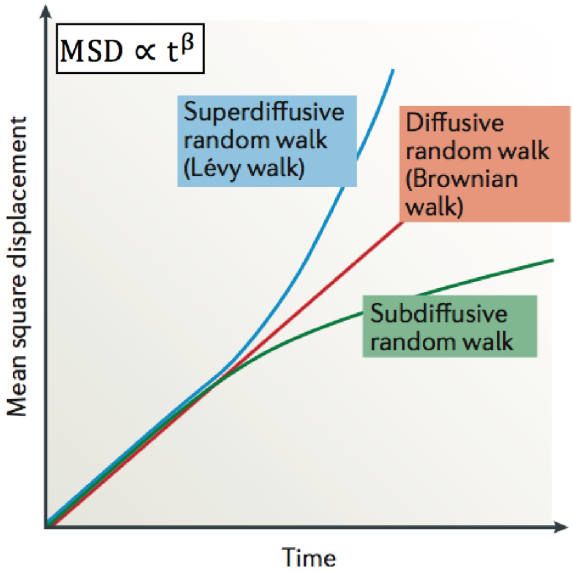

Figure 1.3: Subdiffusive, diffusive and superdiffusive migration modes characterized by mean square displacement (MSD). Diffusive random walk is the random migration with no or short-ranged persistence. Any kind of deviation from diffusive (sub- or superdiffusive) behavior is called anomalous random migration. Random migration occurs when the intrinsic positive feedback loop control, stabilizing the leading edge of the cell is weak [25]. Subdiffusive migration is characteristic for 3D confined migration whereas Lévy walk is an example of superdiffusive migration mode. Image was adapted from Krummel *et al.* [26].

Mean square displacement of multiple tracked cells represents, in essence, the average area that the cells explored in the given time interval [24]. In contrast, direction autocorrelation (DA) evaluates purely the directional component (not biased by cell speed) as it represents the correlation between angles that the normalised displacement vectors make (Fig 1.2C) [24].

Directionality autocorrelation is given by:

$$DA = \frac{1}{N-n+1}\sum_{i=0}^{N-n}\left(\hat{r}_{(i+n)t}\cdot\hat{r}_{it}\right) = \frac{1}{N-n+1}\sum_{i=0}^{N-n}\left(\cos(\alpha_{(i+n)t}-\cos\alpha_{it})\right), \tag{1.2}$$

where α is the angle at each time point of trajectory and t is the time interval. Similarly to MSD analysis, DA for a given t is averaged over the number of cells tracked and plotted over time interval (Fig. 1.2C). The higher the direction autocorrelation values the more persistent is the cell migration. The persistence time is then evaluated through exponential fitting of the autocorrelation curves $\sim e^{-t/\tau}$, where τ is the persistence time. One limitation of direction autocorrelation is that it is sampling interval (Δt) dependent. As the sampling time intervals decrease towards zero, the confounding effects of diffusive motion and human error in cell position measurement are amplified. On the other hand with very large sampling intervals displacement direction may seem not correlated at all [32].

Chapter 2

Temperature effects and neutrophils

With the constant feedback loop between cell intrinsic signaling pathways and extrinsic environment, any changes in the latter may lead to both positive and negative alterations in cell behavior. In context of cell migration, cell speed and directional persistence can be influenced by external factors such as ECM structure, composition or stiffness, application of physical strain or electrical fields, presence of chemoattractants and temperature [33–38]. One of the projects in this thesis focused on investigation of temperature-dependent neutrophil migration studies using differentiated HL-60 model cell line.

2.1 Role of temperature in cell physiology

Temperature is not constant in the human body with temperature gradients existing on both the single cell level and the tissue-scale level [39–41]. These gradients play an important role in many physiological processes such as metabolism, cell division and gene expression [42]. Regulated by the hypothalamus, healthy body's core temperature is kept at approximately 37 °C, whereas at the surface the temperatures range from 28 to 33 °C [43]. During disease, body core temperature may rise up to approximately 41 °C. On the cellular level, Chrétien *et al.* recently demonstrated that mitochondria, the organelle responsible for synthesis of ATP, are physiologically maintained at 50 °C, approximately 13 °C degrees higher than the average cell temperature [44]. Furthermore, temperature gradients have been shown to influence embryonic development in *Drosophila melanogaster* [45]. Mammalian sperm cells also use temperature cues to navigate the female genital tract [46]. Fluctuations in temperature can also affect F-actin polymerization, the diffusion rate of signaling molecules and integrins, cell membrane fluidity and many other processes involved in cell migration [47–50]. Heat and thermal gradients arise in diseased and inflamed tissues as well [51]. Cancer stroma is quite often inflamed and exhibits higher than normal temperatures [52]. Moreover, hyperthermia therapy combined with other, more conventional ones, has been shown to improve patient

treatment in some cancer types [53–55]. Thus, it is not surprising that temperature can also affect vital white blood cell functions, including phagocytic activity in monocytes and superoxide production in neutrophils [56, 57].

2.2 Neutrophils and differentiated HL-60 cell line

Neutrophils, a type of blood polymorphonuclear (PMN) cells, are the most abundant white blood cells in the human body and are the first cells to respond to infection or tissue damage [58]. One of the main morphological characteristics of these cells is the multi-lobulated cell nucleus, which plays a key role in neutrophilic functions [59]. The presence of cytoplasmic granules containing variety of antimicrobial proteins, proteases, and soluble mediators of inflammation is another important feature of these leukocytes [60]. Their ability to swiftly detect signals released by damaged host cells or microorganisms and react by polarizing and migrating towards the source is crucial to the body's initial inflammatory response [61]. The first step in neutrophil activation is rapid F-actin polymerization at the leading edge, polarizing the cell [62]. Many signaling molecules are involved in this step, and a great deal of work has been performed to fully understand the mechanism of neutrophil activation and directional migration [63–65]. Neutrophils make use of multiple mechanisms to fight pathogens: degranulation, phagocytosis or by releasing neutrophil extracellular traps (NETs) [60, 66]. Degranulation causes a problem when working with blood neutrophils, as cells can easily destruct during isolation.

One interesting study on neutrophils relevant to the work presented in this thesis is the possibility of motile cellular fragment formation from blood neutrophils. Malawista *et al.* has shown that there is an uncoupling of actin- and glycogen- rich neutrophil cytoplasm from the cell body when heated briefly at temperatures close to 45 °C [20, 67–69]. Even in the absence of all the organelles, such as the nucleus and microtubule, this cell fragments, or as the authors named them cytokineplasts (CKP), retained many of the characteristics of the parental cells, such phagocytosis, chemotaxis and some residual antimicrobial capacity [69], [20]. The latter was even shown *in vivo* [20]. Additionally, the lack of granules makes the CKPs cryopreservable, which is impossible with the blood neutrophils [20]. One of the apparent advantages of these fragments is their use as a system for identifying minimal components necessary for cell migration. Despite that, it seams that the research of this system was done exclusively by Malawista *et al.* One explanation may be that CKP formation is not a given and depends on neutrophil isolation method. Additionally, as anyone working with blood cells knows, many results are donor-dependent (personal observation). To overcome this issues a model cell line could be used.

One of the most common model cell lines used for *in vitro* studies of neutrophil migration are differentiated HL-60 cells [70–72]. This cell line was first isolated from a patient with acute promyelocytic leukemia in the 1980s. When incubated with Dimethylsulfoxide (DMSO) or all-trans-retionoic acid, these cells mature into fully differentiated neutrophils [73, 74]. Unlike neutrophils isolated from human blood, which are terminally differentiated, short-lived, and cannot be genetically manipulated, HL-60 cells are immortal and can be transfected [75]. Hauert *et al.* systematically compared the response of human peripheral blood neutrophils and neutrophil-differentiated HL-60 cells to different chemical stimuli. They showed that changes in cell morphology and chemotaxis occurring in response to chemoattractants and different inhibitors are both quantitatively and qualitatively comparable to those induced in primary neutrophils. Moreover, they found that levels of signaling enzymes and proteins in HL-60 cells upon differentiation are similar to those found in primary neutrophils [76]. In the presented thesis, the response of neutrophil-differentiated HL-60 cells to temperature changes in their environment was investigated.

Chapter 3

Pancreatic Cancer

According to the World Health Organization cancer is the second leading cause of death worldwide. Cancer is a universal term used to describe a wide variety of heterogenic diseases with their defining feature being uncontrolled in division and spreading of abnormal cells caused by genetic and/or epigenetic mutations. Out of the wide variety of cancer types, pancreatic cancer is one of the deadliest with a 5-year survival rate of the patients being only 7-9 % [77]. This dismal prognosis is notably due to the fact that pancreatic cancer is extremely difficult to diagnose at early stages [78]. Furthermore, the progression of the tumor is very rapid: On average it takes only 1.3 years for this cancer to progress from stage I (carcinoma *in situ*) to stage IV (highly metastatic with multiple secondary tumors), and by the time patients exhibit any symptoms more than 50 % of them have secondary tumors [78, 79]. Currently the only effective treatment for pancreatic cancer is surgery, but the statistics show that by the time of diagnoses only in 20 % of patients the tumor is resectable [78]. Lack of viable treatments and poor survival rates associated with this cancer type drive the science community worldwide to investigate further the underlying processes involved in pancreatic cancer formation, development and to look for new avenues for treatments.

3.1 Progression of pancreatic ductal adenocarcinoma

The pancreas is responsible for synthesis and secretion of hormones (endocrine gland) as well as digestive enzymes (exocrine gland) [80]. There are several varieties of pancreatic tumors, but the majority of them are initiated in the exocrine cells of the pancreas (acini and duct cells) [80, 81]. The most common (90 % of all pancreatic tumors) and aggressive pancreatic cancer is pancreatic ductal adenocarcinoma (PDAC) [80]. The name derives from the fact, that PDAC cells share similar histological and molecular characteristics with ductal cells of the healthy exocrine pancreas [80]. PDAC initiation and progression is associated with combination of multiple oncogenic mutations, inflammatory processes (e.g. chronic

pancreatitis) and inactivation of tumor suppressor genes [80, 82, 83]. Indeed, studies show that pancreatic cancer cells can have hundreds of genetic mutations, which affect numerous signaling pathways and processes [84]. This tumor driving changes can affect not only ductal cells, but also acinar cells. In a process called acinar-to-ductal-metaplasia (ADM), mature acini cells may undergo a transdifferentiation process, forming duct-like PDAC precursor cells [85, 86]. On condition of further oncogenic events these duct-like cells eventually progress into precancerous lesions called pancreatic intraepithelial neoplasia (PanINs) and into malignant adenocarcinoma [87, 88].

Numerous studies have revealed, that one of the crucial tumorigenic events in early PDAC development, is the activation of point mutations in the *KRAS* gene (Ki-ras2 Kirsten rat sarcoma viral oncogene homolog) [89]. Mutational activation of the *KRAS* is indeed found in approximately 90-95 % of pancreatic tumor cells both at early (ADM and PanIN 1, 2 and 3) and late, invasive, stages [90]. The KRAS protein is a small GTP-binding transducer protein involved in activation of several signaling cascades (PI3-K/PDK1/Akt and RAF/MEK1/2/ERK1/2) governing cell proliferation, differentiation and apoptosis [87]. Mutations in this oncogene lead to permanently activated KRAS protein promoting abnormal cellular behavior. As in any type of tumor, KRAS oncogene mutation as a lone factor is not responsible for PDAC progression. Indeed, these mutations may be present in the pancreas of healthy humans as well [87]. However studies in mouse models with switchable KRAS showed that inactivation of this oncogene at early stages hindered tumor progression to more advanced stages, whereas reactivation resulted in rapid disease progression towards PDAC [91]. Unfortunately, leveraging this information for PDAC therapeutic treatment has not been possible as chemical inhibition of the KRAS oncoprotein *in vivo*, despite decades of research, has failed [92]. KRAS is widely considered undruggable. Currently pursued strategies focus on indirect inhibition of KRAS activity by interfering with the kinase proteins involved in downstream signaling pathways [93].

3.2 Carcinogenesis and cancer metastasis

Carcinogenesis is a multi-step process in which healthy cells transform into cancer cells, i.e. cells that exhibit irregular cell growth, high resistance to cytotoxicity as well as defects in programmed cell apoptosis. It is accompanied by various cancer-promoting genetic and epigenetic changes in cells (Fig. 3.1). Depending on tissue type, external factors (e.g. tobacco use, physical activity etc.) and genetic predisposition carcinogenesis may take years or even decades [94]. Extended frame of this process is an important factor in preventing cancer, rather than treating it [95].

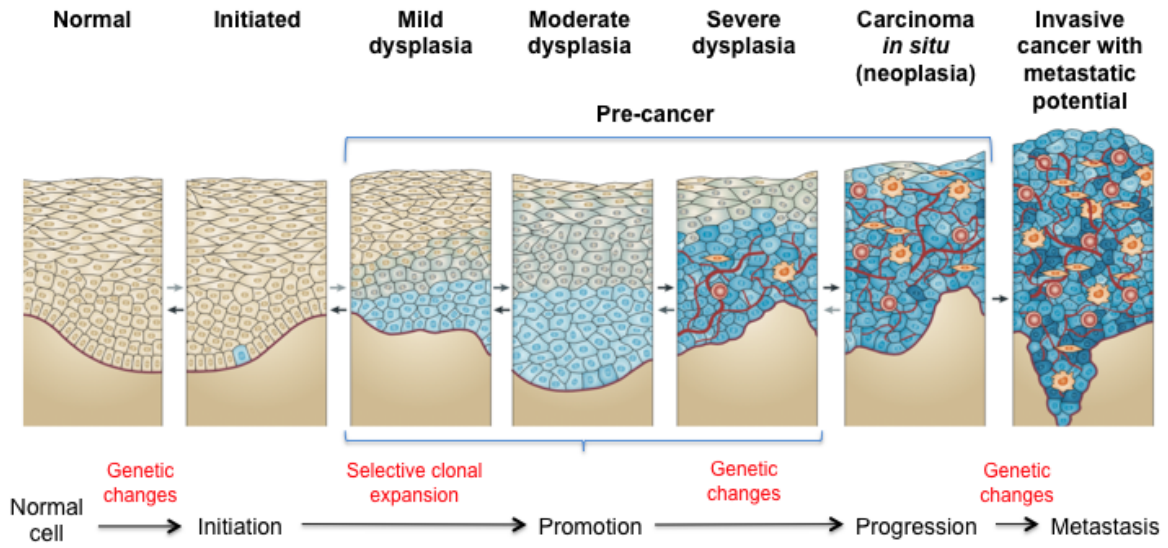

Figure 3.1: Initiation, Promotion and Progression: Three steps of carcinogenesis that characterize the evolvement of normal tissue into invasive cancer. Carcinogenesis is caused by accumulation of abnormal genetic and epigenetic processes promoting activation of oncogenes, altered DNA repair, inactivation of tumor suppressor genes, promotion of cell growth proteins etc. During carcinogenesis the cells develop multitude of defects in growth and proliferation control as well as resistance to cytotoxicity and apoptosis. The end result of carcinogenesis is invasive cancer with metastatic properties. The image was adapted from Umar *et al.* [94].

The first step of carcinogenesis is initiation, which represents a stable irreversible mutation in cell genes creating so-called oncogenes [94, 96]. These mutations deregulate the normal cellular pathways responsible for cell proliferation and development. Initiation may happen randomly or in response to external stimuli, which damage cell DNA [94]. Known carcinogenic catalysts are irradiation, some specific chemicals and viruses, tobacco, etc. The first mutation does not necessarily mean development of invasive cancer, but it allows the possibility of further activation of other oncogenes in the initiated cell and its progeny in case of prolonged exposure to promoting stimuli. The latter may lead to dysplasia, the selective proliferation and clonal expansion of the abnormal cells. This is the second step in carcinogenesis and is called promotion. This step usually takes very long time (years) and is divided into three categories: mild, moderate and severe dysplasia (Fig. 3.1) [94]. Further genetic changes, such as disruption of tumor suppressive genes, prompt the progression of dysplasia into neoplasm or carcinoma *in situ* (a tumor at the site of its formation). Progression is the last pre-cancer step and if left untreated it may further develop into invasive cancer with metastatic properties.

In the promotion stage of carcinogenesis changes happen not only inside the tumor, but also in the surrounding tissue (stroma) [97–99]. Tumor stroma comprises of ECM (primarily collagen) and stromal cells, such as cancer associated fibroblasts (CAFs) and immune cells [100, 101]. During disease, changes are induced not only in ECM biochemistry but also in biomechanical properties. ECM is produced and constantly remodeled by cells and during carcinogenesis, CAFs are responsible for the abnormal, tumor-promoting ECM production and reorganization [99, 102]. Additionally CAFs secrete enzymes, which crosslink collagen fibers inducing decrease in ECM porosity and increase in stiffness, which in turn, drives disease progression further [97, 98, 103]. Tissue fibrosis, which also contributes to matrix stiffening [104], can also be a trigger for carcinogenesis, such as in case of chronic pancreatitis, which quite often precedes or accompanies pancreatic cancer [82, 105]. Besides biomechanical changes, the ECM orientation is also affected, as instead of the non-oriented, anisotropic fibrils surrounding healthy epithelia, in malignant tumors ECM fibers appear straighter and are either aligned parallel or perpendicular to the tumor [106, 107]. This highly structured stroma orientation in the malignancies provides a highway for the migrating cancer cells and promotes cancer metastasis [106, 108].

Primary tumors are rarely the cause of patient death [109]. The majority of cancer related deaths are caused by therapy resistant metastases. Metastasis is defined as the spreading of malignant cells through blood and lymphatic vessels with subsequent colonization at distant organs, resulting in one or more secondary tumors [109, 110]. Similar to carcinogenesis, metastasis is a very complex process, which involves cancer cell dissemination from the primary tumor, invasion into the stroma, intravasation of cells into blood vessels, survival and circulation, attachment of the cells to the vessel walls and extravasation, micrometastases formation and finally metastatic colonization of different tissues (Fig. 3.2) [110]. One crucial step of metastasis is tumor angiogenesis. Angiogenesis, the establishment of new blood vessels, likely starts during carcinogenesis, as supply of oxygen and nutrients is necessary for tumor expansion [111]. During metastasis, angiogenesis provides easily accessible and highly permeable blood vessels for cancer cell intravasation.

There are two accepted models for tumor metastasis: Linear and parallel [112, 113]. In the linear model, the metastatic cascade is believed to start at the last stage of carcinogenesis, when the tumor is fully developed into the invasive phenotype [113]. The second model is based on the premise that the dissemination and metastasis of tumor cells happens in the earlier stages and is initiated in parallel to the primary tumor progression [112, 113]. The latter model is more likely to apply to pancreatic tumor metastasis, as the majority of patients have metastatic lesions at the time of the initial diagnosis. Indeed Rhim *et al.*, using mouse *in vivo* models, have recently shown, that invasion of pancreatic tumor cells into the surrounding

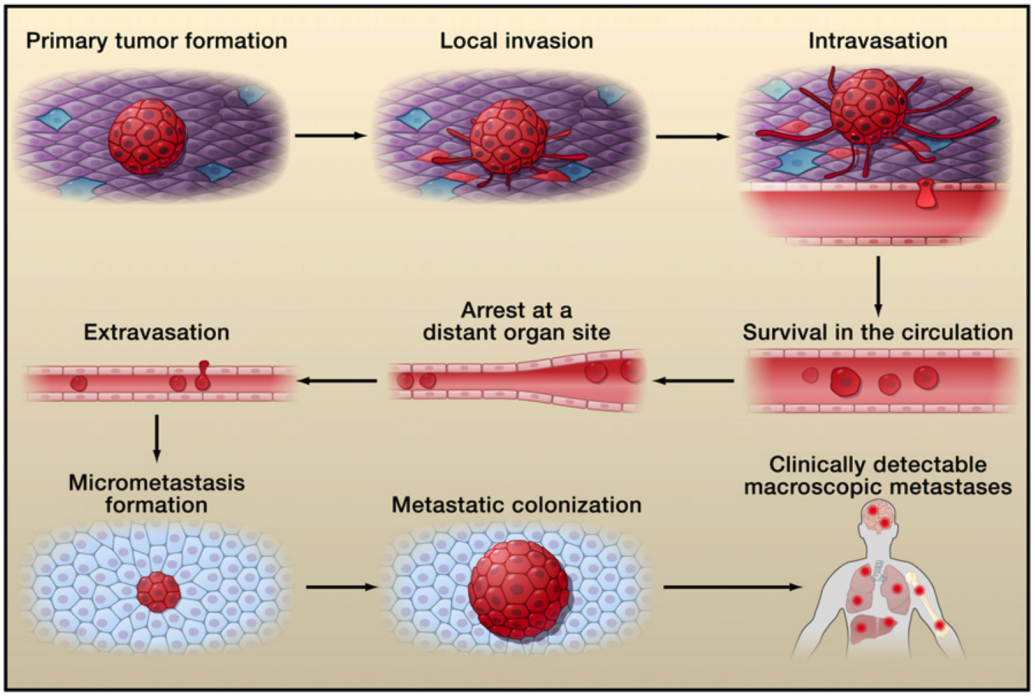

Figure 3.2: Cell-biological events occurring during the invasion-metastasis cascade. The steps involved in cancer cell metastasis are: 1) Metastatic cancer cell detachment from the primary tumor, followed by invasion into the surrounding tissue, 2) intravasation of cells into the blood and lymph vessels, 3) survival and circulation, 4) arrest of cells at the endothelial walls of the vessels, 5) extravasation, and finally 6) formation of microtumors, followed by metastatic colonization. The image was adapted from Valastyan *et al.* [110].

tissue and blood vessels precedes formation of invasive tumor phenotype at the primary site [114].

3.3 Cancer cell invasion and motility

Cancer invasion is a heterogeneous process, requiring constant changes in cell morphology and motility (Fig. 3.3) [100, 115, 116]. Cancer cells display exceptional plasticity and are dynamically able to adapt to, as well as remodel tumor microenvironment. Local invasion of basement membrane (BM) and the stroma can be done by collective or single cell migration [100]. In this work, the focus was given to single cell migration and invasion, as it is of importance not only during the initial invasion of the stroma, but also during intravasation into the bloodstream and later extravasation [117].

In order to successfully escape the confined primary tumor, cancer cells have to transition from epithelial phenotype to highly motile, mesenchymal one. This mechanism by which cancer cells achieve motility is called epithelial-to-mesenchymal transition (EMT) [13, 118,

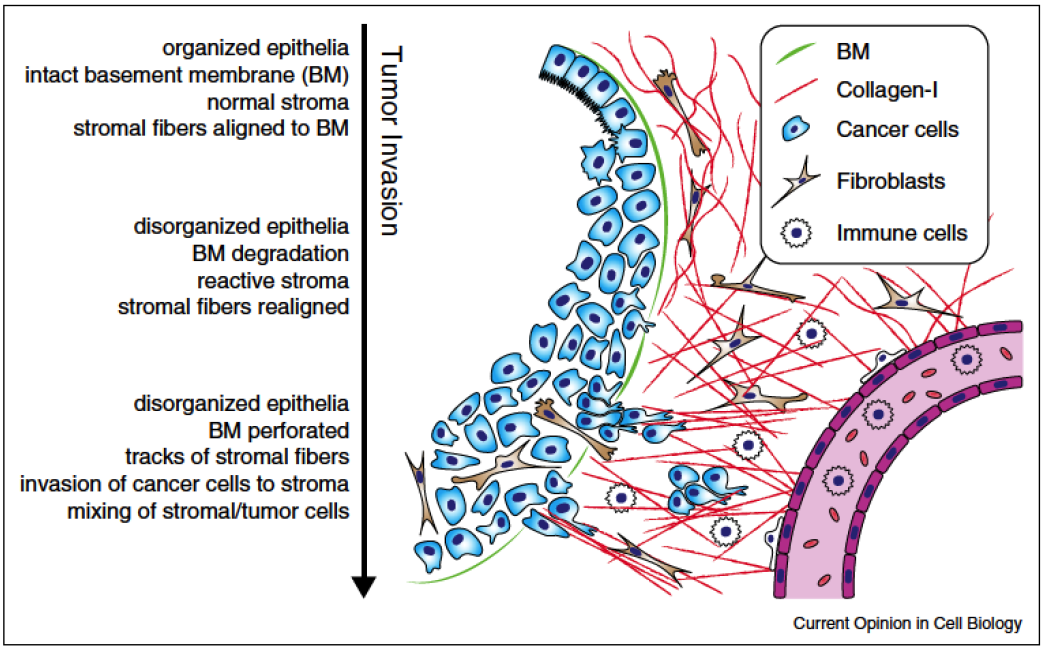

Figure 3.3: Schematic representation of tumor invasion. Cancer cell invasion into the surrounding tissue is a heterogeneous process accompanied by dissemination of the tumor epithelia, Epithelial-to-mesenchymal transition (EMT) of tumor cells, changes in cell biomechanical properties, basement membrane degradation and realignment and stiffening of the tumor surrounding ECM. The image was adapted from Clark *et al.* [100].

119]. EMT is the accepted mechanism of PDAC invasion and has been even associated with development of early drug resistance in many pancreatic cell lines [114, 119, 120]. It is a complex cell-biological process, which is guided by various intrinsic (gene mutations) and extrinsic (growth factor signaling) cues [121]. One important EMT pathway is initiated by overproduction of transforming growth factor β (TGF-β) by CAFs in advanced stages of carcinogenesis, which leads to reduced E-cadherin expression in cancer cells [122, 123]. E-cadherin is a known epithelial marker and is necessary for maintenance of cell-cell junctions [124]. Downregulation and loss of E-cadherin has been reported in many invasive cancer cell lines and is observed in up to 60 % of PDAC cell lines [125–127]. The dynamic interplay between tumor environment and tumor cells is a central factor of cancer invasion [104].

As it was discussed above, the tumor surrounding stroma undergoes drastic changes, such as increased stiffness and reduced porosity. The increased stiffness, among other things, promotes motile cell invadopodia formation and further invasion into the tissue by providing high number of integrin-mediated adhesion sites in the surrounding ECM [104, 128, 129]. Integrin-mediated signaling has also been shown to enhance cancer cell proliferation [130, 131]. Additionally, changes in the ECM topography and realignment (perpendicular to the BM) create “tracks” for the cells to migrate further into the stroma [106, 108]. In contrast with

increased stiffness of tumor stroma, cancer cells, especially the more invasive phenotypes, have been shown to be softer than their healthy progenitors [132–135]. It was suggested, that increase in malignant cell deformability plays an important role during cell transgression of the basement membrane [136]. Degradation of basement membrane and the connective ECM are hallmarks of invasion as well. Intrinsic genetical mutations as well as extrinsic changes trigger increased production of matrix metalloproteinases (MMPs) by the malignant cells [137]. MMPs are enzymes which are responsible for ECM degradation. Malignant cancer cell deformability combined with abnormal MMP secretion facilitates cell migration through the stiff tumor stroma.

3.4 Importance of protein kinases in cancer and Protein Kinase D family

Cell functions, such as proliferation, survival, motility and metabolism, are regulated by numerous kinase signaling pathways. Protein kinases (PTKs) are enzymes which phosphorylate proteins, regulating their biological activity [138]. Deregulation and/or overexpression of PTKs has been linked with numerous oncogenic processes [139]. Inhibiting kinase activity has been proven to be a promising avenue in targeted cancer therapy. In 2001, FDA approved the first protein kinase inhibitor (Imatinib/Gleevec) for the treatment of chronic myeloid leukemia. Since then, 30 more small molecule inhibitors were further approved for treating different tumors and more than hundred are still in clinical trials [140]. The human genome encodes 538 protein kinases and each of them is a potential therapeutic target [141]. In recent years, Protein Kinase D (PKD) enzymes of serine/threonine kinases were found to be key players in progression of many malignancies, especially in pancreatic cancer [142–144].

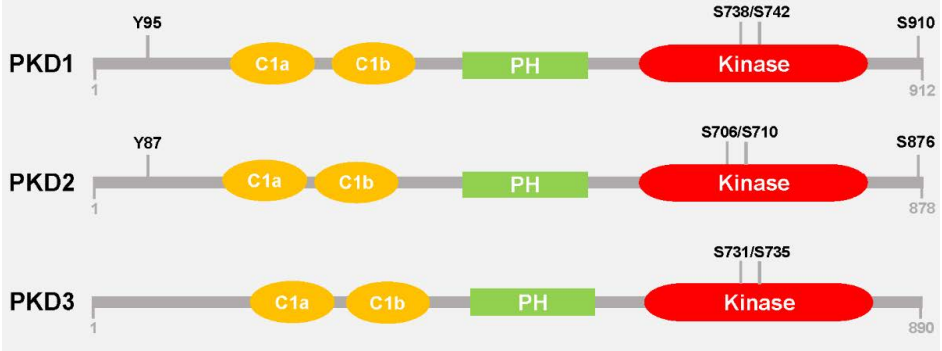

Figure 3.4: Structure of Protein Kinase D 1, 2 and 3 isoforms. All 3 isoforms have high degree of structural homology in their N-terminal regulatory domain, with two cysteine-rich zink finger domains (C1a and C1b) and an auto-inhibitory pleckstin homology (PH) region, as well as in the C-terminal catalytic domain (CD). As an example, PKD1 and 2 have an autophosphorylation site (PKD1^{S910} and PKD2^{S876}), which is absent in PKD3. The image was adapted from Durand *et al.* [145].

Human Protein Kinase D family is a part of calcium/calmodulin-dependent kinase superfamily (CAMK) and consists of 3 structural isoforms called PKD1 (also known as PKCμ), PKD2 and PKD3. PKDs are at crossroads of diacylglycerol and novel Protein Kinase C (DAG-PKC) signaling pathways and are important regulatory kinases for cell migration, proliferation, adhesion, EMT, DNA synthesis, vesicular transport and angiogenesis [145, 146]. PKDs play an important role in physiological processes such as innate immune response initiation [147], insulin secretion from pancreatic cells [148] and increase of cardiomyocyte contractility [149]. All three isoforms share similar domain structures having N-terminal regulatory and C-terminal catalytic domains. They have a high degree of homology in their N-terminal domain, whereas the C-terminal is not conserved (Fig. 3.4). Despite the high structural homology, all 3 isoforms have been shown to participate in different, quite often non-overlapping signaling pathways [146]. The latter may be attributed to differences in their expression patterns in different tissues as well as their structural differences in the phosphorylation motifs. For example, PKD1 and PKD2 contain C-terminal autophosphorylation site (PKD1^{S910} and PKD2^{S876}), which is absent in PKD3 (Fig. 3.4). Subcellular localization also differs for these isoforms. Under resting conditions PKD1 and PKD2 are localized mainly in the cytoplasm and to a lesser degree in the Golgi Apparatus or mitochondria [150]. In contrast PKD3, in addition to cytoplasm localization, can also be found in the nucleus [151].

3.5 Protein Kinase D isoforms in cancer

In recent years more and more studies have reported on PKD involvement in a variety of signal transduction pathways regulating development and progression of cancer [142, 152–154]. Many cancer-relevant functions, such as proliferation, migration, EMT, angiogenesis, MMP production etc., are mediated in an isoform- and tissue-specific way (see Appendix, Table A.1). Moreover, some studies show, that individual isoforms may play contradictory roles by mediating different signaling pathways in carcinogenesis and metastasis [152, 155, 156]. For example, PKD1 is downregulated in highly invasive prostate cancer, and when overexpressed, blocks proliferation and migration by E-cadherin phosphorylation and activating the ERK pathway [157, 158]. In contrast, PKD2 and 3 isoforms are upregulated and promote prostate cancer cell invasion through several recently identified pathways [154, 159, 160]. Findings regarding the role of each of the isoform in different cancer types are summarized in Table A.1 (see Appendix). Pancreatic cancer was excluded from this table as it will be discussed separately in more detail in the next chapter. The role of PKDs in cancer development is not so straightforward and strongly depends on cell type, activation state and expression level. Overall, the majority of research done so far shows that PKD1 has more anti-tumorigenic

functions by inhibiting cell motility of various cancers [152, 153, 155, 158]. Moreover, many malignant cells have reduced PKD1 expression [142, 156, 161, 162]. However, some studies report also pro-invasive functions of PKD1 [163–166]. PKD2 and PKD3 isoforms mediate more-uniformly pro-tumorigenic signaling pathways, such as upregulation of MMPs, inducing drug resistance, excessive tumor proliferation and invasion [154, 159, 167]. In some cancer types PKD2 and 3 isoforms have redundant, overlapping functions [154].

3.6 Role of PKD isoforms in pancreatic cancer progression and pancreatic ductal adenocarcinoma

Recent studies in mice revealed a crucial pro-oncogenic role of PKD1 in early PDAC development. In studies done by the Peter Storz's group and collaborators, 2 different PKD1-facilitated pathways (mutant KRAS/ROS/PKD1/NF-$\varkappa$B/EGFR and TGFα/KRAS/PKD1/Notch) were identified for acinar dedifferentiation, ADM transition and further progression into PanIN precancerous neoplasia [143, 168]. In both studies it was shown that PKD1 is activated downstream of either activated or mutant KRAS and conditional knockdown of PKD1 decreased the progression of ADM and PanIN. The role of PKD2 and PKD3 isoforms was not discussed in this context.

In vitro research sheds more light on individual isoform expression levels and functions in the highly invasive pancreatic cancer cell lines. PKD1 and PKD2 protein expression levels, compared to healthy cells, have been shown to be elevated in Panc1 and Panc89 cell lines [169]. PKD3 expression was not changed in all the cell lines analyzed. Eiseler *et al.* have demonstrated PKD1-driven proliferation and anchorage-independent PDAC growth mediated by Snail1 phosphorylation (transcription factor, which can trigger EMT) [170]. In a different study, the authors demonstrated anti-invasive/antimigratory properties of PKD1 through its control of F-actin polymerization. Cortactin and cofilin-phosphatase Slingshot1L (SSH1L), proteins which control F-actin polymerization and depolymerization, were identified as PKD1 substrates [142, 155]. PKD1 inhibition resulted in higher motility of cancer cells, hence promoting invasive behavior of pancreatic cancer, whereas overexpression of this isoform inhibited migration and invasiveness [155, 169]. The authors argued that presence of PKD1 at early stages of PDAC development is beneficiary for tumor progression, whereas the downregulation at later stages would promote invasion. The seemingly dual role of PKD1 at different stages of tumor progression is likely a direct result of its diverse array of substrates.

On the contrary, the data regarding PKD2 isoform involvement shows uniformly proinvasive quality in pancreatic cancer. Meta-analysis of different pancreatic cancer tissues showed that

PKD2 mRNA expression levels were significantly higher in comparison with control tissues and also in comparison with PKD1 mRNA [169, 171, 172]. PKD2 expressing pancreatic cancer cells have $\sim$ 11-fold time higher concentration of matrix metalloproteinases (especially MMP7 and MMP9) [169]. By regulating expression levels of MMP7/9, PKD2 mediates cancer cell invasiveness not only through ECM degradation, but also by regulating angiogenesis, as MMP7/9 actively contribute to angiogenesis [169, 173, 174]. The opposing functions of PKD1 and PKD2 make it clear that in order to successfully use them in therapy isoform specific inhibitors have to be developed. Less is known about the role of PKD3 in pancreatic cancer.

Chapter 4

Objectives

The goal of the presented thesis was to study two biophysical aspects of single cell migration, a complex process essential to health and disease.

In the first part of the thesis project, presented in Chapters 6 and 7, the effects of temperature and temperature gradients on immune cell motility was investigated. Temperature varies on different length scales form subcellular size to tissue, organ or human body dimension. Knowing how sensitive cells are to any biophysical and biochemical alterations in the extracellular environment, it is surprising that not many studies have investigated the effect of thermal variations on basic cell functions like migration. For example, as part of the body's immune system, leukocytes are required to navigate through various tissues with alternating temperatures in order to successfully migrate towards an injured or infected site. In this regard, one specific aim of the presented work was to elucidate the effect of extracellular thermal changes on immune cell motility. Using differentiated HL-60 cells, a model cell line for blood neutrophils (the fastest human cells and the first responders to infection), 2D cell migration was studied at physiologically relevant temperature ranges of 27 to 43 °C. The migration experiments were carried out both by stepwise increasing the temperature by small increments and using temperature gradients. Therefore, a temperature gradient chamber was developed. Additionally, based on the ability of blood neutrophils to form autonomous motile cell fragments when heat-treated for short periods of time, cell fragment formation was attempted using differentiated HL-60 cells.

Not only external signals such as temperature affect cell motility but also cancer-associated changes of internal signaling can alter cell migration and responses to external signals. Therefore, in the second part of the thesis project, presented in Chapters 8 and 9, pancreatic cancer cell lines with Crispr/Cas9 PKD1, PKD2 and PKD3 knockouts were used for the first

time to study *in vitro* the Protein Kinase D isoform-dependent effects in cancer cell migration associated with invasive behavior.

Protein Kinase D enzymes, a family of three structural isoforms called PKD1, PKD2 and PKD3, have been shown to play a significant regulatory role in cancer motility and invasion but lack of methods to address each isoform specifically limited research. Stable isoform-selective Crispr/Cas9 knockouts, done by a collaboration partner, allowed for controlled deletion of each isoform, which gives an advantage over the previously used methods, such as pan-PKD inhibition with chemicals, PKD isoform partial knockdown or ectopic introduction of one or another isoform.

PKD1 KO, PKD2 KO and PKD3 KO pancreatic cancer cell migration and invasion was studied to elucidate emerging changes in response and migration to the loss of each isoform. Towards this aim, various biophysical *in vitro* migration assays were implemented, starting from cell migration studies on basic glass surfaces, followed by more complex PDMS-based surfaces with microgrooved structures capable of contact guidance induction. Additionally, PKD isoform-selective and MMP-independent pancreatic cancer cell invasion studies were performed using PDMS-based migration chips with precise microchannel architecture. In order to link the altered invasion-associated behavior to mechanical properties, a further aim of this thesis was to characterize the KO cells in this respect.

Part II

Materials and Methods

Chapter 5

Materials and Methods

5.1 Fabrication of migration assays

In this work different *in vitro* migration assays were used to study cell motility in 2D and 3D. Basic 2D migration studies were performed on commercially available glass-bottom petri dishes. Custom temperature gradient chambers were developed and manufactured for differentiated HL-60 cell thermotaxis studies. PDMS-based (Polydimethylsiloxane) substrates and microchips used in pancreatic cancer cell studies were fabricated based on the methods previously developed in our group [36, 175, 176].

5.1.1 Temperature gradient chamber fabrication for 2D and 3D experiments

Temperature gradient chambers were manufactured based on a modification of the system described in Das *et al.* [177], using ridged Plexiglas molds with ridge dimensions of 8.0x2.0x0.2 mm^3 (L:W:H) for 2D experiments and 8.0x2.0x8.0 mm^3 (L:W:H) for 3D experiments (Figs. 5.1 A and B, respectively). As a heat source and heat sink, rectangular hollow copper reservoirs 18x6x8 mm^3 (L:W:H) were used with inlets and outlets to supply heated and chilled water. These were attached to the mold with screws parallel to the microridge. 1:10 PDMS 184 (#2699150, Dow Corning, United States) was poured in the mold and subsequently cured at 65 °C overnight. To be able to inject cells into the 2D PDMS microchambers, two holes with 1 mm diameter were punched into the PDMS. The PDMS chips were bound to a glass coverslip via oxygen plasma treatment (30 seconds at 0.7 mbar oxygen pressure and 200 W power, Plasma System 100, PVA TePLa) of both the glass and the PDMS, followed by an overnight thermal treatment at 65 °C. The copper reservoirs were then detached from the mold and inserted into the PDMS microchamber. The assembled temperature gradient chambers

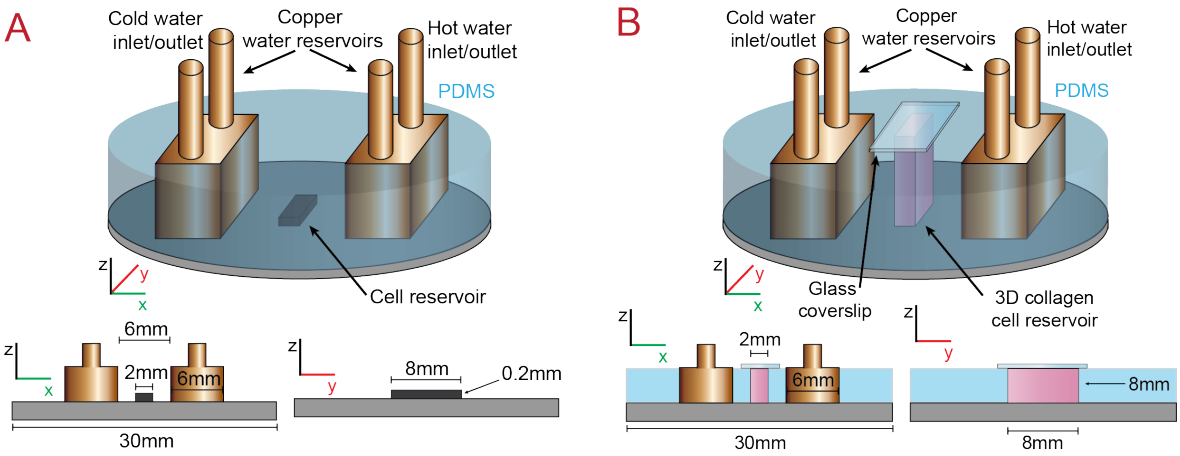

Figure 5.1: Schematic representation of the microfluidic 2D (A) and 3D (B) temperature gradient chambers with cross sections in X and Y directions. Copper reservoirs were used as a heat source and a heat sink, with their temperatures held constant at 65 °C and 5 °C, respectively.

were then sterilized for two hours under UV light. In order to assess the temperature gradient applied to the cells, Comsol Multiphysics 5.1 3D simulations were performed for the geometry used in the experimental setup (Comsol Inc, Sweden). Heat Transfer in Solids mode was applied for the analysis. Several assumptions were made to simplify the computation:

- The liquid in the microchannel is considered to be water, not biological media.
- The copper reservoirs were considered to be solid blocks with a constant temperature corresponding to the temperature used during experiments (65 °C for the heat source and 5 °C for the heat sink).
- The external boundaries of the device were assumed to exchange heat by natural convection only. The ambient temperature and pressure were set to 37 °C and 1 atm.

Computations performed using COMSOL Multiphysics showed a uniform temperature gradient along the whole microchamber with a range from 27 °C to 43 °C (Fig 5.2).

5.1.2 PDMS-based microgrooved substrate and invasion chip fabrication and functionalization

Both microgrooved substrates and microchannel invasion chips were fabricated by replica molding of 1:10 PDMS on silicon (Si) wafers with the desired structures. The microstructured silicon wafers were fabricated using photolithography-based protocols previously developed in our group [36, 175, 176]. Briefly, photoresist coated Si wafers (Siegert Wafer GmbH,

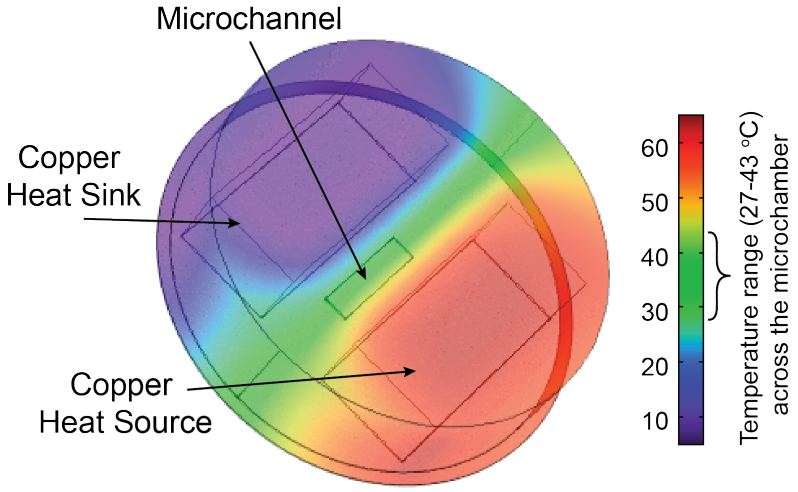

Figure 5.2: 3D Volume temperature gradient distribution computed by COMSOL Multiphysics. A 27-43 °C temperature gradient is generated along the 2 mm wide microchannel.

Germany) were aligned to Chromium photomasks (ML&C GmbH, Germany) with the desired structures. The wafers were then irradiated with UV light ($\lambda = 405$nm) from a mercury lamp source (HBO 350 W, Osram, Germany). Following UV exposure, the structured wafers were developed and baked. For microgrooved substrates, the microstructured silicone wafers were coated with chromium of desired thickness by using physical vapor deposition. After a washing step necessary for photoresist removal, the wafers were placed in petri dishes to be used as molds. For invasion chips with microchannel structures, a two-step photolithography technique with two different photomasks was used to achieve the desired structures.

Microgrooved substrates with 2 and 10 µm wide and 200 and 350 nm deep grooves (Fig. 5.3A) were prepared by replica molding of PDMS in the microgrooved Si molds. 1:10 PDMS mixture of curing agent and polymer base (w/w) were poured into the molds, followed by a 4-hour curing step at 65 °C. The cured PDMS elastomers were then peeled off and placed in 6-well plates (#657160, Greiner Bio-One, Frickenhausen, Germany). After subsequent washing steps with 70 % ethanol (#K928.3, Roth, Germany) and sterile 1x DPBS (Dulbecco's Phosphate-Buffered Saline, #14080-048, Gibco, Germany), the substrates were functionalized by a 1-hour long incubation with 10 µg/mL bovine Fibronectin (bFN) (#86088-83-7, Sigma Aldrich, Germany) in PBS. After a final washing step with cell media, the substrates were ready for cell seeding.

Invasion chips with two different microchannel dimensions (WxHxL 3x11x150 μm^3 and 10x11x150 μm^3) were prepared by PDMS replica molding as described above. Each chip contained 80 microchannels for each dimension. To create enclosed microchips (Fig. 5.3 B) the PDMS replica were bound to glass coverslips via oxygen plasma treatment of both the

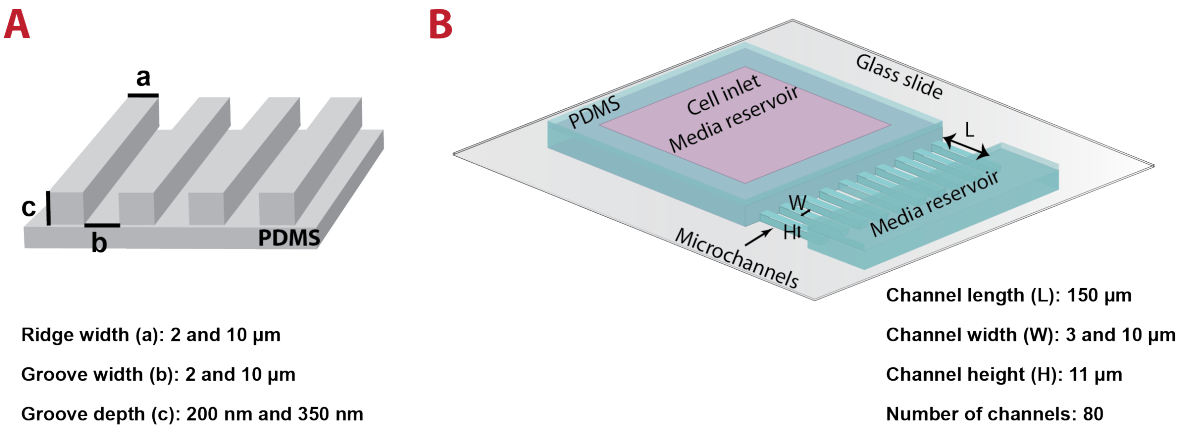

Figure 5.3: Schematic representation of PDMS-based microgrooved substrates (A) and invasion chips with microchannels (B) used for pancreatic cancer cell migration studies.

glass and the PDMS (25 seconds at 0.7 mbar oxygen pressure and 200 W power), followed by a 30-minute thermal treatment at 80 °C. The invasion chips were then incubated overnight at 4 °C with 100 µg/mL Collagen I (#A10483-01, Gibco) solution in PBS. After a washing step with sterile PBS, the chips were exposed to one hour of UV light for sterilization purposes. After a final washing step with cell media the microchips were ready to be seeded.

5.2 Cell biology methods

5.2.1 Cell Culture

5.2.1.1 HL-60 cell culture and differentiation

HL-60 cells were obtained from Deutsche Sammlung von Mikroorganismen und Zellkulturen (DSMZ, Germany) and kept in cell culture at a maximum concentration of 10^6 cells per millilitre. For differentiation purposes, cells (passage numbers 6-9) were cultured with an initial concentration of 10^5 cells per millilitre in the presence of 1.3 % DMSO (Dimethyl Sulfoxide, #D2650, Sigma Aldrich) in cell culture media (RPMI 1640 + GlutaMax, #61870, Gibco) supplemented with 10 % heat inactivated fetal bovine serum (FBS) (#10500, Gibco) and 1 % Penicillin-Streptomycin antibiotics (#15140, Gibco). On Day 2, cells were centrifuged, counted, and cultured again in presence of 1.3 % DMSO with a cell concentration of 10^5 cells per millilitre. On Day 4 the media was changed. On Days 5-7 cells were sufficiently differentiated and could be used for experiments.

5.2.1.2 3-D cell culture for temperature gradient studies

Differentiated HL-60 cells were cultured in Collagen I hydrogel scaffolds as described by Shin *et al.* [178]. Briefly, 20 µL of 10x DPBS (#14080, Gibco) was thoroughly mixed with 11 µL of 0.5 N NaOH solution (#1.06498.0500, Merck, United States), 133 µL of 3 mg/mL rat tail Collagen I stock solution (#A10483, Gibco) and 36 µL of cell suspension (200,000 cells overall) for a final concentration of 2.0 mg/mL collagen. All ingredients and vials were precooled and hydrogel solution preparation was performed on ice.

5.2.1.3 Neutrophil isolation

Human blood neutrophils were isolated from fresh venous blood of two donors. Heparin-Calcium (Ratiopharm, Ulm, Germany) was used as an anticoagulant. Fresh blood was left to sediment at an angle of 45° for two hours. The middle layer, containing white blood cells, was then pipetted, suspended in DPBS without Ca^{2+} and Mg^{2+} ions (#D8537, Sigma Aldrich), and centrifuged gently. After centrifugation, the cells were re-suspended in human blood plasma.

5.2.1.4 Pancreatic cancer cell culture

PKD1, PKD2, PKD3 Crispr/Cas9 knockout Panc1 (PKD1 KO, PKD2 KO, PKD3 KO, respectively) and wild type Panc1 pancreatic cancer cell lines were kindly provided by Dr. Tim Eiseler from Dr. Thomas Seuferlein's laboratory at University Clinic Ulm. The cells were cultured in Dulbecco's Modified Eagle Medium (DMEM) (#31966, Gibco) with the addition of 10 % FBS and 1 % Penicillin-Streptomycin. The cells were passaged when at 80-90 % cell confluence using pre-warmed 0.25 % Trypsin/EDTA (#25200, Gibco). Following inhibition of trypsin with DMEM+10 % FBS (twice the amount of Trypsin used), the cell suspension was centrifuged at 600 rpm for 5 minutes. After resuspending the cell pellet in fresh growth media, the cells were counted using a Neubauer chamber for cell seeding for the experiments.

5.2.2 Immunocytochemistry

5.2.2.1 Giemsa-Wright staining of differentiated and non-differentiated HL-60 cells

Giemsa-Wright staining was performed according to the manufacturer's instructions (#WS16, #GS500, Sigma Aldrich). Briefly, 10^5 cells in 300 µL media were spun onto a Cytospin slide and subsequently fixed with methanol for 15 minutes. After drying, slides were incubated with 500 µL of Wright solution for 2 minutes, rinsed with dH_2O and incubated with a 1:20 Giemsa solution diluted with dH_2O for one hour. Afterwards, the slides were thoroughly washed

with dH_2O and dried. Imaging was performed using a Zeiss Axiovert200M microscope, a Plan-Apochromat 63x oil objective (Zeiss) and an AxioCam IC camera (Zeiss).

5.2.2.2 Pancreatic cancer cells

Filamentous Actin (F-actin), nuclei, focal adhesion (FA) protein vinculin and cell-cell adhesion molecule E-cadherin of fixed PKD1 KO, PKD2 KO, PKD3 KO and Panc1 control cells seeded on a glass surface were fluorescently labeled and imaged using confocal fluorescence microscopy. Cells were seeded in 6-well glass-bottomed petri dishes (#P06-1.5H-N, In Vitro Scientific, United States), incubated overnight at 37 °C and 5 % CO_2 and fixed with 3.7 % Parafomaldehyde (PFA) (Sigma Aldrich) in PBS for 15 minutes at 37 °C, followed by cell membrane permeabilization with 0.1 % Triton X-100 (#93421, Fluka, Germany) in PBS for 15 minutes at room temperature. After thorough washing step with PBS, antibody unspecific binding sites were blocked by treating the cells with 5 % bovine serum albumin (BSA) (#9048-46-5, Sigma Aldrich) for one hour at room temperature, following another one hour incubation with primary antibodies solution in 5 % BSA at 37 °C. Afterwards, the cells were rinsed again with PBS and incubated with secondary antibody solution in 5 % BSA for 30 minutes at room temperature. After a final washing step with PBS, the cells were ready for imaging. The list of the primary and secondary antibodies and the concentrations used is given in Table 5.1.

Table 5.1: List of antibodies used for modified and non-modified Panc1 cells staining

	Primary antibody, dilution factor	**Secondary antibody, dilution factor**
F- actin	N/A	Alexa Fluor 568 Phalloidin (#A12380, Life Tech., Germany), 1:500
Nuclei	N/A	Hoechst 33342 (#H3570, Life Tech., Germany), 1:5000
Vinculin	Mouse anti-Vinculin (#V9131, Sigma Aldrich), 1:400	Goat anti-Mouse488 (#A-11029, Life Tech.), 1:500
E-cadherin	Mouse anti-E-cadherin (#610182, BD transduction lab), 1:25	Goat anti-Mouse488 (#A-11029, Life Tech.), 1:500

Imaging was carried out using an inverted confocal Laser-Scanning-Microscope (SP5, Leica Germany) equipped with an argon and a white light laser (WLL). Images were acquired using a 63x oil-immersion objective (HCX PL APO 63x/1.40-0.60; Leica Microsystems GmbH, Germany). The pinhole for data acquisition was set to 1 Airy unit. Fluorophores

were excited at 350, 488 and 558 nm and the detection windows were set at 380-450 nm, 500-540 nm and 568-610 nm, respectively. 10 to 15 images (0.99 µm apart) in z direction were acquired. Images were processed with Fiji software [179]. Using the Z project function of the software, z-stack images were projected into one image. Maximum Intensity projection type was applied. Brightness and contrast of the images was then modified for each image.

5.2.3 Cell seeding, cell imaging and image analysis: Differentiated HL-60 cells

5.2.3.1 2D glass surfaces

Cell seeding: Differentiated HL-60 cells (Days 5-7) were centrifuged at 1000x g for 5 minutes, the supernatant was removed, and the cells were resuspended in corresponding RPMI-1640 media not containing DMSO. 200,000-1,000,000 cells in 250 µm media were placed in sterile 20 mm or 35 mm glass-bottom petri dishes (#627860, Greiner Bio-One, Germany) and incubated for one hour at 37 °C and 5 % CO_2. Afterwards, in order to remove as many non-adherent cells as possible, media was aspirated and the petri dishes were washed three times. After addition of 2 mL of fresh pre-heated (37 °C) media, the petri dishes were placed on a heating plate and time-lapse movies were generated.

Three different seeding conditions were used for experiments with static temperatures: control, bovine fibronectin (bFN) glass coating, and 5X FBS. Cells seeded on the glass surface of the petri dish without any coating and with media containing 10 % FBS was used as a control. For bFN experiments, the petri dish was incubated with 100 µg/mL bFN (Gibco) for two hours at room temperature and subsequently washed with PBS three times for 5 minutes each. Afterwards, they were filled with media containing 10 % FBS and stored until cell seeding. For the third seeding condition, a 5-fold increase of FBS in the media compared to the control was used for the duration of the experiment.

Cell imaging: After cell seeding, samples were placed on a transparent thermoplate (Tokai Hit, Model TP-KI05-60, Thermofisher, Darmstadt, Germany), which was then placed on the stage of an Axiovert200M microscope. Time-lapse movies were taken with a 10x objective (EC Plan-Neofluar, Zeiss) every 10 seconds. Cells were heated from 30 °C to 42 °C. During this process, the temperature was held at 30 °C, 33 °C, and 35 °C for one hour each and at 37 °C for 30 minutes. Starting with 37 °C, the temperature was changed every 10 minutes by 0.5 °C until a final temperature of 42 °C. The temperature change of the plate caused thermal expansion, which resulted in gradual defocusing of the images. To address this, imaging was shortly paused at 39 °C for focus adjustment.

Image analysis: To assess cell attachment at different seeding conditions and temperatures, the number of attached and floating cells in 10 positions (each with an area of 0.6 mm^2) from two independent experiments was counted and averaged.

To investigate the effects of temperature on cell velocity, for each condition and each temperature, 39-78 cells were manually tracked for 8 minutes (50 frames) using Fiji's Manual CellTracker plug-in [179]. At 39 °C and 40 °C on bFN coating, 117 cells were tracked. For the lower temperatures (30 °C to 37 °C), videos taken from the last 10 minutes of each corresponding temperature were analyzed. The instantaneous speed of each cell was then calculated and averaged. The mean speed results presented in this work are averaged from the number of cells tracked for each specific condition at a given temperature.

To evaluate differentiated HL-60 cell persistence at different temperatures, autocorrelation analysis was performed on the tracked data of the cells. Autocorrelation was computed over 1/3 of the track length for each condition and temperature using the DiPer macro provided by Gorelik *et al.* [24]. Exponential fitting of the autocorrelation data was done in MATLAB R2016a using the following equation:

$$\alpha e^{-t/\tau} + c\,, \tag{5.1}$$

where τ is the persistence time. The average persistence length was then calculated by multiplying the persistence time by the average speed at each temperature.

5.2.3.2 Temperature gradient studies

The temperature gradient was initiated by supplying hot and cold water to the copper reservoirs being continuously exchanged through two peristaltic pumps. The temperature of the supplied water was kept constant via a heating plate and an ice bath. A thermocouple was attached to each copper reservoir to monitor the temperature of the reservoirs for the duration of the experiments.

2D experiments were performed by injecting cells into the microchamber at a concentration of 150 cells/mm^2 and imaging every 15 seconds. Prior to temperature gradient initiation, cells were imaged for 30 minutes at 37 °C. To achieve the desired temperature gradient range of 27 °C to 43 °C, the hot and cold sources were supplied with 65 °C and 5 °C water, respectively. After gradient initiation, cells were imaged for 40 minutes. 50 cells in total were tracked. The mean cell speed was then calculated as described above.

To investigate cell behavior in 3D temperature gradients, 50 µL of collagen I gel solution containing 2x10^5 cells was loaded into the 3D cell reservoir. To promote collagen gelation, gradient chips were incubated for 50 minutes at 37 °C and 5 % CO_2. Afterwards, the cell reservoir was covered with a glass coverslip and sealed from all sides using addition-curing silicone (Picodent twinsil® speed, Wipperfürth, Germany). Cells were then imaged via phase contrast every 5 minutes with a 10x objective. Multiple 2D planes were acquired throughout the 3D collagen scaffold at a z-spacing of 20 µm. Prior to initiation of the temperature gradient, cells were imaged for one hour at 37 °C. After initiation, cells were imaged for eight hours. 20 cells in total were tracked in 20 different z planes. Mean cell speed was then calculated as described above.

5.2.3.3 Shear flow assay

Channel slides with dimensions of 50 x 5 x 0.2 mm^3 (LxWxH) (Ibidi GmbH, Germany) were used to investigate differentiated HL-60 cell behavior under shear flow. The flow rate, controlled by syringe pumps (Pump11Elite, Harvard Apparaturs, USA), was kept at either 30 µL/hour or 40 µL/hour. Media was injected with 1 mL syringes (Omnifix®-F, B.Braun, Germany) connected by a cannula (Sterican®, 0.4 x 20 mm^2, BL/LB, B.Braun, Germany) and PTFE-tubing (0.4 x 0.9 mm^2, Bola, Germany). The cells were kept under constant flow for one hour and imaged at a 1-minute interval. For each of the two flow conditions, two independent experiments were performed. In total, 50 cells from at least five different chamber positions were tracked.

5.2.4 Cell seeding, cell imaging and image analysis: Blood neutrophils

Freshly isolated blood neutrophils, suspended in blood plasma, were seeded on glass-bottomed petri dishes and left for 10 minutes at 37 °C and 5 % CO_2 to ensure neutrophil attachment. After gentle washing with preheated blood plasma, the samples were placed on a transparent thermoplate (Tokai Hit, Model TP-KI05-60, Thermofisher, Darmstadt, Germany), which was then placed on the stage of an Axiovert200M microscope. Time-lapse movies were taken with a 40x air objective (LD Plan-Neofluar, Zeiss) every 5 seconds. Cells were imaged at 37 °C for 10 minutes, followed by a 10-minute long heating step at 45-47 °C, necessary for cell fragment formation (also known as citokineplasts). Afterwards, the temperature was cycled back to 37 °C and the cells were imaged for another 10 minutes. Blood Neutrophil velocity was assessed at 37 °C by manually tracking 20 cells isolated from two donors using Fiji's Manual CellTracker plug-in [179]. The instantaneous speed of each cell was then calculated

and averaged. The mean speed results presented in this work are averaged from the number of cells tracked.

5.2.5 Cell seeding, cell imaging and image analysis: Pancreatic cancer cells

5.2.5.1 2D glass surfaces

Cell seeding: PKD1 KO, PKD2 KO, PKD3 KO and Panc1 control cells were seeded at a concentration of approximately 30 cells/mm^2 on commercially available glass-bottom petri dishes (Greiner Bio-One). All experiments were carried out 24 hours after the initial seeding to ensure full cell attachment and spreading.

Cell imaging: For cell attachment, proliferation and morphological studies phase contrast images were taken 24 hours after cell seeding at 10 separate positions for each sample.

For cell migration studies, phase-contrast imaging was performed in a heated chamber (37 °C and 5 % CO_2) of an inverted AxioObserver (Zeiss) microscope equipped with a halogen lamp (Hal 100). Time-lapse movies were taken with a 10x objective (LD Plan-Neofluar, Zeiss) every 5 minutes over a 24-hour period.

Image analysis: To assess cell attachment efficiency of Panc1 cells in the absence of each PKD isoform, the number of attached cells in 20 positions (each with area of 0.6 mm^2) from two independent experiments was counted 24 hours after cell seeding. The rounded cells were considered to be non-adherent. Cell attachment efficiency was then calculated as:

$$Attachment\ Efficiency\,(\%) = \left(\frac{Cell\ No\ at\ 24h}{Cell\ No\ at\ seeding}\right) * 100\,. \tag{5.2}$$

After 72 hours the cells were passaged and the total number of cells was estimated by using flow cytometer. The proliferation rates of each cell line were expressed as:

$$Cell\ Proliferation = \frac{Cell\ No\ at\ 72h}{Cell\ No\ at\ 24h}\,. \tag{5.3}$$

To assess pancreatic cancer cell velocity for each knockout and control 45-50 cells were manually tracked for 24 hours using Fiji's Manual CellTracker plug-in [179]. The instantaneous speed of each cell was calculated and averaged. The mean speed results presented in this work are averaged from the number of cells tracked. Three independent experiments were performed. For morphological studies, 30 cells for each cell line were manually outlined in Fiji. Using the Measure function in Fiji, cell area and cell aspect ratio (AR) were measured. AR is defined in more details in section 5.2.5.2.

To evaluate cell persistence, mean square displacement (MSD) analysis was performed on the tracked data of the cells (see Introduction, Section 1.2). MSD was computed over 1/6 of the track length (four hours) for each condition using the DiPer macro provided by Gorelik *et al.* [24]. Obtained MSD curves were fitted with persistent random walk model (PRW) in MATLAB R2016a using the following equation:

$$MSD(t) = 2S^2P_t\left(t - P_t\left(1 - e^{-t/P_t}\right)\right), \tag{5.4}$$

where P_t is the persistence time and S is the cell speed. Time dependent changes of MSD follow a power law MSD $\propto t^{\beta}$, where β is a dimensionless number between 0 and 2, indicating different migration modes. β(t) was obtained from the logarithmic derivative of MSD curves:

$$\beta(t) = \frac{d(\ln MSD(t))}{d(\ln t)}. \tag{5.5}$$

5.2.5.2 PDMS-based microgrooved substrates

Cell seeding: PKD1 KO, PKD2 KO, PKD3 KO and Panc1 control cells were seeded at a concentration of approximately 30 cells/mm^2 on bFN-coated microgrooved PDMS substrates. All experiments were carried out 24 hours after the initial seeding to ensure full cell attachment and spreading.

Cell imaging: For cell migration studies, phase-contrast imaging was performed in a heated chamber (37 °C and 5 % CO_2) of an inverted AxioObserver (Zeiss) microscope equipped with a halogen lamp (Hal 100). Time-lapse movies were taken with a 10x objective (LD Plan-Neofluar, Zeiss) every 10 minutes over a 20-hour period.

Image analysis: Morphological studies and cell alignment of the grooves was carried out by manually outlining 30-50 cells (from two independent experiments) on each groove dimension 24 hours after seeding. Cell aspect ratio and orientation parameter were then measured by fitting an ellipse to the cell outlines as shown in Figure 5.4. The AR is then defined as:

$$AR = \frac{a_{major}}{a_{minor}}, \tag{5.6}$$

where a_{major} and a_{minor} are major and minor axes of the best fitting ellipse of the cell outline. Cell alignment on the grooves is given by cell orientation parameter S averaged over all cells:

$$S = \frac{1}{n}\sum \cos(2\theta), \tag{5.7}$$

where n is the number of the cells and θ represents the angle in radians between major axis of the fitted ellipse and the groove direction, here x-axis (Fig. 5.4). S is a dimensionless

parameter with values ranging from -1 to 1, with S = 1 denoting perfect, S = 0 random and S = -1 perpendicular alignments.

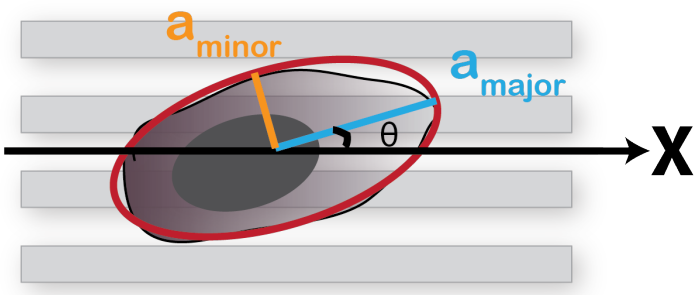

Figure 5.4: Best fitting ellipse of a cell on a microgrooved substrate used for cell AR and alignment analysis.

To assess pancreatic cancer cell velocity for each cell line and groove dimension 30-50 cells were manually tracked for 20 hours using Fiji's Manual CellTracker plug-in [179]. The instantaneous speed of each cell was then calculated and averaged. The mean speed results presented in this work are averaged from the number of cells tracked. Migration displacement angles with respect to the groove direction were also calculated from cell migration vectors. Steps smaller than 3 µm were disregarded.

5.2.5.3 PDMS-based microchannel invasion assay

Cell seeding: PKD1 KO, PKD2 KO, PKD3 KO and Panc1 control cell suspensions, containing approximately 40x10^3 cells in 80 µL media, were injected into the cell inlet of collagen-coated invasion microchips (Fig. 5.3 B). Cell reservoirs located opposite of the cell inlet were filled with cell culture media. After one hour incubation at 37 °C and 5 % CO_2, the petri dish containing the chips was filled with 2 mL cell media to ensure sufficient nutrition for long-term experiments. All experiments were carried out 24 hours after the initial seeding to ensure full cell attachment and spreading.

Cell imaging: Life phase-contrast imaging was performed in a heated chamber (37 °C and 5 % CO_2) of an inverted AxioObserver (Zeiss) microscope equipped with a halogen lamp (Hal 100). Time-lapse movies were taken with a 10x objective (LD Plan-Neofluar, Zeiss) every 10 minutes over a 48-hour period.

Image analysis: Image processing was performed in Fiji. Single cell-channel interactions were divided into three categories: Penetration, invasion and permeation (Fig. 5.5). Cells that partially extended into the channels (up to 50 % of the channel length), without fully entering them, were classified as penetrating cells. Cells that completely entered or penetrated

$\geq$ 50 % without leaving the channels from the opposite side were considered invasive cells. And lastly, the cells that completely migrated through the channels were termed permeative.

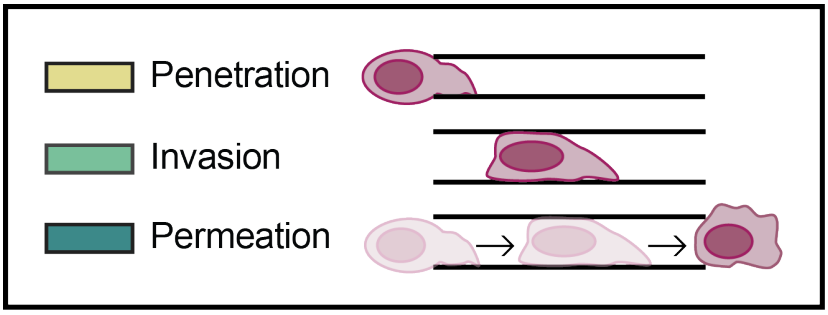

Figure 5.5: Three categories of cell-channel interactions.

To evaluate average migration speed of permeating cells, the leading edge of the cells was tracked using Fiji's Manual CellTracker plug-in [179]. The tracking was stopped as soon as the front of the cells reached the opposite edges of the channel. Cells undergoing mitosis inside the channels were excluded from this analysis. The instantaneous speed of each cell was then calculated and averaged. The mean speed results presented in this work are averaged from the number of cells tracked. Three independent experiments were performed.

5.3 3-D optical stretching of pancreatic cancer cells

To estimate PKD-isoform dependent changes in mechanical properties of Panc1 cancer cell line, a 3D optical stretcher was used (RS Zelltechnik, Germany). The optical stretcher is a dual laser tool that was first introduced by Guck *et al.* [180], that uses light force to trap and deform small biological objects, such as cells and lipid vesicles. The working principle of the optical stretcher is based on momentum transfer from the light to the object, which results in forces exerted on the object. As a ray of light hits the cell, changes of photon momentum occur due to differences in refractive indices of the surrounding media and cell. The conservation of momentum leads to forces acting perpendicular to the cell surface. Using two identical, counterpropagating laser beams allows for a symmetric stretching of the cells along the laser beam axis (Fig. 5.6A).

The setup of the 3D optical stretcher consists of an optical measurement chamber mounted on an inverted microscope (AxioImager, with a 63x air objective, LD Plan-Neofluor, Zeiss) equipped with a high-resolution camera (Zyla 5.5 sCMOS, Andor Technology-Oxford Instruments, Northern Ireland). Inside the measurement chamber a glass capillary, which serves as cell flow channel, is situated between two optical fibers (Fig. 5.6B). 1064 nm laser (Fibolux, FIBOTEC, Germany) with two separately controllable outputs and a maximum power of

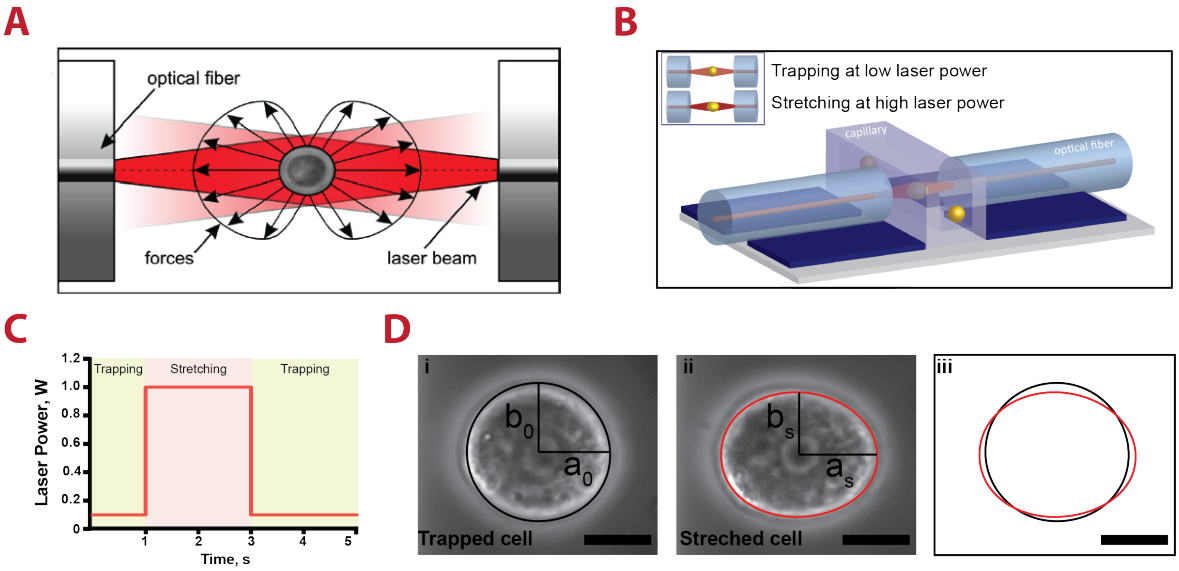

Figure 5.6: Working principle of 3D optical stretcher. **A.** Forces exerted on the cell surface due to momentum transfer lead to cell deformation along the beam axis. Image adapted from Lautenschläger *et al.* [181]. **B.** Optical measurement chamber, consisting of a glass capillary situated between two optical fibers. Image was adapted from RS Zelltechnick marketing material. **C.** Laser power profile used in the measurements. The cells, supplied into the capillary with a microfluidic pump, were trapped at low (100 mW) and stretched at higher (1000 mW) laser powers. 1064 nm laser was used as a light source. **D.** Phase contrast images of a representative cell being optically trapped (t = 0s) (i) and stretched (t = 3s) (ii). The black and the red lines represent the cell boundaries, with a_0, b_0 and a_s, b_s being the semi-axes of trapped and stretched cell, respectively. (iii) Overlap of trapped and stretched cell outlines. Scale bars: 10 µm.

2 × 2 W attached to the chamber serves as light source. The microscope, with the mounted measurement chamber, was situated in a housing with a temperature control system to ensure stable temperature during measurements. The temperature was kept at 23 °C. The cell suspension, containing approximately 10^5, was supplied into the capillary using a microfluidic pump. The flow rate was controlled automatically by the program provided by the manufacturer. During object trapping and stretching the flow was stalled. The cells were trapped for 1 s at low laser power of 100 mW, stretched for 2 s at 1000 mW, followed by a 2-second long relaxation period at 100 mW (Fig. 5.6C). 30 images per second were obtained for each cell throughout the measurement. The program was equipped with a cell-edge detection algorithm, which allowed automatic and swift image processing. One important factor for automatic image processing is the sharp white contrasting ring around the cell surface appearing in the phase contrast images (Fig. 5.6.D). This is necessary for the algorithm to precisely detect object shape by detecting the borders. Cell shape irregularities and bleb formation during stretching would lead to inconsistent measurements.

To quantify cell deformability, relative change in cell ellipticity was calculated for each cell:

$$Cell\,deformability = \left(\left(\frac{a_s - b_s}{a_s}\right) - \left(\frac{a_0 - b_0}{a_0}\right)\right) * 100\,, \tag{5.8}$$

where a_0, b_0 and a_s, b_s are the semi-axes of trapped and stretched cell, respectively (Fig. 5.6D). The average deformability of each cell line at each time point was then estimated by averaging over all the cells measured.

5.4 Statistics

Autocorrelation and MSD data is presented as mean ± SEM. All other data is presented as mean ± 95 % confidence intervals (CIs). Statistical analysis was performed in GraphPad Prism (San Diego, CA, USA). Significance was evaluated where applicable either by standard unpaired one-way ANOVA, unpaired two-way ANOVA or by unpaired Welch's t-test. The normality of the t-test was assessed using the D'Agostino & Pearson normality test.

Part III

Temperature-sensitive migration dynamics in neutrophil differentiated HL-60 cells

Chapter 6

Results

In the study described in this chapter, differentiated HL-60 cells were used as a model cell line to investigate temperature-dependent neutrophil migration. HL-60 cells are immortal human blood promyelocytic leukemia cells capable of terminal differentiation into more mature white blood cell types such as neutrophils or monocytes.

6.1 HL-60 cell differentiation

HL-60 cells were differentiated into neutrophil-like cells using 1.3 % DMSO. Differentiation was induced for five to seven days, after which cells were resuspended in DMSO-free media. To qualitatively confirm the success of the differentiation into neutrophil-like cells, Giemsa-Wright staining was performed prior to and after the differentiation protocol. Prior to induction, HL-60 cells had rounded nuclei typical of that cell line, whereas the majority of differentiated cells exhibited multi-segmented nuclei characteristic of neutrophils (Fig. 6.1A).

Non-differentiated HL-60 cells are non-adherent and cultured in suspension. Further confirmation of successful differentiation was the presence of adherent cells: By the third day of differentiation, cells adhering to the bottom of the culture flasks were observed. By the seventh day post-induction, the number of adherent cells increased five-fold (Fig. 6.1B).

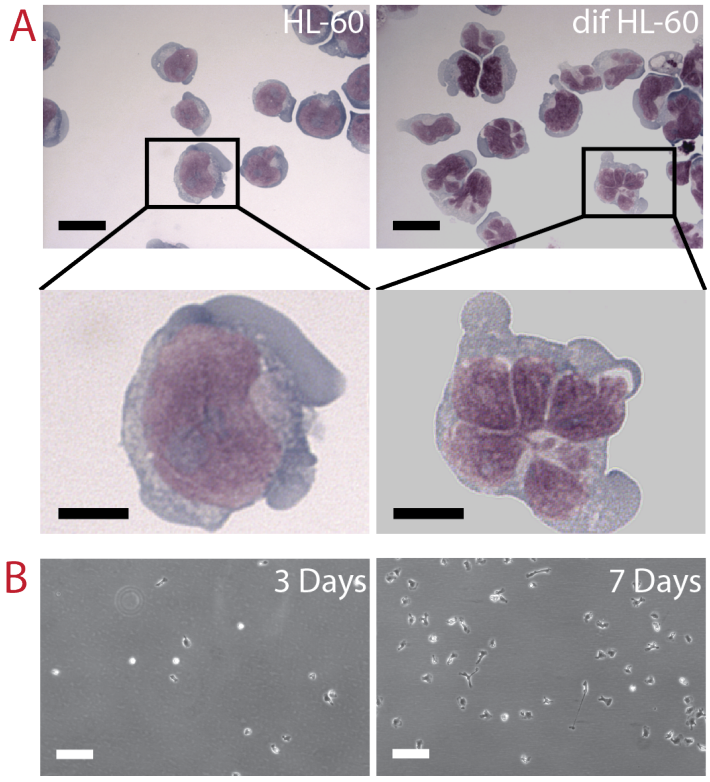

Figure 6.1: Successful differentiation of HL-60 cells into neutrophil-like cells. **A.** Giemsa-Wright staining of HL-60 cell nuclei before (left) and seven days after differentiation (right) (Scale bars: 50 µm and 20 µm top and bottom row, respectively). The majority of differentiated HL-60 cells exhibit lobed nuclei characteristic to blood PMN cells. **B.** 10x phase contrast images thee days and seven days after the start of differentiation. The amount of attached cells increases up to 10-fold. Scale bars: 50 µm.

6.2 Heat induced formation of motile cell fragments

Malawista *et al.* have demonstrated the ability of human blood polymorphonuclear leukocytes to separate the motile machinery from the cell body under short-termed (8 to 10 minutes) heat treatment [21]. The authors reported that despite the uncoupling from cell body, the cell protopods retained their ability to attach to surfaces and exhibit directed migration towards a chemotactic signal both *in vitro* and *in vivo* [20, 67–69]. Despite this fascinating discovery made already in 1982, very little has been done to date to understand the mechanism of the uncoupling and to further study these motile fragments, named cytokineplasts (CKPs). This is likely due to the drawbacks involved in working with blood neutrophils, as well as the challenging procedure of fragment formation (see Introduction, Section 2.2).

In this work, CKP formation was attempted both in blood neutrophils and neutrophil differentiated HL-60 cells. Blood neutrophils were isolated from fresh venous blood obtained from willing donors (see Materials and Methods, Section 5.2.1.3).

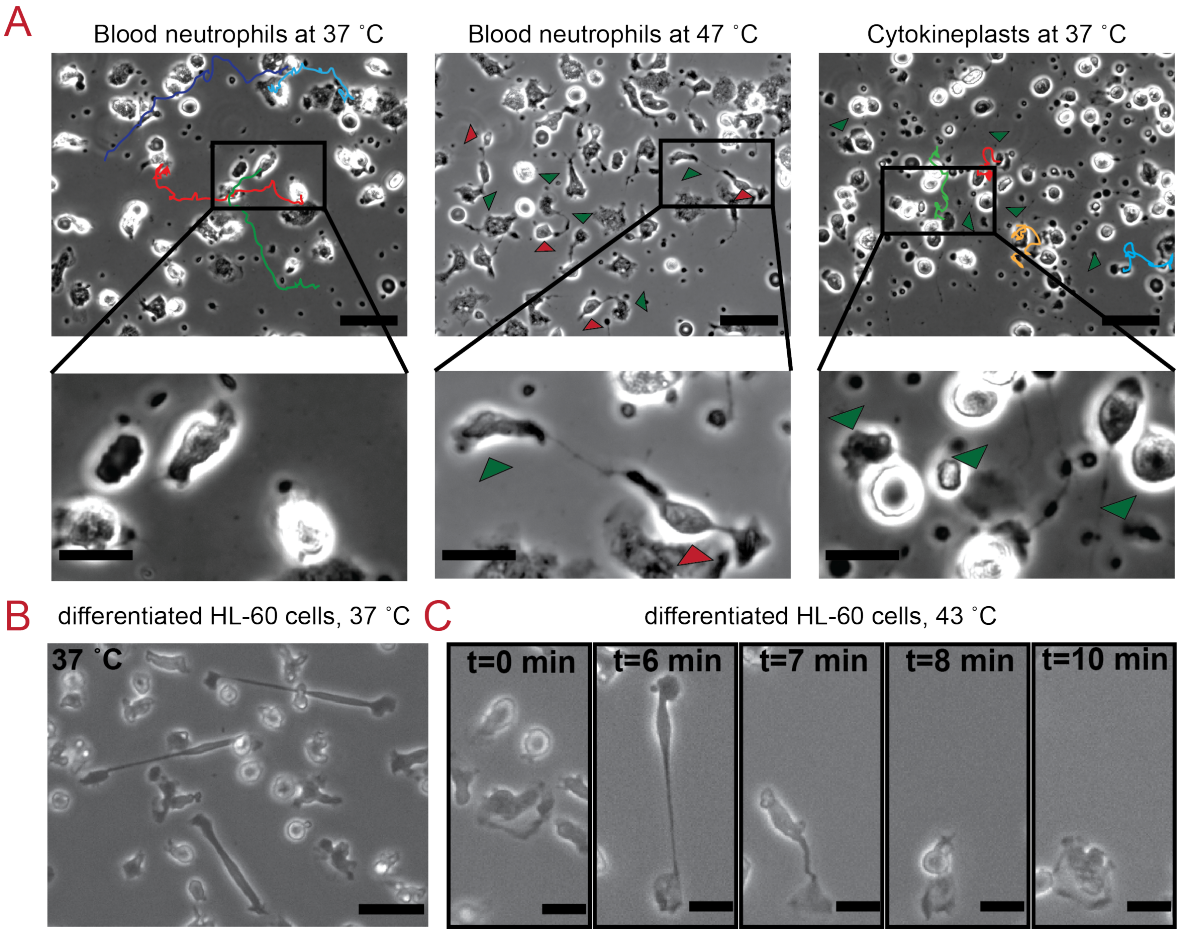

Figure 6.2: Motile fragment formation was possible in human blood neutrophils but not in differentiated HL-60 cells. A. Representative phase contrast images of fully intact blood neutrophils plated on glass slide at 37 °C (left), heated for 5 minutes at 47 °C (middle) and the formed CKPs at 37 °C (right). When heated to 45-47 °C, the cell protopods (green triangles) migrated away from the cell body (red triangle). The motile cell fragments stayed attached to the cell body through a thin filament. If the heating temperature and time were sufficient, the fragments fully detached from the bodies, forming CKPs (right image, green triangles). Scale bars: 50 µm and 20 µm top and bottom row, respectively. **B.** Representative phase contrast images of neutrophil differentiated HL-60 cells at 37 °C. Some of the cells exhibited extreme cell elongation already at 37 °C, with motile front and cell bodies connected with a thin filament. Scale bar: 50 µm. **C.** Heating at 43 °C, the maximum temperatures at which some cells stayed adherent, was not sufficient for CKP formation. Nucleus containing bodies retracted towards the motile front and the cells reassemble without any visible damage to them. Scale bars: 20 µm.

Blood neutrophils were plated on glass slides, sealed with a coverslip and placed on a heating plate on the stage of a microscope. Phase contrast imaging was used to observe neutrophil migration and CKP formation. After ten minute-long imaging at 37°C, the heating stage was set to 45-47 °C for another ten minutes. Afterwards, the temperature was cycled back to 37 °C and the samples were imaged (Fig. 6.2A).

In general, the number of motile neutrophils, their fragment formation and full decoupling (i.e. exact temperature and heating period) highly depended on the donor. Only the fast migrating cells formed CKPs. Upon heating, the motile fronts of the cells moved away from the cell body staying attached to it with a thin filament (Fig. 6.2A). Longer heating periods (9-10 minutes) led to the full decoupling of the motile fragments. If stored at 4 °C, the CKPs were motile after 24 hours. As CKP formation from blood cells was extremely heterogeneous, the same procedure was performed using neutrophil differentiated HL-60 cells, a model cell line used for neutrophil studies. Extended motile protopods connected to cell body with a thin filament were observed in this cell line already at 37 °C (Fig. 6.2B). However, heating neutrophil-like HL-60 cells did not lead to fragment formation. Poor adherence of differentiated HL-60 cell at temperatures higher than 40 °C was one of the biggest obstacles (Fig. 6.3). As described in the next section, already at 43 °C most of the cells were detached. Regardless of temperature applied, the extended motile front of the model cell line stayed adherent to the cell body. After a period of some minutes the cell part containing the nucleus would detach from the glass, retract towards the motile front and the cells would reassemble and continue movement (Fig. 6.2C). Although differentiated HL-60 cells were not a successful neutrophil substitute for CKP formation, they were further used to study cell migration under physiologically relevant temperatures.

6.3 Temperature-dependent attachment and migration speed in differentiated HL-60 cells.

Differentiated HL-60 cells were used to investigate neutrophil migration under the effect of physiologically relevant temperatures (30-42 °C). Here, this thermal range is divided into 3 increments: hypothermic (30-35 °C), normal (35-39 °C), and hyperthermic (39-42 °C). Cells were cultured on untreated glass bottom petri dishes and monitored migration monitored using phase contrast microscopy. Differentiated HL-60 cells remained motile throughout the entire temperature range applied (Fig. 6.3A). Elevated temperatures in the hyperthermic range significantly reduced the amount of adherent cells. At 40 °C, approximately 50 % of previously attached cells were observed floating in the media (Fig. 6.3Aiii). Detached cells did not appear to be dead or apoptotic, as reduction of the temperature back to 37 °C resulted in reattachment to the substrate (Fig. 6.3B).

To improve cell adhesion at higher temperatures, elevated serum concentration (5X FBS) and a 100 µg/mL fibronectin (bFN) surface coating were both tested. Fibronectin coating did not improve cell attachment in any of the temperature regimes (Fig. 6.4A). However, higher

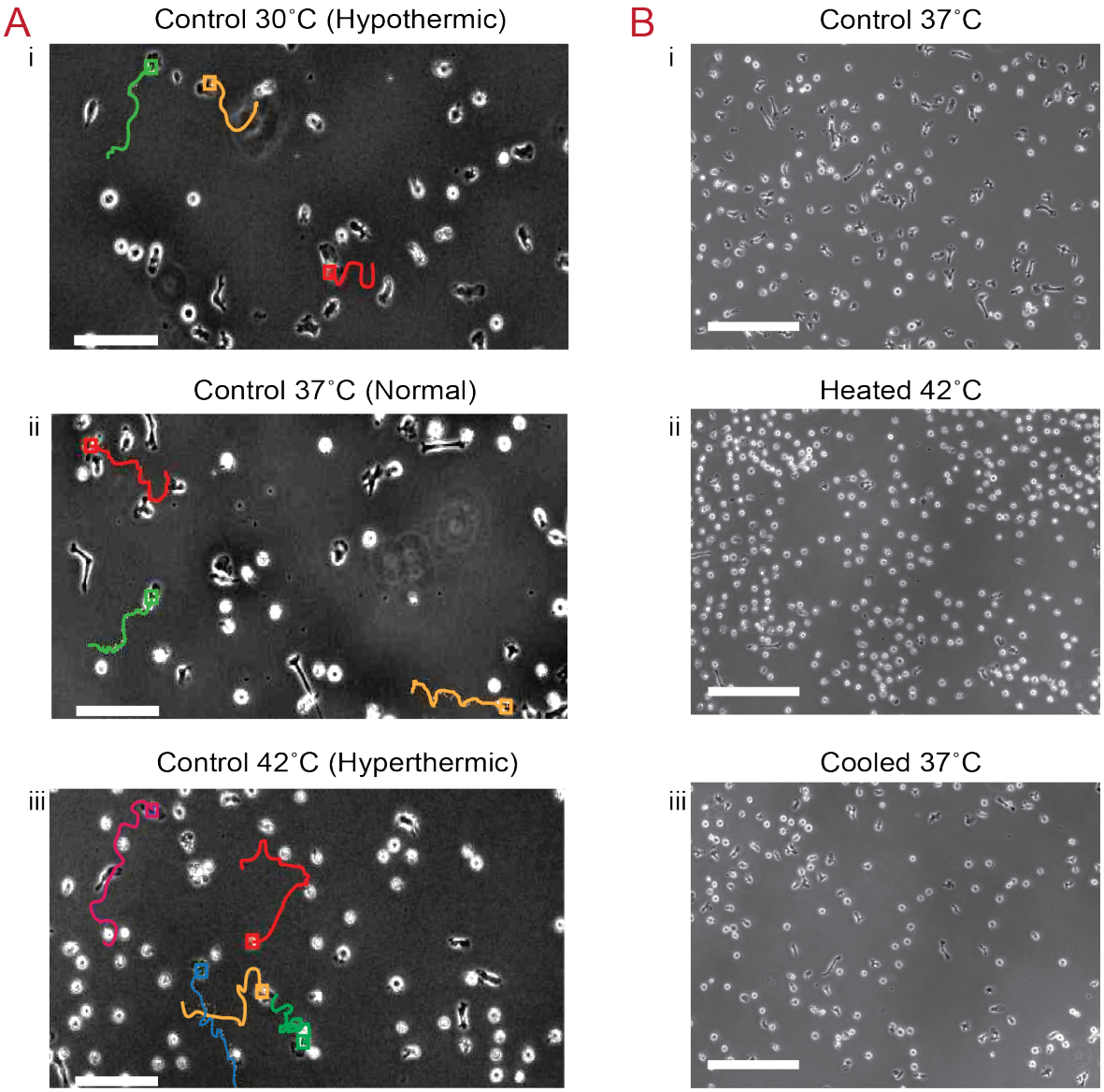

Figure 6.3: Representative phase contrast images of differentiated HL-60 cells at different heating conditions. **A.** Phase contrast images of control cell tracks at 30 °C (hypothermic), 37 °C (normal) and 42 °C (hyperthermic). A large number of cells detached under hyperthermic conditions. Scale bars: 100 µm. **B.** Phase contrast images of cells under control conditions at 37 °C, heated to 42 °C and cooled back to 37 °C. Detached cells did not appear to be dead or apoptotic, as reduction of the temperature back to 37 °C resulted in cell reattachment to the substrate. Scale bars: 200 µm.

serum concentration resulted in a 20-30 % increase in cell attachment for the entire range of temperatures analyzed. The mean speed of differentiated HL-60 cells varied between different conditions and as a function of temperature. For all three seeding conditions, the mean migration speed increased nearly linearly with increasing temperature, with each increasing degree Celsius causing a commensurate increase in cell speed of approximately 0.87 µm/min

for control surfaces, 0.65 µm/min for 5X FBS, and 0.71 µm/min for fibronectin-coated surfaces. No significant difference in mean speed was observed between cells cultured in media containing 10 % FBS or 5X FBS. Fibronectin coating significantly reduced cell speed (Fig. 6.4B).

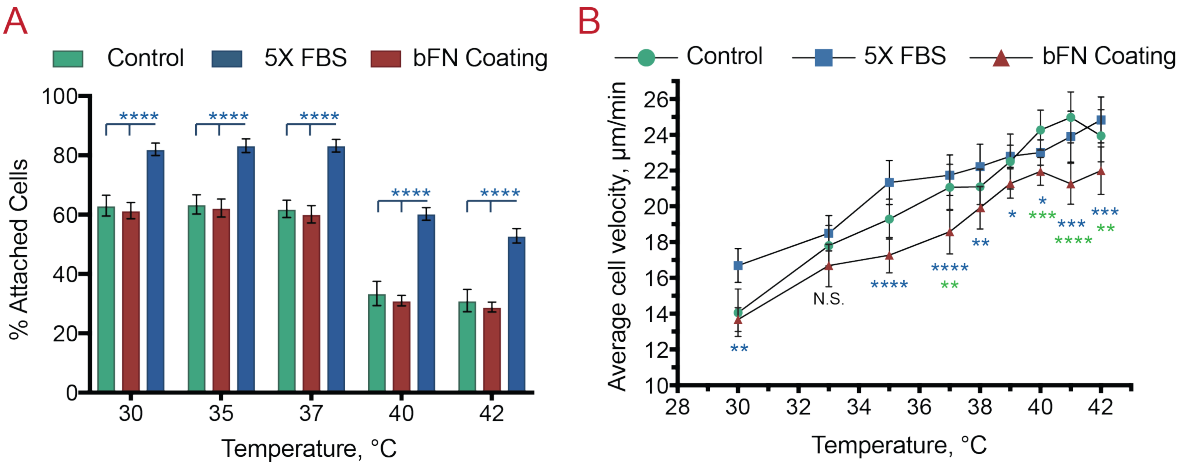

Figure 6.4: Temperature-dependent attachment and migration dynamics of differentiated HL-60 cells. **A.** Cell attachment at different seeding conditions. In control samples under hyperthermic conditions, approximately 50 % of the initially attached cells detached. 100 µg/mL bovine fibronectin (bFN) coating did not improve cell attachment compared to the control condition (no coating, 10 % FBS), whereas a 5-fold increase in FBS (5X FBS) in the media resulted in a significantly higher (20-30 %) number of attached cells throughout the entire (30-42 °C) temperature range. **B.** The average cell speed ± 95 % CIs of differentiated HL-60 cells at each experimental temperature. Cell speed increased linearly with increasing temperature for all conditions. Cells seeded in the presence of 5X FBS did not show any significant increase in average speed. 100 µg/mL bFN surface coating significantly reduced average cell speed at normal and hyperthermic temperatures. 39 and 78 cells were tracked for all conditions in hypothermic and normal/hyperthemic temperature ranges, respectively. At 39 and 40 °C on bFN coating, 117 cells were tracked. **For all:** N = 2 independent experiments were performed. $^{*}P < 0.05$, $^{**}P < 0.01$, $^{***}P < 0.001$, $^{****}P < 0.0001$, N.S. not significant. Significance was evaluated by two-way ANOVA.

6.4 Temperature-dependent effects on differentiated HL-60 cell directionality

Direction autocorrelation was calculated in differentiated HL-60 cells for 3 conditions and 9 temperatures using an algorithm published by Gorelik *et al.* [20, 67–69] (Figs. 6.5A-C). This describes the correlation in migration path orientation over increasing time intervals. Direction autocorrelation coefficients were computed by averaging the cosine of all angle differences over increasing time intervals between two migration vectors that have been normalized to the same length. These coefficients were then averaged for all cells tracked over all pairs of time points and plotted against applied time intervals. The resulting curves can be understood as follows: The steeper the decay of the plotted curves, the more frequently the cells turn in different directions.

To quantitatively approximate the persistence length of the cells, autocorrelation curves were fitted to Equation 5.1 (Materials and Methods) to yield the persistence time, which is the time period below which directional orientation remains correlated. Average persistence length was estimated by multiplying persistence time by the average speed at a given temperature. The three seeding conditions did not affect cell average persistence length significantly at any given temperature (Fig. 6.5D). While cells exhibit longer persistence lengths at hypothermic temperature regimes, persistence length remained similar throughout normal and hyperthermic regions. For all three surface coatings, cells cultured between 35 °C and 42 °C had consistent persistence lengths between 9.8 and 14.9 μm.

To determine whether an increase in temperature was altering the fibronectin layer, an experiment utilizing pre-heated fibronectin was performed. Fibronectin-coated glass was heated for 1 hour at 41 °C. After cooling, differentiated HL-60 cells were seeded onto the heat-treated fibronectin and time-lapse movies were taken at 37 °C for 1 hour. The heat treatment of the coating significantly reduced average cell speed compared to non-treated fibronectin (Fig. 6.5E). Interestingly, autocorrelation was not affected by fibronectin heat treatment, further supporting the hypothesis that intrinsic cell persistence is not affected by the ECM composition (Fig. 6.5F).

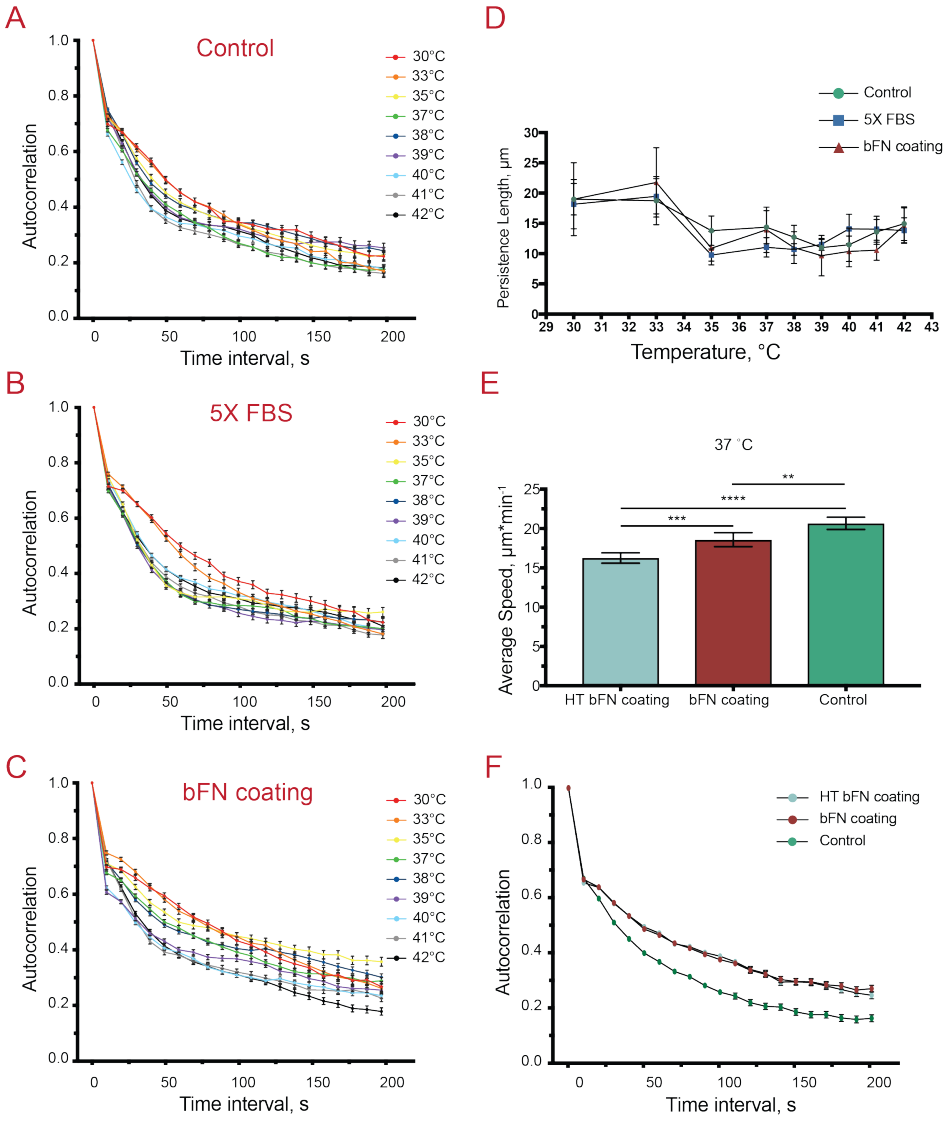

Figure 6.5: Temperature- and ECM-dependent direction correlation of differentiated HL-60 cell migration. A-C. Direction autocorrelation analysis of differentiated HL-60 cells under 3 different conditions (control, 5X FBS and bFN coating) and 9 different temperatures between 30 and 42 °C. At hypothermic temperatures, directional autocorrelation peaks for all conditions. On bFN coating, cells maintain directionality for longer time periods. Error bars represent S.E.M. **D.** Persistence length (µm) of differentiated HL-60 cells was calculated by multiplying the persistence time by average cell speed. The persistence time was evaluated by fitting equation 1 to the autocorrelation curves. At normal and hypothermic conditions, the persistence length was preserved. Error bars represent 95 % CIs. **E.** Average cell speed of differentiated HL-60 cells without coating (control), on 100 µg/ml bovine fibronectin coating (bFN coating), and on heat-treated bovine fibronectin coating (HT bFN coating). Heat treatment of the coating significantly reduced average cell speed. Error bars represent 95 % CIs. **F.** Direction autocorrelation of differentiated HL-60 cells on control, bFN and HT bFN coatings at 37 °C. Heat treatment of bovine fibronectin did not influence cell persistence. Error bars are S.E.M. **For all:** N = 2 independent experiments were performed. $^{**}P < 0.01$, $^{***}P < 0.001$, $^{****}P < 0.0001$.

6.5 Thermotaxis in differentiated HL-60 cells on 2D surfaces

The ability of the neutrophil-differentiated HL-60 cells to sense temperature gradients and thermotax in response was investigated on 2D glass surface using a microfluidic temperature gradient system (see Materials and methods, Fig. 5.1A). Computations performed using COMSOL Multiphysics showed the temperature gradient along the whole microchamber was uniform with a range from 27 °C to 43 °C (see Materials and Methods, Fig. 5.2). For 2D studies, differentiated HL-60 cells were injected into the microchamber at a concentration of 150 cells/mm^2. The temperature gradient in the 2D microchamber resulted in heat transfer by convection, which caused media flow from the heat sink to the heat source above the glass surface. Up to 60 % of cells detached in the microchamber, possibly due to elevated temperatures in regions of the chamber (Fig. 6.6A). Of the cells that remained adherent, the majority ($\sim$ 70 %) either remained in place or migrated very little from their position. These cells were considered to be non-mobile cells (Fig. 6.6A). The remaining mobile cells were classified into three subpopulations based on their final positions within equally-sized 120° polar divisions: cells migrating toward the heat source (positive thermotaxis), cells migrating toward the heat sink (negative thermotaxis), and cells moving perpendicular to the temperature gradient (Fig. 6.6A and C). Based on these divisions, 40 % of cells were found to exhibit positive thermotaxis and 50 % of cells negative thermotaxis. Interestingly, only approximately 10 % of motile cells finished in the perpendicular subpopulation, compared to an expected value of 33 % for unbiased migration (Fig. 6.6A). To quantify this tendency, the relative angles θ between each cell step greater than 2 μm were calculated and plotted as a polar histogram, revealing significant migrational bias along the temperature gradient (Fig. 6.6D). The migration speed of motile differentiated HL-60 cells was also evaluated. Independent of migration direction, the average cell speed in the presence of the temperature gradient was approximately half the average speed of cells in a constant 37 °C environment. No significant difference was found between the average speed of positively or negatively thermotaxing cells (Fig. 6.6B).

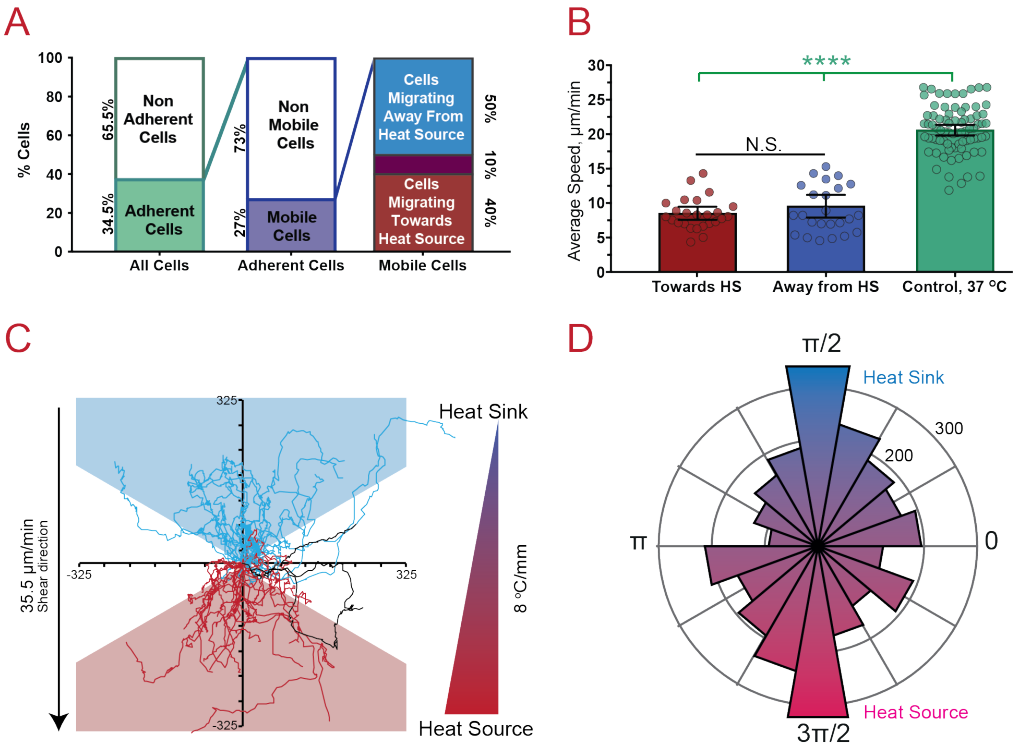

Figure 6.6: Differentiated HL-60 cell thermotaxis in response to temperature gradients in 2D microchambers. **A.** Temperature gradient effects on cell adhesion and migration in 2D. After application of the gradient, $\sim$ 40 % of cells remained attached. 72 % of the attached cells were non-mobile. Of the mobile cells, approximately 50 % migrated towards the heat sink (negative thermotaxis) and 40 % migrated towards the heat source (positive thermotaxis). **B.** Differentiated HL-60 cell speed in 2D in the presence of the temperature gradient. 25 cells in each direction were tracked. No significant differences in cell speed were found between those moving towards the heat source and those toward the heat sink, but both were approximately 50 % slower than those in a constant 37 °C environment. **C.** Migration tracks of 50 cells migrating both towards and away from the heat source. Cells that migrated at an angle of 60° or less with respect to temperature gradient direction (in this case the Y axis) were considered to have directed migration towards either the heat source or sink (red and blue triangles). 10 % of cells showed non-directed migration. **D.** Polar histogram of the relative angles from cell step to cell step calculated for 50 cells tracked under temperature gradient in 2D. Small steps less than 2 µm were disregarded. **For all:** N = 2 independent experiments were performed. Error bars represent 95 % CIs of the data. ****P $<$ 0.0001, N.S. not significant. Significance was evaluated by ordinary one-way ANOVA.

6.6 Differentiated HL-60 cell migration under shear flow

To determine whether directed migration towards the heat source was affected by the gradient-generated fluid shear stress, additional migration studies of differentiated HL-60 cells under laminar flow were performed. To approximate the flow rate created in the 2D temperature gradient chamber, the average floating speed of 60 detached cells at different positions was calculated (35.5 μm/min). Using a commercial microchamber flow cell with the same height as the temperature gradient microchannel and a syringe pump, it was established that flow rates of 30 μl/hour resulted in an average detached cell floating speed of 37 μm/min, i.e. similar to that observed in the 2D temperature gradient chamber. A higher 40 μL/hour flow rate was also applied, resulting in a higher shear flow rate that doubled the floating speed of detached cells (80.5 μm/min).

The speed with which the differentiated cells migrated under the applied flow conditions was significantly lower than the speed of the control cells at 37 °C without any external stimuli (Fig. 6.7A). Although 40 μL/hour flow resulted in slower cell migration than 30 μL/hour flow, neither flow rate was sufficient to induce directional bias (Fig. 6.7B). This suggested that cells in the 2D temperature gradient microchannel were unlikely to be affected by the gradient-induced convective flow, and thus, their directional bias was a result of the temperature gradient.

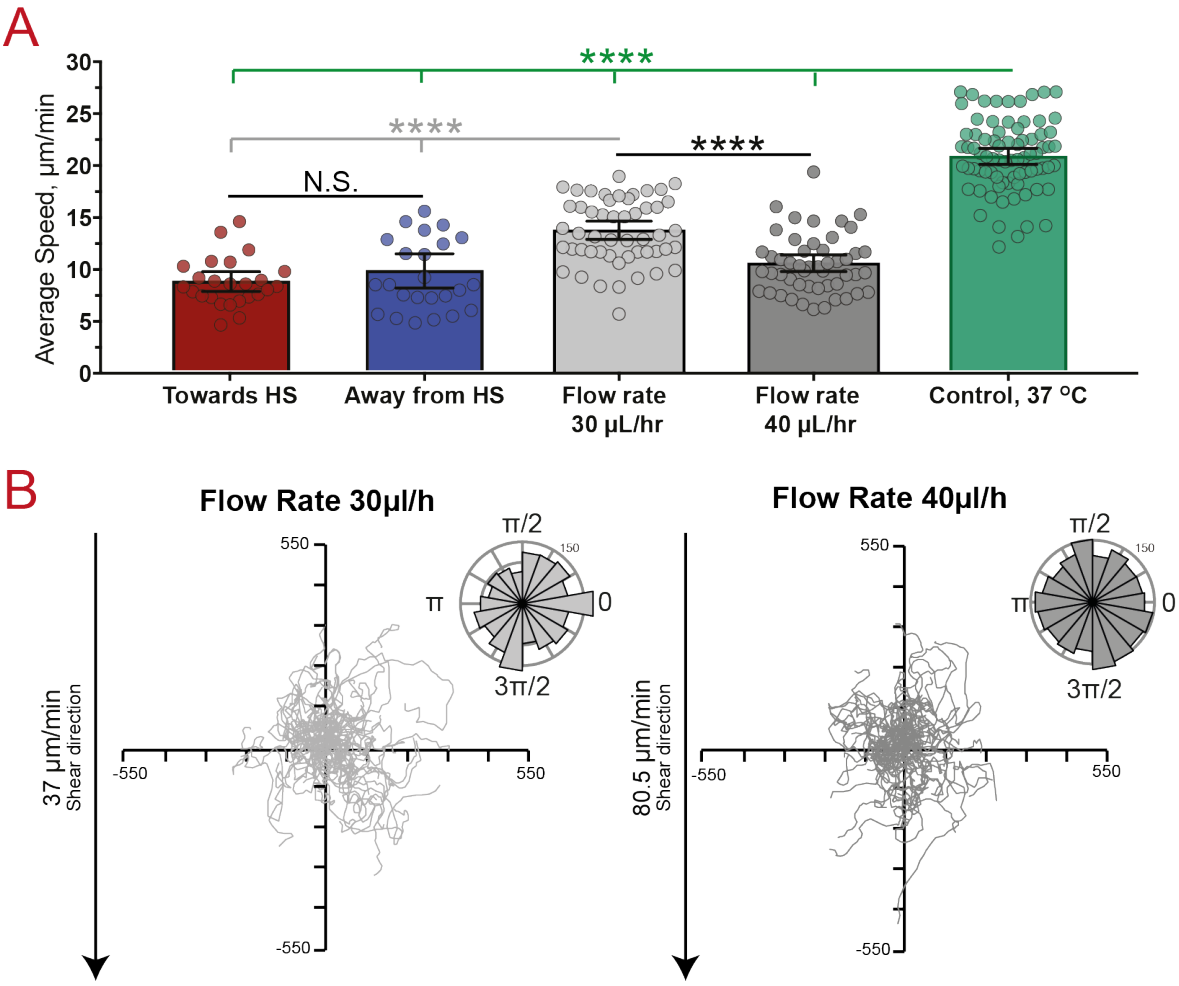

Figure 6.7: Fluid shear flow of a similar magnitude to that produced by temperature gradients does not induce directed migration. **A.** Cell speed of differentiated HL-60 cells in 2D in the presence of a temperature gradient and under laminar flow of 30 and 40 µL/hour. The average speed of 50 cells in total was evaluated for each condition. In the 2D temperature gradient chamber, 25 cells in each direction were tracked at a sampling interval of 15 seconds. No significant difference between migration speed of cells moving towards either heat source or sink was found by Welch's t-test. When compared with cell speed in a constant 37 °C environment (sampling interval 10 seconds), cell speed was reduced by approximately 50 %. Application of shear flow also resulted in significant cell speed reduction. Lower cell velocities could partially be an artifact of the lower cell tracking rate of 60 seconds, but the significant differences in cell speed under lower and higher flow rates indicate that cell migration speed has an inverse relationship to flow rate. **B.** Migration tracks and polar histograms of θ for 50 cells migrating under laminar flow conditions. Application of 30 and 40 µL/hour flow rates did not result in directional cell migration.

6.7 Thermotaxis in differentiated HL-60 cells in 3D collagen gels

Cell migration on 2D surfaces differs considerably from migration in the 3D microenvironment *in vivo*. To better mimic *in vivo* confinement, a new 3D temperature gradient chip was produced featuring a 3D cell reservoir (see Materials and Methods, Fig. 5.1B). 20 cells were tracked at both a constant 37 °C and under temperature gradient conditions equal to those produced in the 2D microchannel (8.0 °C/mm). In the absence of the gradient, cells exhibited migration without directional bias (Fig. 6.8A). When the temperature gradient was applied, 65 % of the tracked cells migrated towards the heat source. Cells in the 3D microchamber migrated much slower than cells on 2D surfaces, in agreement with the literature [28], with no significant difference found between cells at a constant temperature and those in the temperature gradient (Fig. 6.8B).

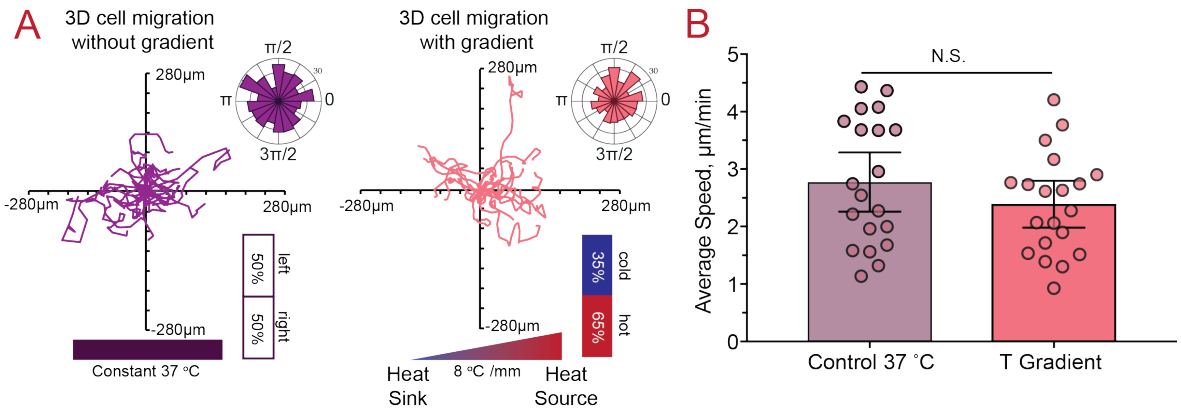

Figure 6.8: Differentiated HL-60 cell thermotaxis in response to temperature gradients in 3D microchambers. A. Migration tracks and polar histograms of θ for 20 cells each, migrating in 3D collagen matrix with and without temperature gradients. Application of the temperature gradients in 3D revealed a higher percentage of cells migrating towards the heat source. **B.** Cell speed of differentiated HL-60 cells in a 3D collagen matrix at a control temperature of 37 °C and in the presence of the temperature gradient. The average speed of 20 cells in each condition was evaluated. **For all:** Error bars represent 95 % CIs of the data. N = 2 independent experiments were performed. N.S. not significant.

Chapter 7

Discussions

Many external factors affect cell behavior. Despite 37 °C being the average core temperature of the human body, thermal variations still occur both on macro (tissue) and micro (cell) scales. As an example, inflammation is accompanied by increased heat due to the augmented blood flow in the injured or infected tissue. It is reasonable to assume that these extracellular changes in temperature can have an influence on the cells, in particular the immune cells recruited to the inflammation sites. However, very little studies have been done to understand temperature effects on cell behavior in general and cell migration in particular.

One of the most notable studies of temperature effects on immune cells, done by Malawista *et al.*, showed an interesting ability of neutrophils to form autonomous motile fragments (CKPs) through detachment of cell protopods from the cell body under short-termed heat treatment of approximately 45 °C [20, 21, 67, 68]. In another study, Díaz *et al.* [182] showed that fever-range hyperthermia combined with low pH in the environment, which is often present in inflamed and cancerous tissues, significantly increased neutrophil survival. In the present study, the role of physiologically relevant temperatures (30-42 °C) on immune cell adhesion, migration speed, and directionality was systematically analyzed using neutrophil differentiated HL-60 cells as a model cell line.

7.1 CKP formation was not possible in neutrophil differentiated HL-60 cells due to the reduced cell adherence at elevated temperatures

Results presented in Section 6.2 showed that human neutrophils isolated form venous blood formed autonomous motile cytokineplats when heated to approximately 47 °C (Fig. 6.2A). In contrast, CKP formation was not observed with neutrophil differentiated HL-60 cells. According to Malawista *et al.*, neutrophil attachment and motility play a key role in fragment formation. Their experiments with non-adherent blood neutrophils and less motile leukocyte cells, such as monocytes, did not lead to motile fragment production [21]. As average cell velocities of differentiated HL-60 cells are comparable to that of blood neutrophils (see Appendix, Fig. A.1), the inability of these cells to form CKPs at elevated temperatures is likely due to the cell detachment observed already at 40 °C (see Results Chapter 6, Figs. 6.3B and 6.4A).

Two different seeding conditions were used to improve cell adherence: bovine fibronectin coating (bFN) and media containing elevated serum concentration (5X FBS). To recapitulate, fibronectin coating did not improve cell adherence, whereas increased levels of FBS led to significantly higher numbers of adhering cells at all the applied temperatures (see Results Chapter 6, Fig. 6.4A). This could be due to high levels of surface-adsorbable ECM proteins commonly found in serum [183], which provide an increased number of binding ligands at the cell-surface interface. As the elevated levels of serum were maintained throughout the experiment, it is also possible that the resulting increase in soluble protein concentration in the media also encouraged attachment and cell migration. Regardless of the seeding condition, the highest temperature at which any adherent and migrating cells were observed was 44 °C, a temperature, which was insufficient to produce autonomous motile fragments in differentiated HL-60 cells.

7.2 Temperature-dependent increase in cell speed and reduction in cell persistence time lead to equal persistence length in migrating neutrophil-differentiated HL-60 cells

Temperature-dependent differentiated HL-60 cell motility was studied by stepwise increasing the temperatures from 30 to 42 °C (see Materials and Methods, Section 5.2.3.1). In the Results Chapter 6 (Section 6.4) it was shown that with increasing temperature cell average velocity

rose nearly linearly independently of seeding conditions. The results may be explained by acceleration of actin polymerization corresponding to increases in temperature, as described by Rosin *et al.* [47]. Additionally, it has been shown that overall F-actin concentration in PMNs increases in response to external signals. Howard *et al.* [47] showed that both chemoattractant signaling and the application of elevated temperature are sufficient to cause an increase in F-actin concentration in human blood neutrophils. They showed that between temperatures of 30 °C and 40 °C, F-actin concentration increases linearly, resulting in doubling by 40 °C. Assuming that these temperature-driven changes in actin occur similarly in HL-60 cells, these previous findings support the above-mentioned hypothesis that linear increases in the average speed of the neutrophil-like cells could be a result of higher F-actin polymerization rates and subsequent increases in absolute F-actin levels as a result of increasing temperature.

Independent of the temperatures applied, fibronectin coating significantly reduced cell speed compared to cells migrating under control and 5X FBS conditions. This decrease might be due to the stronger adhesion promoted by fibronectin, resulting in an altered cell migration speed, as observed by other studies [34, 184]. As fibronectin is known to unfold and expose additional binding ligands [185], it is possible that the heat treatment encourages irreversible unfolding or altered refolding. Such changes may lead to the significant reduction of cell speed on heat-treated fibronectin coatings (see Results Chapter 6, Fig. 6.5E).

As part of the motility studies, temperature dependent cell persistence was also evaluated using direction autocorrelation analysis (see Results Chapter 6, Fig. 6.5). To obtain the average persistence time, autocorrelation curves were fitted with a one phase exponential decay model $c + ae^{-t/\tau}$, where τ is the persistence time. Using non-zero values for constant term "c" significantly improved the quality of the fit. The nonzero value of the constant could imply a correlation between cell directionalities at large time offsets. As these experiments were performed by homogeneously increasing the temperatures throughout the samples, i.e. in absence of external directional signal, the non-zero values could imply an inherent cell directionality at migration on large time scales. There are several examples of cells exhibiting correlated migration even in the absence of external directional signals. Li *et al.* [28] showed that *Dictyostelium discoideum*, an amoeba exhibiting fast motility and chemotactic behavior similar to neutrophils, are capable of directed motion by "remembering" their last turn, even in the absence of an external signal. This improves their search efficiency relative to random walk and allows them to search more territory. Of course, the autocorrelation data could have been fitted well by a double exponential model, meaning that the autocorrelation curves reflect at least two processes. However, it would be difficult to elucidate what these processes represent during cell migration and give the appropriate weight to each of them.

As described in the Results Section 6.4, the estimated persistence time for all conditions showed a decrease with increasing temperature. This decrease meant that at higher temperatures, despite higher migration velocities, the cells made more frequent turns. The relationship between cell persistence time and cell speed has been examined in a number of cell models [186, 187]. In general, as cell speed increases, cell persistence increases concomitantly, up to a plateau value [186]. Here, when increases in speed are a function of increases in temperature, the opposite effect was observed, as persistence time decreased with increasing temperature (see Appendix, Fig. A.2).

The drop in the persistence time could be due to the temperature-dependent changes in membrane fluidity. Houk *et al.* have shown that membrane tension plays a pivotal role during directed neutrophil migration by restricting the signaling molecules to the leading edge of the cells [64]. Accordingly, decreases in membrane tension cause a loss of polarity. An increase in temperature results in higher membrane fluidity, which in turn reduces membrane tension and can cause cells to stop and turn more frequently, resulting in a decrease in cell persistence time. In contrast, as previously mentioned, increases in temperature also increase the rate of F-actin polymerization and the total amount of F-actin in the cell, which leads in higher cell migration velocities. Based on the results presented in Figure 6.5D (see Results Chapter 6), it can be speculated that these two factors combine to balance each other out, causing cells to have an approximately constant persistence length at temperatures higher than 33 °C. Furthermore, even in conditions that cause a significant reduction in cell speed, like fibronectin coating (see Results Chapter 6, Figs. 6.4B and 6.5F), persistence length remains constant. These results could indicate, that adherent immune cells have an innate persistence, unaffected by ECM composition or temperature, allowing them to navigate microenvironments with diverse protein compositions and thermal conditions. It can be theorized that the preservation of persistence length confers an advantage to immune cells migrating at higher temperatures, as they are able to cover more ground in search of their target independent of extracellular matrix composition. The effect of elevated temperatures on membrane fluidity may also be favorable to immune cells, as it allows for faster adaptation of migration direction in response to obstacles.

7.3 Differentiated HL-60 cells exhibited "positive" and "negative" thermotaxis in 2D

The ability of HL-60 neutrophils to sense and react to temperature gradients was examined both on 2D glass surfaces and in 3D collagen gels. Despite the high number of detaching cells in 2D, the remaining motile cells could be divided into two subpopulations exhibiting "positive" (migration towards heat source) and "negative" thermotaxis (migration towards heat sink) (see Results Chapter 6, Fig. 6.6). While primary neutrophils have been shown to exhibit positive thermotaxis [188], negative thermotaxis has not been observed. Based on the previous observations, a significant number of the differentiated HL-60 cells detach in response to increasing temperatures (Results Chapter 6, Fig. 6.3 and 6.4A). Hence, the "negative" thermotaxis of the second cell population could be attributed to cell migration from a weakly adherent surface to strongly adherent surface in a manner similar to haptotaxis. The cells embedded in 3D collagen also showed a small, but not significant, tendency of differentiated HL-60 cells to migrate along the temperature gradient as 65 % of the tracked cells migrated in the direction of heat source. These findings, especially on 2D surfaces, show that neutrophil differentiated HL-60 cells can be a valuable tool for investigating immune cell thermotaxis, a complex process that is not yet well understood.

Part IV

In vitro studies of Protein Kinase D isoform dependent pancereatic cancer cell invasion related motility

Chapter 8

Results

In the study described in this chapter, Crispr/Cas9 PKD1, PKD2, PKD3 Panc1 and control Panc1 cell lines were used to investigate PKD isoform-mediated pancreatic cancer cell migration and invasion.

8.1 PKD-isoform dependent Panc1 cell attachment, proliferation and morphology

PKD isoforms have been reported to modulate cancer cell proliferation and morphology [170], [161]. To assess cell attachment efficiency and proliferation rate of CRISPR/Cas9 PKD1, PKD2 and PKD3 Panc1 knockout cells, the cells were seeded into petri dishes and the cell number was then monitored over 72 hours (Fig. 8.1). The data suggests that PKD1 KO cells had significantly lower attachment efficiency (see Materials and Methods, Equation 5.2) compared to the wild type, the PKD2 KO and PKD3 KO cell lines. The proliferation rate, estimated as the change in cell number over 48 hours (see Materials and Methods, Equation 5.3), was also reduced, although not significantly. On the contrary, PKD2 KO cells exhibited significantly better attachment efficiency and proliferation rates approximately 1.8 times higher than the control cells. No changes in attachment and proliferation were observed for PKD3 isoform knockout in comparison with the control.

PKD isoform dependent changes in cell morphology were observed as well (Fig. 8.2). Qualitatively, based on their shape, the cells could be classified into 3 categories: epithelial-like, mesenchymal-like and mixed (Fig. 8.2A). Maupin *et al.* described similar cell classification for different pancreatic cancer cell lines [171]. Based on this division, Panc1 wild type and PKD3 KO cells were in the mixed category, as both epithelial (rounded cells with cell-cell contacts) and mesenchymal (elongated cells with little cell adhesions) phenotypes were present.

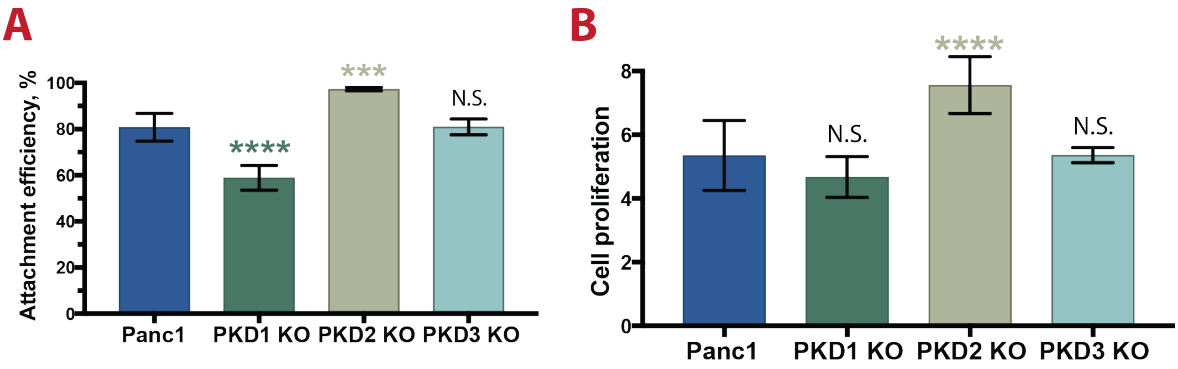

Figure 8.1: Attachment efficiency (A) and cell proliferation (B) over 48 hours of PKD1 KO, PKD2 KO, and PKD3 KO cells. Loss of PKD1 isoform led to significantly lower attachment efficiency as well as reduced proliferation rates of the Panc1 cells. On the contrary PKD2 knockout cells exhibited increase in cell propagation. No changes in either cell attachment efficiency (Equation 5.2) or cell proliferation (Equation 5.3) were observed for PKD3 KO cells. **For all:** Error bars represent 95 % Confidence Interval. N = 3 independent experiments; $^{***}P < 0.001$, $^{****}P < 0.0001$, N.S. not significant. Significance was evaluated by ordinary one-way ANOVA.

PKD1 KO exhibited clear mesenchymal-like spindle-shaped morphology. Concurring with this observation, quantitative analysis of cell morphologies also showed significant increase in PKD1 KO cell aspect ratio (Fig. 8.2C). Interestingly, PKD2 KO cells exhibited the opposite behavior and would grow in clusters creating epithelial-like sheets (Fig. 8.2A). Knockout of either isoform did not influence cell area (Fig. 8.2B).

E-cadherin, a crucial transmembrane glycoprotein involved in cell-cell adhesions, is one of the main epithelial cell markers. Indeed, during epithelial-to-mesenchymal transition (EMT) many cells exhibit E-cadherin downregulation. Panc1 cancer cell line has been shown to have low E-cadherin expression [171]. E-cadherin re-expression and/or upregulation has been also linked to the reverse process of mesenchymal-to-epithelial transition (MET) [189], [190]. Immunofluorescent staining of this glycoprotein in the Panc1 control, PKD1 KO and PKD3 KO cells showed only E-cadherin cytoplasmic localization (Fig. 8.3). PKD2 KO cells exhibited distinct patterns of membranous E-cadherin expression at the intercellular borders. This indicates that the PKD2 isoform is a positive regulator of EMT transition in Panc1 cells and loss of it drives the reverse change from mesenchymal to epithelial phenotype.

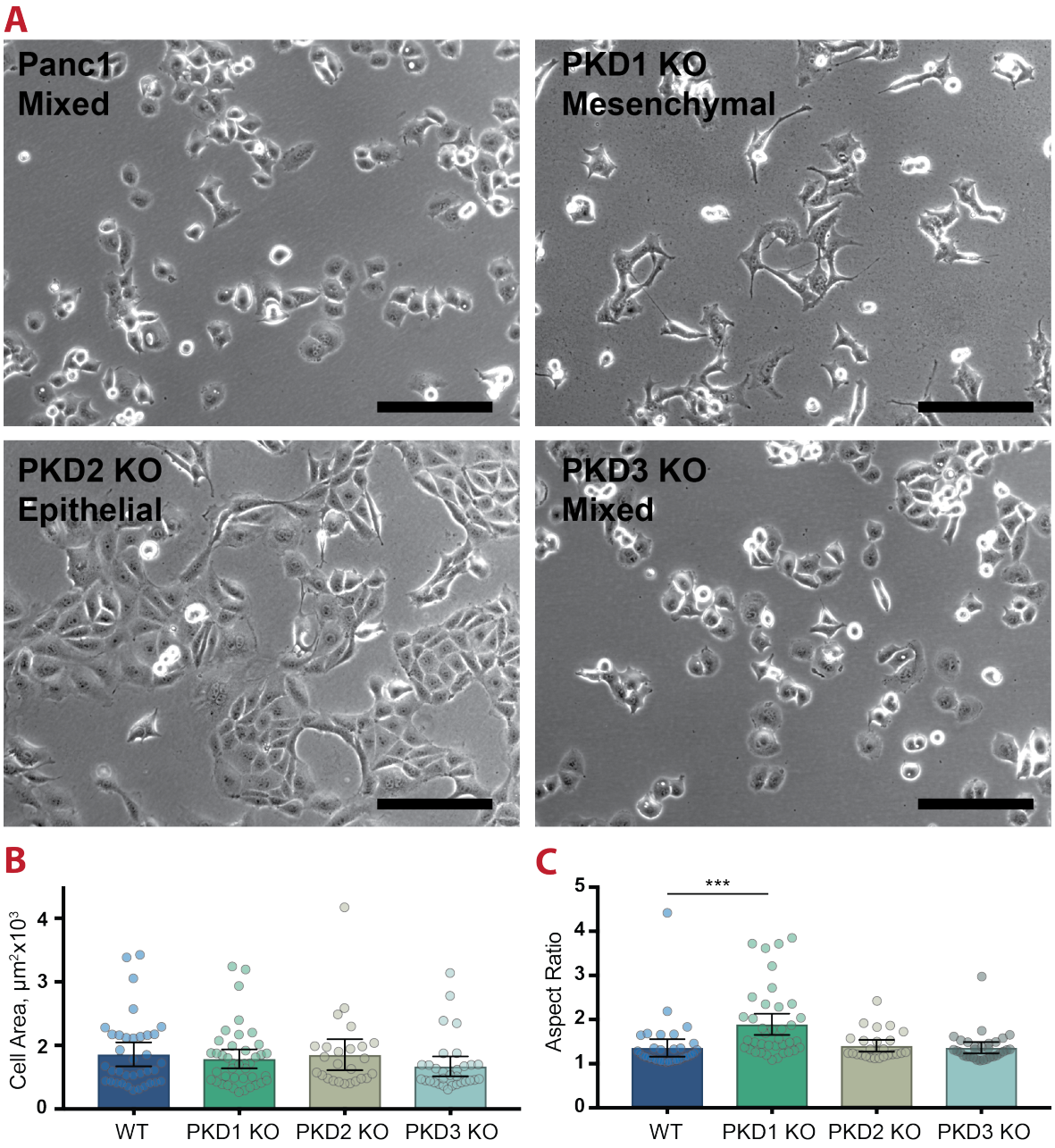

Figure 8.2: PKD enzymes regulate cell morphology in an isoform specific way. A. Representative phase contrast images of Panc1 control, PKD1 KO, PKD2 KO and PKD3 KO cells in 2D culture. Based on morphological presentation the cells were divided into 3 categories: mesenchymal (PKD1 KO cells), epithelial (PKD2 KO cells) and mixed (Panc1 control and PKD3 KO cells). PKD1 knockout cells exhibited defined spindle-like morphology, whereas in absence of PKD2 the cells grew in epithelial like clusters. Scale bars: 200 µm. **B.** Cell area was evaluated after 24 hour cell culture on glass slides as described in Materials and Methods (Section 5.2.5.1). The cell area was not influenced in absence of either isoform (N = 2). **C.** Significant increase ($^{***}P < 0.001$) in PKD1 KO aspect ratio further proved PKD isoform involvement in cell morphology regulation. **For all:** Error bars represent 95 % Confidence Interval. N = 2 independent experiments; $N^* = 30$ total cells analyzed; significance was evaluated by ordinary one-way ANOVA.

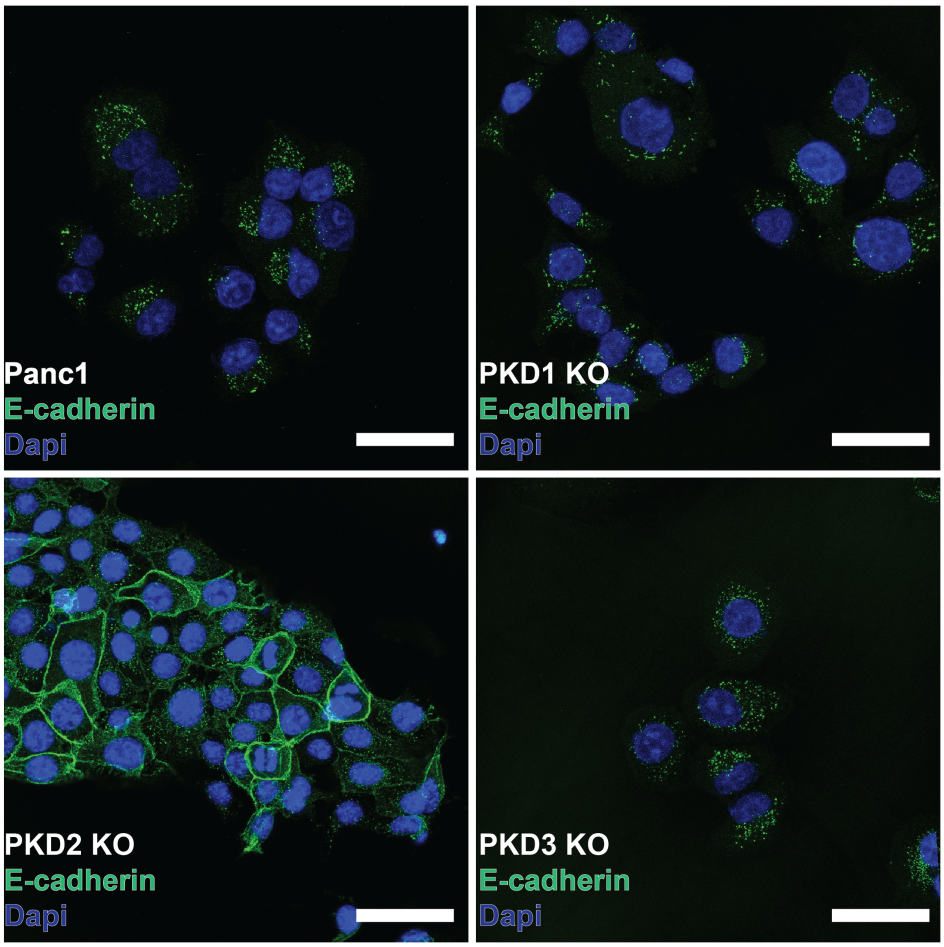

Figure 8.3: Representative immunofluorescent confocal images of E-cadherin (green) and nuclei (blue) in fixed Panc1 cells with PKD1, PKD2 and PKD3 knockouts. Brightness and contrast of the images were adjusted for each cell line. Strong membranous E-cadherin expression could be observed at the intercellular borders in PKD2 knockout cells further attesting to the adaptation of the epithelial phenotype. Panc1 control, PKD1 and PKD3 knockout cells exhibited primarily cytoplasmic E-cadherin expression indicative of mesenchymal phenotype. **For all:** Scale bars: 20 µm

8.2 PKD isoform dependent cell motility in 2D

A major factor defining the highly malignant and invasive cancer cell lines is the enhanced motility they exhibit both *in vitro* and *in vivo*. In order to assess changes in cell migration speed and persistence with regards to the absence of one of the PKD isoforms in 2D, the cells were seeded on glass-bottomed petri dishes. After overnight incubation at 37 °C, the cells were imaged at a 10–minute interval for 24 hours. The cells were then tracked manually and the average cell velocity was calculated (Fig. 8.4). The cell average speed of the Panc1 cells did not change in response to PKD1 knockout (Fig. 8.4A).

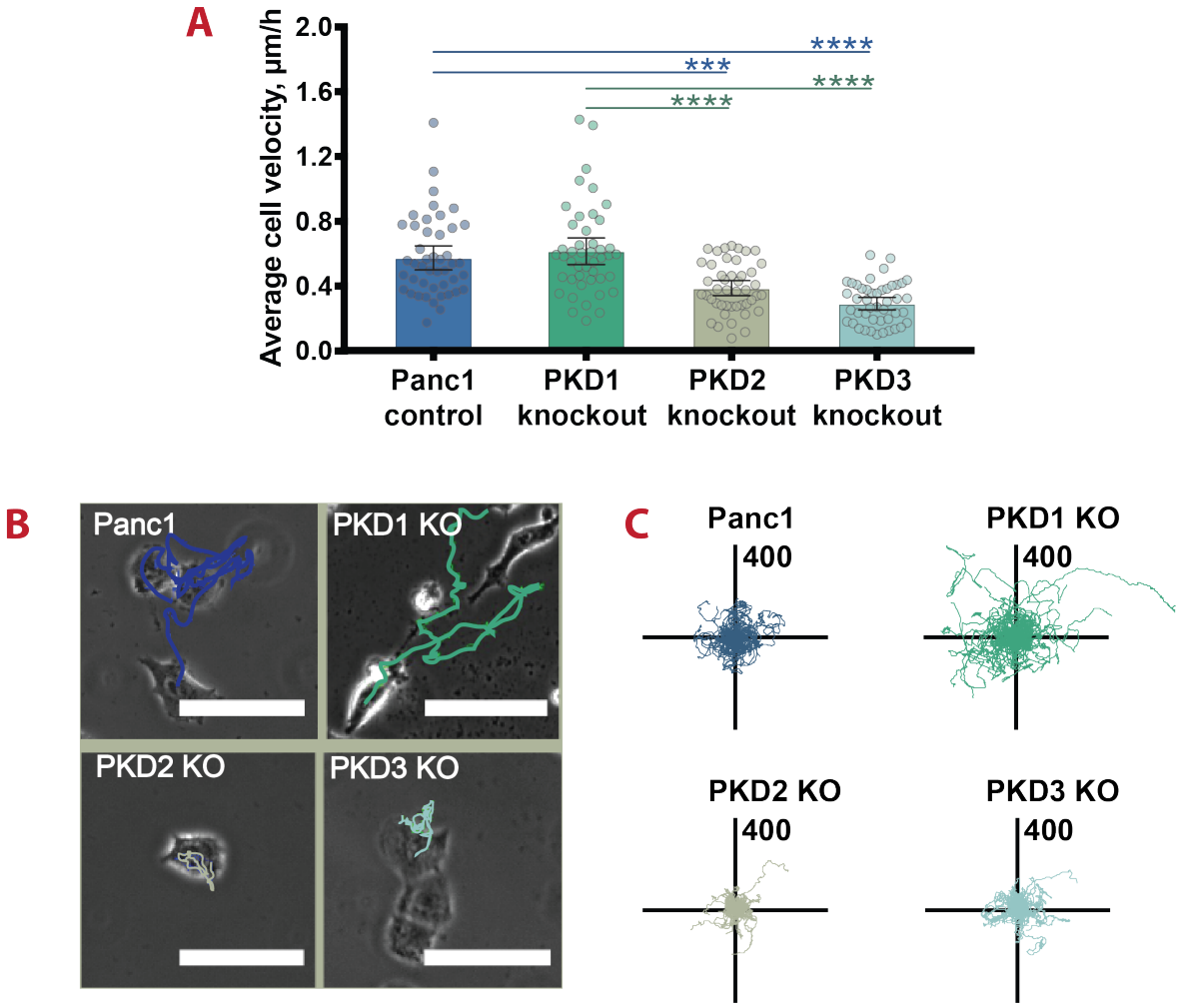

Figure 8.4: 2D Panc1 cell migration speed is dependent on the presence of PKD2 and 3 isoforms. **A.** Average cell velocity was evaluated by tracking the cells over a 24-hour period. PKD1 knockout in Panc1 cells did not affect the average cell velocity. In contrast, deletion of PKD2 and PKD3 isoforms significantly ($^{***}P < 0.001, ^{****} P < 0.0001$) reduced cell speed. **B.** Representative tracks of migrating Panc1 control and PKD1, PKD2 and PKD3 knockout cells. PKD2 KO and PKD KO cells retained their rounded shape and would migrate only small distances from their original tracking position. **C.** Rose plots of cell migration tracks. Although PKD1 KO did not affect cell speed, Panc1 cell persistence improved with the knockout of that isoform. **For all:** Error bars represent 95 % Confidence Interval. N = 3 independent experiments; $N^* = 45 - 55$ total cells analyzed; significance was evaluated using ordinary one-way ANOVA.

In contrast, absence of PKD2 and PKD3 significantly hindered Panc1 cell migration. In both cell lines the average speed drastically slowed down (approximately 1.5 - 2-fold decrease) and the cells, retaining their rounded shape, would migrate only small distances from the original position of tracking (Fig. 8.4B). Very small number of single cells exhibited migratory behavior in the PKD2 KO cell line. As described in the previous chapter, these cells would proliferate and grow in epithelial-like sheets, preferring collective migration at high cell densities. An important parameter describing cell motility is the persistence. As described

in the Introduction (Section 1.2), cells have innate persistence regardless of extracellular signaling.

From the rose plots of cell tracks (Fig. 8.4C), it is clearly visible that, despite no significant changes in cell average velocity, PKD1 KO cells could cover larger area, which is a sign of higher persistence in these cells. To quantify this observation, mean square displacement (MSD) analysis was performed on the cell tracks (see Materials and Methods, Section 5.2.5.1).

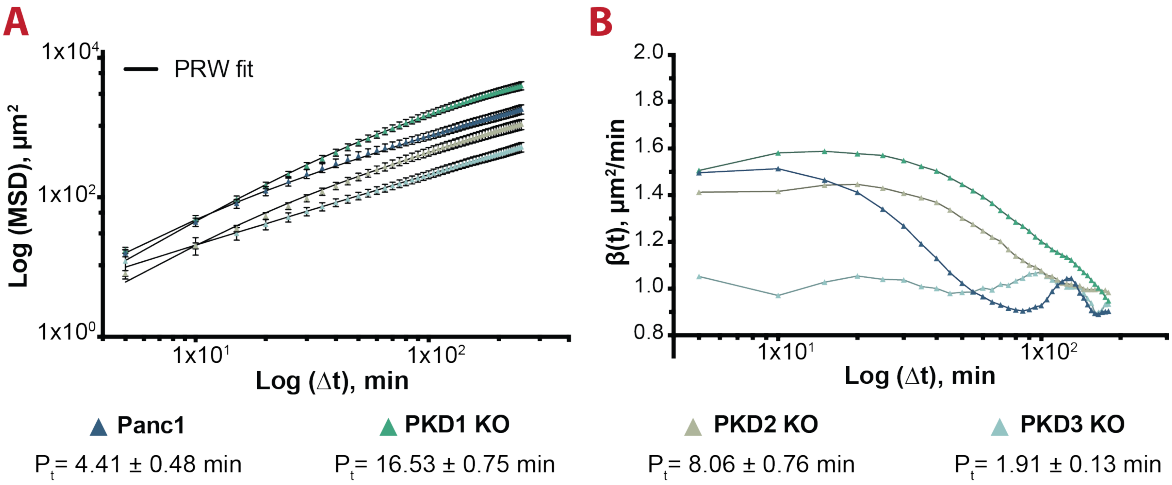

Figure 8.5: Mean square displacement (MSD) analysis of cell migration dynamics in 2D revealed strong PKD isoform dependence of the cell persistency. A. Double logarithmic plot of the average MSD of cell trajectories over a 4-hour migration period fitted with persistent randpm walk (PRW) model (black line). Average persistence time (P_t) of PKD1 KO cells, acquired from PRW fit, was 4 times higher than of control Panc1 cells. The higher persistence resulted in increased MSD values over extended time periods. PKD2 knockout cells had an approximately 2-fold increase in P_t, but due to the reduced cell speed, they exhibited lower MSD values. PKD3 KO cells were the least persistent P_t approximately 2 times lower than the control cells). Error bars represent S.E.M. **B.** Log-log MSD slopes showing time-dependent changes in cell persistency. Knockout of both PKD1 and PKD2 isoforms resulted in extended transition periods from semi-persistent ($\beta(t) \sim 1.5$) to random migration modes ($\beta(t) \sim 1.0$). **For all:** N = 3 independent experiments; $N^* = 45 - 55$ total cells analyzed.

Figure 8.5A depicts double logarithmic plot of the average MSD of the cells over a 4-hour observation period. To obtain the persistence time, the average time period during which cells migrate in a correlated fashion, MSD curves were fitted with a persistent random walk (PRW) model (see Materials and Methods, Equation 5.4). PKD1 KO cells showed 4-fold increase in average persistence time (16.53 ± 0.75 min) compared to the control cells (4.41 ± 0.48 min), confirming the previous observation that absence of *PRKD1* gene (the gene that produces the PKD1 enzyme), leads to more directed migration of pancreatic cancer cells and overall to a bigger area explored. Interestingly, knockout of the PRKD2 gene also led to higher persistence time (9.06 ± 0.76 min). Nevertheless, due to reduced cell speed, the overall MSD of PKD2 KO was lower than that of the Panc1 cells (Fig. 8.5A). In contrast, PKD3 KO

cells exhibited 2-fold drop of persistence time. The latter, combined with low cell speed, lead to the least lowest MSD values.

Mean square displacement has a time interval dependence that follows a power law MSD $\propto t^{\beta}$, with $0 < \beta < 2$. The linear dependence is associated with Brownian motion, i.e. random migration. Deviation from the linear behavior denotes subdiffusive, constraint ($0 \leq \beta \leq 1$) or superdiffusive ($1 \leq \beta \leq 2$) migration modes. In the absence of an extracellular guiding signal, cells migrate in a correlated manner in shorter time intervals and at longer observation periods they loose the persistency ($\beta \sim 1$). To illustrate time dependent changes in the directional persistence, the logarithmic derivative of MSD ($\beta(t)$) (see Materials and Methods, Equation 5.5) was plotted as a function of time interval (Fig. 8.5B). As it can be seen, PKD1 KO and PKD2 KO cells had longer transition periods from semi-persistent ($\beta(t) \sim 1.5$) to fully random ($\beta(t) \sim 1.0$) migration mode. PKD3 KO cells exhibited only random motion with $\beta(t)$ fluctuating around 1.0.

8.3 Changes in F-actin arrangement and focal adhesion morphology in response to PKD isoform specific protein deletion in Panc1 cell line

Taking into consideration the dependence of cell morphology and motility on cytoskeletal organization, filamentous actin (F-actin) and the focal adhesion (FA) protein Vinculin were immunofluorescently stained to reveal any possible changes in response to PKD isoform deletion. Figure 8.6 contains representative confocal images of F-actin (red) and Vinculin (green). In Panc1 control cells, F-actin stress fiber bundles were disorderly arranged throughout the cell body, with elongated focal adhesions anchoring the cells to the substrate. FAs could be observed both in the cell interior and its periphery. PKD1 KO cells had similar F-actin organization, but FAs were smaller and formed primarily at the cell periphery. PKD2 KO cells exhibited drastic changes both in F-actin and FA organization and localization. Actin bundles were absent in the cell center but formed very organized stress fibers at the cell periphery, with very large focal adhesions present at the cell membrane protrusions. The distinct features of PKD3 KO cell cytoskeleton were mesh like F-actin organization with little to no stress fibers, and small, rounded FAs dispersed throughout the cell body.

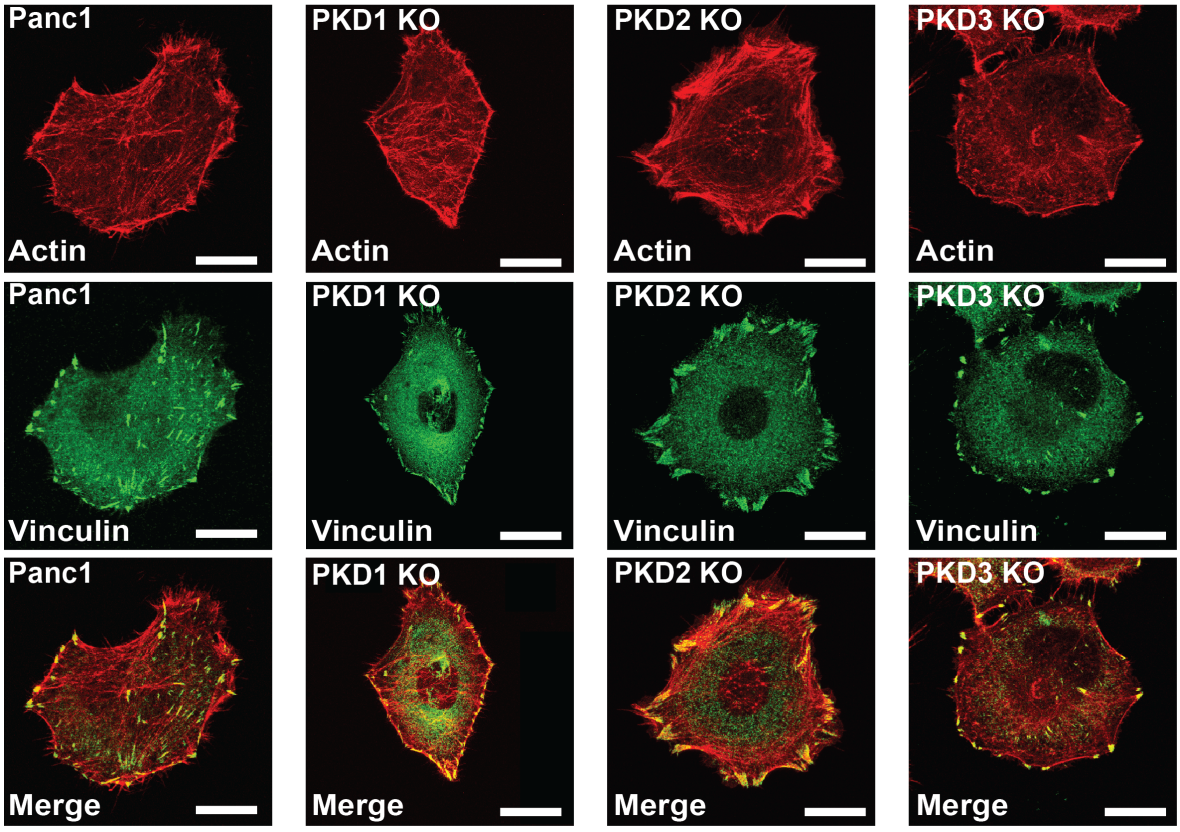

Figure 8.6: Representative immunofluorescent images of F-actin (red) and Vinculin (green) in fixed Panc1 cells with PKD1, PKD2 and PKD3 knockouts. The images were taken with a confocal microscope; the brightness and contrast of the images were adjusted for each cell line. Changes in F-actin organization and focal adhesion size and distribution were observed in all three knockout cells. PKD1 knockout led to no FA formation in the cell exterior and smaller focal adhesion areas at cell periphery. PKD2 knockout cells had no F-actin fibers in cell interior, but exhibited high density and highly oriented F-actin stress fibers, as well as very large focal adhesions at the cell periphery. PKD3 knockout cells had mesh-like F-actin organization with little to none stress fibers and formation of small, rounded FAs throughout the cell body. **For all:** Scale bars: 20 µm.

8.4 PKD-isoform dependent Panc1 cell contact guidance on microgrooved substrates

One phenomenon observed in invasive cancer types *in vivo* is the high cross-linking of tumor-surrounding extracellular matrix with increased directional orientation of ECM fibrils. The changes in ECM alignment create topographical signaling cues for directed cancer cell invasion into the stroma. *In vitro* studies of cell contact guidance, which is the ability of the cells to orient towards geometrical patterns and migrate along them in a directed manner, were carried out using micro- and nano- structured surfaces developed previously in our group [36].

Cells were seeded on fibronectin functionalized PDMS substrates with defined 200 and 350 nm deep, 2 and 10 µm wide grooves. After overnight incubation, the cells were imaged for 20 hours using phase contrast microscopy. Cell morphology, orientation and motility were then evaluated as described in Materials and Methods (Section 5.2.5.2).

All cell lines exhibited some degree of contact guidance, but the most significant changes were observed in PKD1 knockout cells (Fig. 8.7). When looking at cell morphology, these cells exhibited extreme cell body elongation, which was quantified as a change in cell aspect ratio (Fig. 8.7B). Both on 200 and 350 nm deep grooves, PKD1 KO cells had approximately 1.5- to 2-fold increase in the average aspect ratio compared to the same cell line on a flat PDMS surface. Correlated with cell elongation, cell-spreading area was also affected and was significantly reduced on these substrates. The biggest changes were observed on 2 µm wide grooves. On average, Panc1 control cells exhibited higher AR values – yet only on the 350 nm deep and 2 µm wide grooved structures, which is the geometry that provides the strongest guiding cues. PKD2 and PKD3 knockout cells seeded on the structured substrates did not exhibit any morphological changes.

Cell alignment along the grooves was estimated using the apolar orientation parameter S (see Materials and Methods, Equation 5.7). S is a dimensionless parameter, with $-1 < \mathrm{S} < 1$. The closer S is to 1, the better the cell is aligned along the grooves, whereas S = 0 and S = -1 are random and perpendicular alignments respectively. As it can be seen from Figure 8.8, S was highly dependent on structural characteristics of the substrates, as well as on the absence of specific PKD-isoforms. All the cell lines exhibited some degree of alignment $(\mathrm{S} > 0)$, but the architecture of the substrates had the most prominent effect on PKD1 KO cells. The general tendency for all the cells was that the finer the spacing and the deeper the grooves were the more prominent the cell contact guidance was. Regardless of groove dimensions PKD1 KO cells had the highest Order Parameter values compared with the rest of the cells. On 2 µm wide grooves SPKD KO reached the significantly high values of 0.8 (D: 200 nm) and 0.93 (D: 350 nm). Despite the fact that no changes in cell morphology were induced by structured surfaces, PKD2 and PKD3 knockout cells exhibited higher groove-sensitive cell alignment compared to the control Panc1 cells. Already on 200 nm deep and 2 µm wide grooves, these cells exhibited an improved contact guidance with order parameter values twice as high as the ones measured for the control cells. Panc1 wild type cell orientation was affected only on the more structurally defined surfaces (D: 350 nm, W: 2 µm).

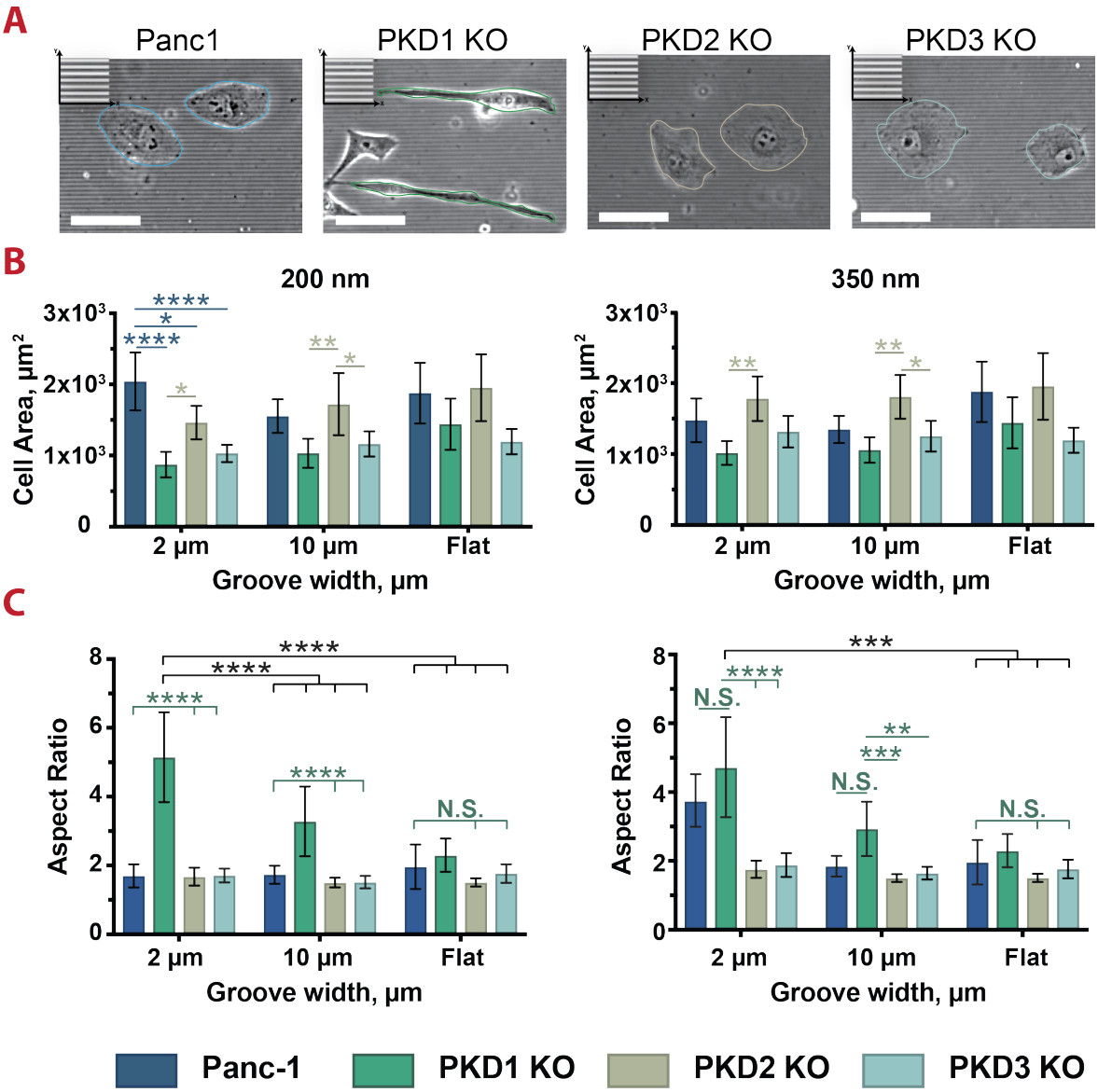

Figure 8.7: Only PKD1 knockout had effect on Panc1 cell morphology plated on microgrooved substrates. **A.** Panel of representative phase contrast images of Panc1 control, PKD1 KO, PKD2 KO and PKD3 KO cells on 350 nm deep and 2 µm PDMS substrates with wide grooves. Noticeably PKD1 KO cells exhibited extreme cell body elongation. Scale bars: 50 µm. **B** and **C.** Cell area and aspect ratio (AR) ratio were significantly affected in PKD1 KO cells independent of groove dimensions. The extreme cell body elongation along the grooves led to cell area reduction. Microgrooved surfaces did not induce any morphological changes in the control, PKD2 KO and PKD3 KO cells. **For all:** Error bars represent 95 % Confidence Interval. N = 2 independent experiments; $N^* = 30 - 50$ total cells analyzed; $^*P < 0.05$, $^{**}P < 0.01$, $^{***}P < 0.001$, $^{****}P < 0.0001$, N.S. not significant. Significance was evaluated by ordinary two-way ANOVA.

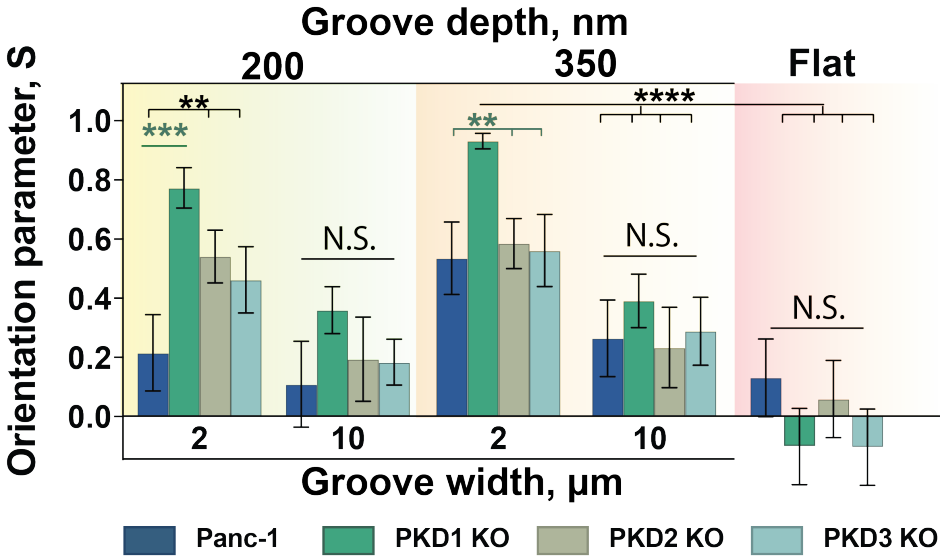

Figure 8.8: PKD isoform-specific knockouts in Panc1 cells induce enhanced cell alignment on structured substrates. Orientation Parameter S, which ranges between $-1(\text{perpendicular}) < 0(\text{random}) < 1(\text{parallel})$, was used to quantify cell alignment as a function of groove depth and width. All the cells plated on microgrooved PDMS substrates exhibited some degree of alignment along the structures. All three isoform specific knockouts led to higher Orientation Parameter values regardless of microgroove dimensions with the strongest alignment shown by PKD1 KO cells. The absence of PKD1 led to almost perfect cell ordering on the grooves with 2 µm spacing ($S^{PKD1\ KO}{}_{200nm} = 0.8$ and $S^{PKD1\ KO}{}_{350nm} = 0.93$). Higher groove depth (350 nm) and lower groove width (2 µm) architecture provided the strongest cues for all the cell lines. **For all:** Error bars represent 95 % Confidence Interval. N = 2 independent experiments; $N^* = 30-50$ total cells analyzed. $^{**}P < 0.01$, $^{***}P < 0.001$, $^{****}P < 0.0001$, N.S. not significant. Significance was evaluated by ordinary two-way ANOVA.

Cell contact guidance leads not only to cell alignment along the grooves but also in directed movement along them. Migration displacement angles with respect to the groove direction were plotted to reveal the degree of directional bias created by the surface architecture (Fig. 8.9). The Rose plots show strong migration persistence in the x-direction parallel to the grooves for all the cell lines, although PKD2 KO and PKD3 KO cells exhibited the lowest persistency especially on wider 10 µm grooves. Panc1 control and PKD1 KO cells had a very similar angle distribution profile. Independent of the cell line, the biggest bias was induced by the narrow (2 µm) and deep (350 nm) grooves.

Due to the directional bias presented by the surface architecture, cell speed was also affected. The average cell velocity as a function of groove dimension and isoform knockdown is shown in Figure 8.10. As expected all the cell lines had significantly elevated mean cell velocities on the grooved PDMS surfaces. The changes in cell velocity followed the same trend as described above. On average, PKD1 KO cells had the higher cell speed on the 200 nm deep grooves.

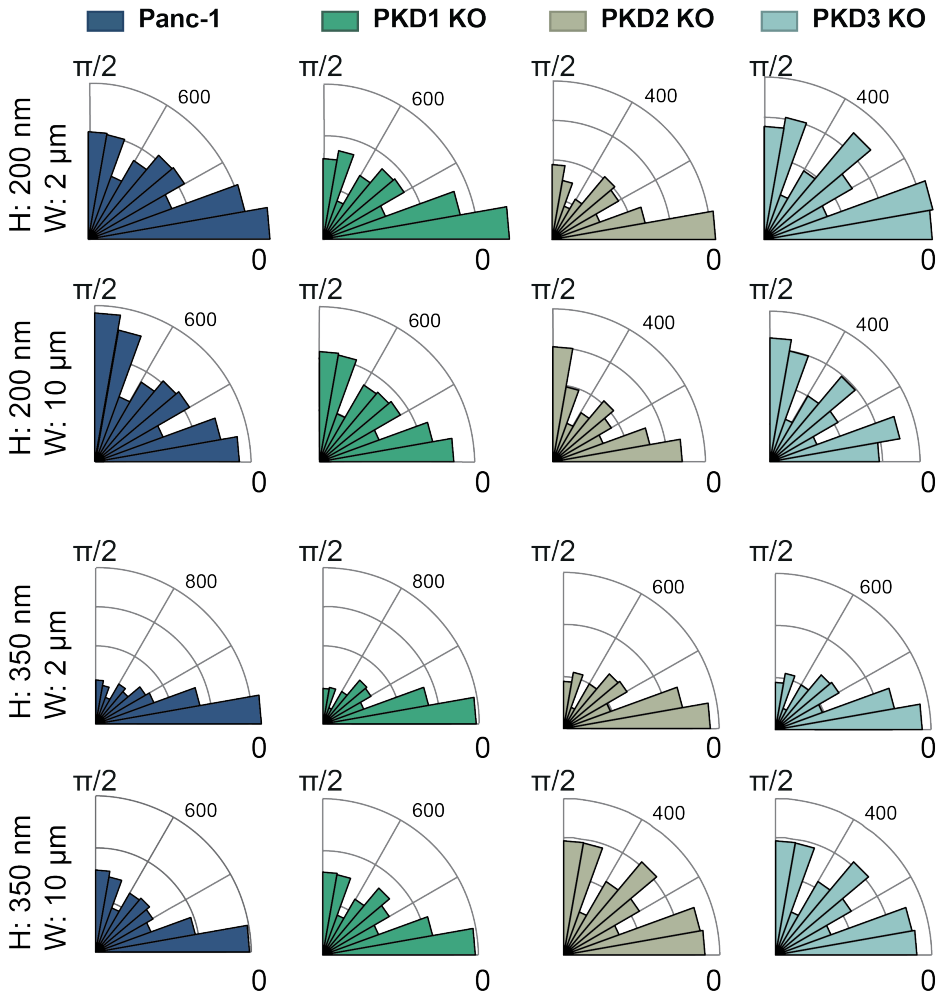

Figure 8.9: Rose plots of cell displacement angles. The angles were calculated from cell migration vectors with respect to the groove direction (here x-axis). Steps smaller than 3 µm were disregarded. Tall and narrow grooves were the most effective in biasing cell migration in all the cell lines. Loss of PKD1 made the cells "sensitive" to the shallower structures (200 nm deep and 2 µm wide). 10 µm wide grooves provided a strong signal for directed migration only combined with 350 nm depths. Concurrent with the results on 2D glass surfaces (Section 8.2), PKD3 KO cells exhibited the lowest persistency on all substrates except the deeper and narrower ones (D: 350 nm, W: 2 µm).

In contrast, on 350 nm deep structures, Panc1 control cells were faster, showing significant differences on 2 µm wide grooves.

To summarize all the results described in this section, absence of PKD1 isoform in Panc1 cells resulted in significant morphological changes, such as extreme cell elongation along the grooves. No morphological changes were observed for the rest of the cell lines plated on the structured substrates. In contrast, cell alignment parallel to the grooves, average velocity and migration persistence were affected to some degree in all the cell lines, with the strongest effect observed for PKD1 KO cells. All the cells had higher contact guidance efficiency on smaller groove spacing (2 µm combined with higher groove depth (350 nm).

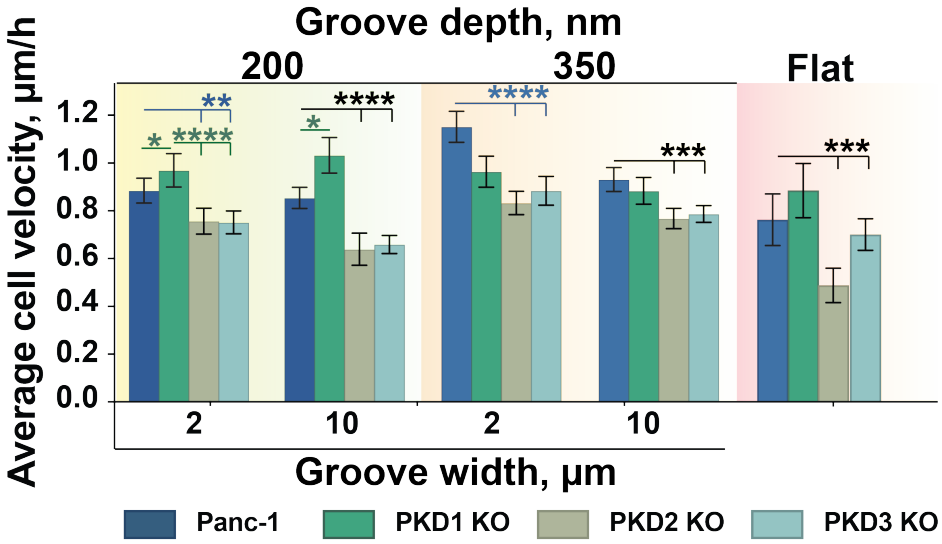

Figure 8.10: Cell average velocity as a function of groove dimensions and PKD isoform-specific knockout. All the cell lines migrated faster on microstructures compared to the flat PDMS surface. Concurrent with the directionality analysis, all cell lines were faster on the deeper and narrower ones (D: 350 nm, W: 2 µm), with Panc1 control and PKD1 KO cells being significantly faster than PKD2 and PKD3 KO cells. PKD1 KO cells were also significantly faster ($^{*}P < 0.015$) than the control cells on 200 nm deep and 2 µm wide grooves. **For all:** Error bars represent 95 % Confidence Interval. N = 3 independent experiments; $N^{*} = 30 - 50$ total cells analyzed. $^{*}P < 0.015$, $^{**}P < 0.01$, $^{***}P < 0.001$, $^{****}P < 0.0001$. Significance was evaluated by ordinary two-way ANOVA.

8.5 PKD isoform-specific knockout Panc1 single cell invasion studies

One of the goals of this work was to understand Protein Kinase D isoform-specific involvement in pancreatic cancer cell invasive behavior. Among the key aspects of invasion is the ability of cancer cells to deform their body in order to migrate through gaps of different sizes in the highly cross-linked ECM network. To mimic this environment in well-controlled manner, PDMS-based devices with micron scale channels were used, to investigate cell migration in stiff confined environment. These microchips were previously developed in our group and are a powerful tool for single cell *in vitro* invasion studies [175]. By using two different channel dimensions of 3x11x150 µm^3 and 10x11x150 µm^3 (WxHxL) the degree of cell mechanical deformability could be assessed as well. Considering that the diameter of pancreatic cancer cells in suspension is approximately 20-25 µm, migration through 3 µm channel would require dramatic deformations of cell cytoskeleton and the nucleus. At the same time, migration through 10 µm wide confinement would not necessitate such extreme morphological changes.

The cell lines were seeded in the microchips, and after overnight incubation, the cells were imaged for a 48-hour period using phase contrast microscopy (see Materials and Methods, Section 5.2.5.3). Only single cell-channel interactions were then analyzed. The interactions were divided into three categories: Penetration, invasion and permeation [175]. Cells that partially extended into the channels (up to 50 % of the channel length), without fully entering them, were classified as penetrating cells. Cells that completely entered or penetrated $\geq$ 50 % without leaving the channels from the opposite side were counted as invasive cells. And lastly, the cells that completely migrated through the channels were termed permeative cells (see Materials and Methods, Fig. 5.5). Summary of the interaction categories with respect to cell type and channel dimensions is presented in figure 8.11A and B. Permeating cell migration velocity inside the channels was analyzed as well (Fig. 8.11C).

Each of the cell lines exhibited different behavior inside the microchannels. In 3 µm channels, Panc1 control cells were more permeative than any of the PKD isoform knockout cells. Upon contact with the channels 46 % of the control cells were able to fully permeate (Fig. 8.11A). Moreover, only 18 % of the cells were invasive, meaning that once the cells squeezed and entered the channels they would likely migrate all the way through. In the absence of PKD1 or PKD2 isoforms the ratio of the cell-channel interactions changed and became more uniform (approximately 33 % each permeation, invasion and penetration). From the perspective of PKD1 knockout, this result was quite surprising, as their ability to elongate on the microstructures would hint to them being more deformable and hence more permeative in the narrow channels. In contrast, the deletion of PKD3 in the Panc1 cells reduced the number of the fully permeating cells by 17 % percent. As mentioned before, 10 µm channels do not pose a big challenge with respect to cell deformation. Hence the cells had higher percentage of fully permeating cells: Panc1 cells 1.4- fold increase, PKD1 KO 2- fold increase, PKD3 KO 1.7- fold increase. PKD2 knockout cells were the only exception with approximately the same ratio of penetration, invasion and permeation as in 3 µm channels. Figure 8.11B shows the number of the cells that interacted per one channel in one-day period. Surprisingly, PKD1 KO cells were least likely to initiate contact and invade the 3 µm wide channels.

In the next step, the migration speed of the cells inside the channel was evaluated by tracking the leading edge of the cells. As it can be seen from Figure 8.11C channel dimensions did not affect migration speed of the Panc1 control, PKD2 KO and PKD3 KO cells. Surprisingly, absence of PKD1 significantly reduced cell speed (approximately 2.5- fold drop) in 3 µm wide channels both compared to the control cells and the PKD1 KO cells in the wider (10 µm) channels. It is obvious, that the highly confined environment had a very strong effect on PKD1 KO cell invasive behavior *in vitro*.

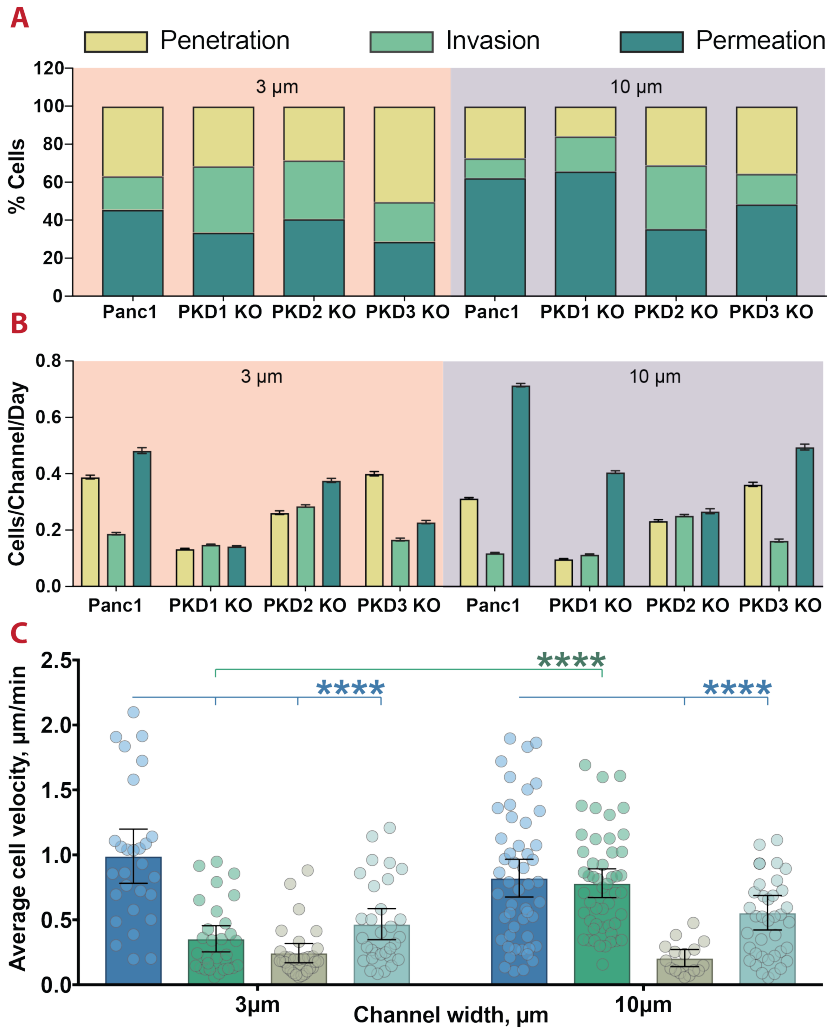

Figure 8.11: Single cell-channel interactions and confined cell average migration speed of Panc1 control, PKD 1, PKD2 and PKD3 knockout cells. **A.** Cell-channel interactions were divided into 3 categories: Penetration, invasion and permeation. Panc1 control cells were more effective at permeation in 3 µm channels than any of the knockout cells. Out of 237 cells evaluated 36 % were penetrative, 18 % were invasive and 46 % permeative. PKD1 and PKD3 knockout cells exhibited similar and relatively equal ratio of interaction types. Deletion of PKD3 was more effective at reducing cell permeation in the narrow channels (29 % out of 167 cells). Higher percentage of Panc1, PKD1 KO and PKD3 KO cells permeated the 10 µm wide channels. PKD2 KO cell-channel interactions were not affected by changes in channel dimensions. N = 3 independent experiments; $N^*_{3\mu m} = 237$ Panc1, 143 PKD1, 194 PKD2, 167 PKD3 and $N^*_{10\mu m} = 337$ Panc1, 190 PKD1, 200 PKD2, 200 PKD3 total cells analyzed. **B.** Number of interacting cells in a 24-hour period normalized by the total number of channels available. PKD1 isoform knockout led to reduced number of total number of interacting cells and poor permeation in 3 µm channels. **C.** In the absence of PKD1 enzyme average permeating cell velocity in 3 µm wide channels was significantly ($^{****}P < 0.0001$) reduced compared to the control cells and the PKD1 KO cells in 10 µm channels. Significance was evaluated by ordinary two-way ANOVA.

To better understand these changes, the phase contrast time-lapse movies were investigated in greater detail. Figure 8.12A presents the image series of each of the cell lines migrating inside the channels. Three important observations could be made:

- Control cells had no difficulty in permeating the narrow channels. As soon as the cells deformed enough to squeeze through, they migrated promptly and left the channels from the opposite side. PKD3 knockout cells behaved similarly, although due to the speed decrease in these cells, they required much longer times to fully permeate.

- PKD1 KO cells exhibited extreme shape deformation in the 3 μm wide channels. Their cell body could elongate to span the whole length of the channel, i.e. 150 μm, yet their nucleus had difficulty deforming and entering the confined space (Fig. 8.12A). To illustrate this, cell nuclei of fixed PKD1 KO and control cells inside the microchannels were immunofluorescently stained. As it can be seen from the representative images in Figure 8.12C, in Panc1 control cells the nuclei deformed almost immediately upon cell entrance into the channels. In contrast, the nuclear deformation of PKD1 KO cells happened when the cell body would reach approximately 80 % the length of the channel, hence playing a role of a "plug" hindering cell permeation. This led to the significant decrease in cell speed in the used confinement (Fig. 8.11C). The cell membrane ruptured sometimes under such strain, which led to channel blockages (Fig. 8.12B). Additionally, the channels were occupied for longer time periods since one PKD1 KO cell could spend up to thirty hours inside one. This two factors combined explained the calculated low number of cell interactions with the channels.

- PKD2 KO cells also behaved quite differently in the system used. As it can be seen from Figure 8.12A (10 μm channels) and concurrent with the previous observations the cells preferred collective cell migration, so-called cell streaming throughout the channels. At low concentrations, single cells were able to interact with the channels and permeate them in the same fashion as Panc1 control cells (8.12 2 μm channels). The single cell migration inside the channels was as slow as on 2D surfaces. However, due to much higher proliferation rates of Panc1 cells in the absence of PKD2 enzyme, the cells created connective cell layers on both sides of the channels already after a 24-hour period.

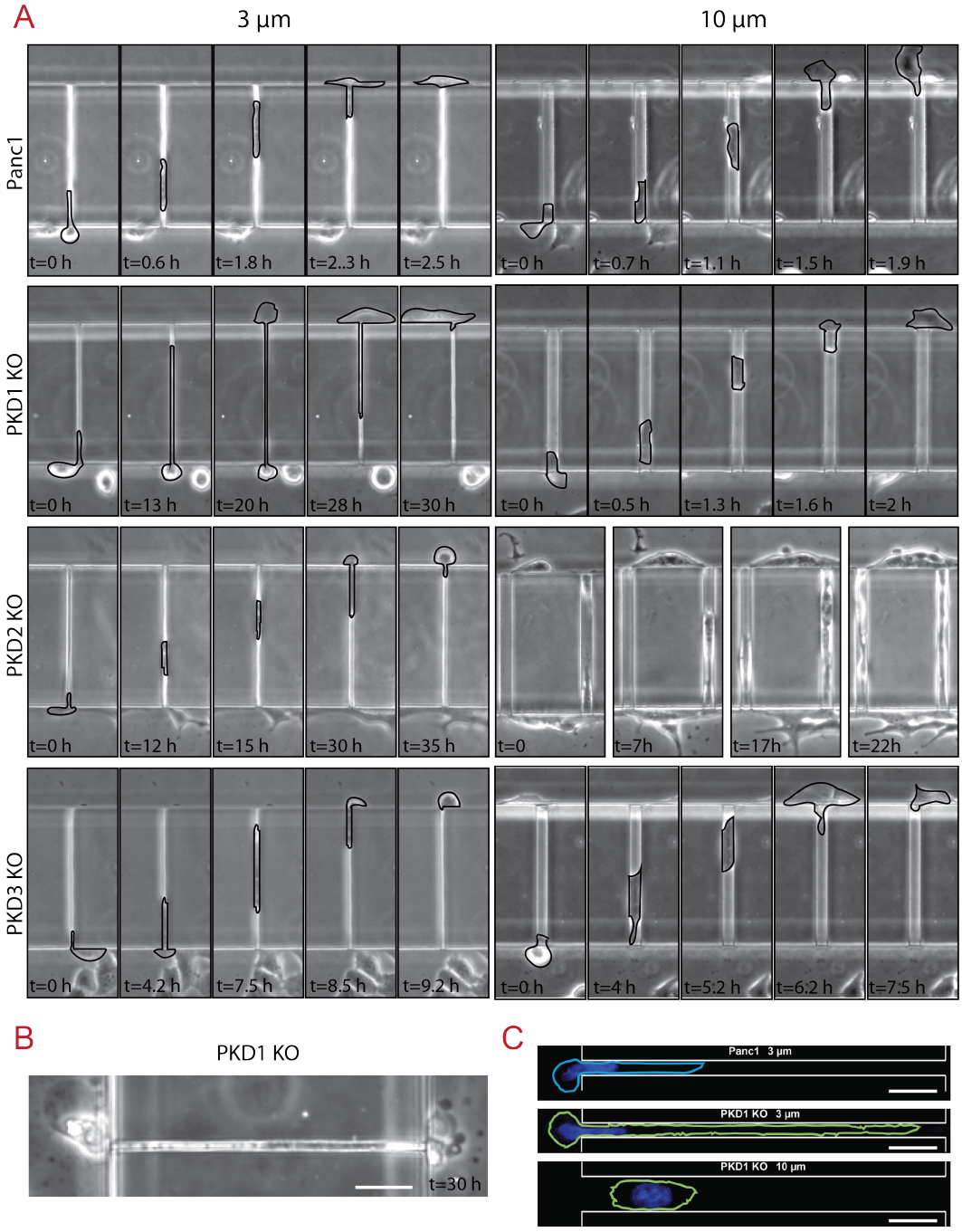

Figure 8.12: Representative phase contrast cell and immunofluorescently labeled nucleus images inside 3x11x150 and 10x11x150 μm^3 (WxHxL) wide channels. **A.** For each of the cell lines different permeation behavior was observed (see Section 8.5 for explanation). Cells were manually outlined to improve visibitlity. **B.** PKD1 KO cells would sometimes rupture inside the narrow channels, due to extreme and prolonged deformation inside them. **C.** Immunofluorescent staining of cell nuclei of Panc1 control and PKD1 KO cells inside 3 and 10 µm wide channels. Nuclear deformation in PKD1 KO cells starts when cell body of PKD1 KO cells reached approximately 80 % the length of the channels. Scale bars: 50 µm.

8.6 PKD1 isoform knockout induces changes in pancreatic cancer cell mechanical properties

The ability of PKD1 KO cells to drastically deform was an indicator of changes in cell mechanical properties of the cell. 3D optical stretcher was used to quantify cell stiffness. The results are presented in figure 8.13. Cell deformability of PKD3 KO cells could not be quantified due to both cell shape irregularity in suspension and bleb formation during stretching (see Materials and Methods, Section 5.3 and Fig. 8.13A). The other three cell lines were stretched at 1W laser power for two seconds. Cell deformability was measured as a relative change in cell ellipticity (see Materials and Methods, Equation 5.8) and is shown in Figure 8.13B as a function of time. Absence of PKD1 had a significant effect on cell viscoelasticity. At maximum stretch time (t = 3s), PKD1 KO cells had approximately 1.6 % and 2.6 % more change in cell ellipticity than the control and PKD2 KO cells respectively. This confirmed the previous observations that these cells were much softer.

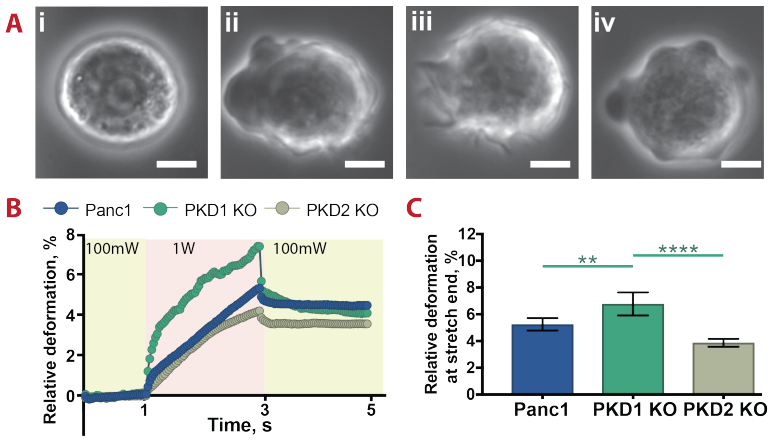

Figure 8.13: PKD1 KO cells are significantly more deformable. **A.** (i) Typical Panc1 cell in suspension. The illuminated ring at the cell boundaries allows for automatic edge detection necessary for deformation measurements. (ii-iv) Many of PKD3 KO cells had very irregular non-spherical shapes in suspension (ii and iii), which rendered it difficult for the software to detect cell boundaries. Additionally the cells with circular shapes would often form blebs upon stretching, possibly due to actin cortex rupture (iv). Combined, these factors made it impossible to accurately measure PKD3 KO cell deformation with the used assay. Scale bars: 10 µm. **B.** Average deformability curves of Panc1 control, PKD1 KO and PKD2 KO cells shown as relative change of cell ellipticity. The cells were trapped at low laser power (100 mW) for 1 second, followed by 2 seconds stretching at 1 W laser power ($\lambda = 1064$nm). PKD1 KO cells, which were previously identified as more invasive, are significantly softer. **C.** At stretch end (t = 3 s), PKD1 KO cells had relative change of ellipticity of approximately 6.8 % and 1.6 % more than the control Panc1 cells (5.2 %). PKD2 KO cells were the least deformable (4.2 %). **For all:** Error bars represent 95 % CI. N = 4 independent experiments; $N^* = 270$ Panc1, 310 PKD1 KO, 320 PKD2 KO cells analyzed. $^{**}P < 0.01$, $^{****}P < 0.0001$. Significance was evaluated by ordinary one-way ANOVA.

Chapter 9

Discussions

Currently the 5-year survival rate for patients with pancreatic cancer is only 7-9 % [77]. Although it has slightly improved in the past few years, the long term projections of cancer-related deaths predict that by 2030 pancreatic cancer will become the second most deadly form of cancer in the United States, surpassed only by lung cancer [191]. At the core of this poor prognosis are pancreatic cancer's fast progression, late diagnosis, and lack of viable treatments [78, 79]. In recent years, the protein kinase D family has received increasing attention as a possible inhibition target in pancreatic cancer [142, 143, 155, 168, 170]. A number of compelling *in vitro* and *in vivo* (murine) studies have shown PKD-based regulation of both early acinar-to-ductal metaplasia [143, 168] and later stage pancreatic ductal adenocarcinoma (PDAC) invasion and metastasis [169, 173]. Additionally, the available literature supports the notion that the three PKD enzymes control tumor progression and invasion in an isoform-specific manner and have seemingly opposing pro- and anti-invasive roles [169].

In this work, Panc1 pancreatic cancer cell lines with Crispr/Cas9 knockouts of *PRKD1, 2* and *3* genes were used, first time, for systematic studies of *in vitro* PKD-isoform dependent pancreatic cancer migration and invasion. Using these modified cell lines, a deeper understanding was obtained on the different functions of the three PKD isoforms in cancer cell motility, contact guidance, MMP-independent invasion, and cell mechanical properties. As all three isoform knockout lines exhibited unique migratory behavior, they will be discussed separately.

9.1 Loss of PKD1 leads to a more invasive pancreatic cancer phenotype

The data presented in Chapter 8 suggest that PKD1 activity may inhibit invasiveness in Panc1 cells, as loss of this isoform led to improved cell persistence, enhanced contact guidance and significant cell softening (see Results Chapter 8). In order to explain the observed changes in the panc1 phenotype and migration in the absence of PKD1, it is necessary to refer to unpublished data obtained by collaborators, Dr. Tim Eiseler and Thomas Seufferlein at the University Clinic Ulm. They measured among other markers expression levels of different Epithelial-to-mesenchymal (EMT) transition markers and intermediate filament (IF) proteins in the three different PKD KO cells using qPCR.

EMT transition is one of the main mechanisms of cancer invasion into the stroma [114, 119, 120]. PKD1-dependent EMT inhibition has been shown in various cancer types (see Appendix, Table A.1). According to the literature, both mesenchymal and epithelial phenotypes have been observed in different PDAC cell line [171]. In the present study, PKD1 KO pancreatic cells exhibited mesenchymal characteristics, as qualitative comparison of PKD1 KO cells with wild type cells showed lack of cell-cell contacts and spindle shaped morphology typical to mesenchymal phenotype (see Results Chapter 8, Fig. 8.2A). Additionally, immunofluorescence staining of E-cadherin in these cells showed no enhanced expression at cell-cell junctions (see Results Chapter 8, Fig. 8.3). These observations are in agreement with the microarray data obtained by the collaborators. They found that compared to control cells, PKD1 KO cells exhibit a significant upregulation of EMT markers, including N-cadherin, ZEB2 and vimentin. Combined, these results support the notion that PKD1 can function as EMT suppressor in pancreatic cancer, which may explain also other observations made in the different migration experiments of this work.

Panc1 motility was affected as well by the absence of PKD1. Although PKD1 KO cell speed was not affected, cells migration persistence time was four times higher (see Results Chapter 8, Section 8.2). It has been reported in multiple cancer cell lines, including PDAC cell lines, that PKD1 plays an inhibitory role in cancer cell migration (see Apendix, Table A.1). Dynamic actin polymerization and remodeling is necessary for cell migration [18, 19]. Protrusion of the cell's leading edge (lamellipodia) is driven by free barbed end formation of actin filaments [192]. Eiseler et al. reported two independent mechanisms through which PKD1 controls F-actin polymerization and remodeling [142, 155]. By inhibiting SSH1L (slingshot protein phosphatase 1), PKD1 inactivates the actin-remodeling protein cofilin at the lamellipodium, thus inhibiting directed cell migration [155]. Additionally, PKD1-mediated

cortactin phosphorylation decreases actin dynamics through its affinity to the WAVE2 complex, resulting in decreased lamellipodia protrusion velocity [142]. Thus, the 4-fold increases in persistence time of Panc1 cells migrating on 2D glass surfaces (see Results Chapter 8, Fig. 8.5) might be linked to rapid F-actin remodeling and polymerization in the absence of PKD1.

Panc1 cell deformability seems to be consistently enhanced in the absence of PKD1 in all the migration assays presented in Chapter 8. PKD1 KO cells had significantly higher aspect ratios (AR) both on glass and on microstructured PDMS surfaces (see Results Chapter 8, Figs. 8.2C and 8.7C). In the PDMS-based microchannels, cells were able to elongate and permeate 150 µm-long constrictions (see Results Chapter 8, Fig. 8.12). Finally, optical stretching of the suspended cells revealed 1.6 % higher (statistically significant) Panc1 cell deformability in the absence of PKD1 (see Results Chapter 8, Fig. 8.13). Changes in biomechanical cell properties are increasingly being correlated with malignant phenotypes of different cancers [136, 193, 194]. Cell mechanical properties are directly linked to cell cytoskeleton biochemistry and organization [195]. It has been proposed that cell viscoelastic measurements may be a marker for malignant transformation, as many studies have revealed a direct link between the stage of malignancy and cell viscoelasticity [133, 135, 193, 196]. It is thus reasonable to deduce that changes in the mechanical properties induced by PKD1 knockout may be advantageous to pancreatic cancer cell invasion potential. Intermediate filaments (IF), such as keratin, contribute to the maintenance of cell shape and protect cells from mechanical stresses [197, 198]. PDAC cancer cells express some keratin heteropolymers, with the Panc1 cell line in particular known to express keratin 8 (K8) and keratin 18 (K18) [197, 199]. In the absence of PKD1, the levels of K8 and K18 in Panc1 cells were downregulated 3.2- and 2.9-fold, respectively (unpublished collaborator data). This downregulation may account for the observed softening of PKD1 KO cells. This assumption is supported by the studies done with Sphingosylphosphorylcholine (SPC) treated Panc1 cells [199]. SPC is known to induce keratin reorganization and reduction of cell peripheral keratin, which significantly reduces the elastic modulus of the cell. This altered cell deformability has been shown, to enhance Panc1 cell migration and higher cell invasion in Boyden chamber assays and in PDMS microchannels [199], [175].

In this work, experiments on Panc1 cell migration on microgrooved surfaces capable of inducing contact guidance showed that PKD1 knockout caused not only morphological changes, but also significantly enhanced cell alignment along the grooves (see Results Chapter 8, Fig. 8.8). Improved cell alignment on surfaces with smaller depths (200 nm deep, 2 µm wide) also led to significantly higher cell speed and better migration directionality (see Results Chapter 8, Figs. 8.9 and 8.10). Similar behavior has been reported in SPC treated Panc1 cells [36]. Thus, the downregulation of K8/18 observed in PKD1 KO cells likely plays a role in

the observed enhancement of contact guidance. The dependence of intermediate filament expression on PKD1 isoform has not been investigated so far. It may represent a new avenue through which PKD1 regulates pancreatic cancer invasive features, as along with vimentin upregulation, alterations or loss of keratin expression are another biomarker of cell EMT transition [200, 201].

One unexpected result observed in the PDMS microchannel assay was that despite the significant deformability of the PKD1 KO cells, they did not exhibit enhanced invasion through the highly confined 3 μm channels. On the contrary, the inability of the nucleus to squeeze into the narrow channels may have led to a reduction in the number of permeating PKD1 KO cells and significantly lowered migration speed inside channels with this geometry (see Results Chapter 8, Figs. 8.11 and 8.12). That interpretation is in alignment with the widely accepted observation that the nucleus is one of the limiting factors for effective confined migration. As the largest and stiffest organelle in the cell, it requires significant deformation to squeeze into the small pores comprising the dense extracellular matrix [202], [203]. The mechanisms involved in nucleus deformation are not yet fully understood. During migration and especially confined migration, cell cytoskeleton compresses the nucleus, so the nucleus is elongated along the migration direction [204–206]. One may speculate, that the softening of cell cytoskeleton observed in PKD1 KO cells may result in inability of the cytoskeleton to deform the nucleus, which could explain the inability of the nucleus to squeeze into the 3 μm wide channels. Further investigations would be necessary, to elucidate the changes in the perinuclear region of these cells, which could attribute to the observed behavior.

9.2 PKD2 knockout reverses EMT but enhances cell proliferation

In the absence of PKD2, pancreatic cancer cells exhibited epithelial characteristics such as strong cell-cell and cell-surface adherence, and reduced cell speed (see Results, Chapter 8). These changes might not only be due to the PKD2 KO but could be attributed to PKD1 isoform activity in the PKD2 KO cells. PKD1 has been shown to promote the epithelial phenotype in breast and prostate cancer cell lines by upregulating E-cadherin expression [153, 157]. Similarly, PKD2 KO cells, used in the current study, adapted the epithelial phenotype, with E-cadherin expression at cell-cell borders and cell growth in epithelial-like sheets (see Results Chapter 8, Figs. 8.2 and 8.3). Additionally these cells exhibited significantly lower single cell migration speed and stronger cell-cell and cell-surface attachment. As discussed in the previous section, PKD1 inactivates the actin-remodeling protein cofilin at the lamellipodium

by inhibiting SSH1L [155]. It has been also reported that in NIH/3T3 fibroblasts PKD1 negatively controls FA dynamics (decrease FA turnover and increase FA maturation) through phosphorylation of PIP5Klγ enzyme [207]. The presence of highly defined F-actin stress fibers and large focal adhesions (FA) at the cell lamellipodia observed in immunofluorescent stainings of PKD2 KO cells may indicate similar function of PKD1 in Panc1 cells in the absence of PKD2 isoform (see Results Chapter 8, Fig. 8.6). Combined with elevated E-cadherin levels this function of PKD1 might explain the observation of increased cell-surface attachment of PKD2 KO cells (see Results Chapter 8, Fig. 8.1).

F-actin and FA spatiotemporal remodeling regulates cell migration and inactivation of the dynamic changes in both leads to the reduced cell migration speed observed in the PKD2 KO cell line. Despite migrating slower, PKD2 KO cells had 2-fold higher cell persistence time compared to the parental Panc1 cells. This also is likely a result of altered F-actin and FA dynamics, as due to reduced F-actin and FA remodeling lamellipodia in the migration direction may be stabilized for longer time periods.

The hyperproliferation of Panc1 cells in the absence of PKD2 could be attributed to PKD1 signaling as well. Eiseler *et al.* have shown PKD1 phosphorylation of zinc-finger transcriptional factor Snail1 in the nucleus which upregulates pancreatic cancer cell proliferation [170].

Upregulaton of E-cadherin and hyperproliferation also explains PKD2 KO cell invasive behavior in the PDMS-based microchannel assay. The cells were not affected by channel dimensions and after 24 hours permeated the channels rather in a collective fashion (cell streaming) retaining their cell-cell contact (see Results Chapter 8, Figs. 8.11 and 8.12). The channel permeation was then the result of not enhanced invasive behavior but more of volume exclusion principle caused by the excessive proliferation of these cells.

From the observed behavior of PKD2 KO cells, one may hypothesize that in the parental cells, where both PKD1 and PKD2 are present, PKD1 regulatory functions are downplayed or suppressed, as loss of PKD2 leads to the PKD1-governed phonotypical changes in pancreatic cancer cells.

9.3 PKD3 regulates cell motility

The PKD isoform PKD3 is the least known member of the PKD family. While it has been reported that PKD3 expression is unchanged in cancerous pancreatic cells compared to their healthy counterparts [169, 171], there is a lack of literature describing PKD3-specific activity in pancreatic cancer progression.

The results in Chapter 8 showed that despite not causing any morphological changes, PKD3 knockout did significantly hinder the motility of Panc1 cells (see Results Chapter 8, Figs. 8.24 and 8.5). PKD3 KO cells saw a reduction in both cell speed and directionality, as opposed to PKD2 KO cells in which cell speed was significantly reduced but cell persistence increased (see Results Chapter 8, Fig. 8.2). Additionally, likely due to their reduced migration speed, PKD3 KO cells did not efficiently permeate PDMS microchannels, either at extreme (3 μm) or moderate (10 μm) levels of confinement (see Results Chapter 8, Fig. 8.11). This PKD3-dependent pancreatic cancer cell behavior has not been reported in the literature. As PKDs are involved in many cellular processes, it is difficult to pinpoint how exactly PKD3 may regulate pancreatic cancer motility. It has been reported that in prostate cancer, PKD3 inhibition impairs cell migration through downregulation or inhibition of MMP9 and growth factors such as IL-6, IL-8 and GRO_{α}, tumor promoting cytokines involved in cancer cell proliferation, migration and angiogenesis [160]. However, it is clear that PKD3 knockout can drive notable changes in cytoskeletal organization, as F-actin staining revealed an absence of the distinct F-actin bundles that are visible in the control cells (see Results Chapter 8, Fig. 8.6). This observation is supported by the additional result that PKD3 KO cells formed membrane blebs during 3D cell stretching experiments (see Results Chapter 8, Fig. 8.13), which could mean either that the membrane has dissociated from the actin cortex or that the cortex itself has ruptured [208, 209]. Alterations in the normal actomyosin network could also explain the observed inhibition of cell motility, as F-actin polymerization and myosin-mediated contractility are the canonical drivers of cell migration.

Part V

Summary and Outlook

Chapter 10

Summary

Immune cell recruitment and subsequent migration is a complex process guided by the combined effort of many different extracellular cues, including chemical gradients, shear flow and possibly changes in temperature. In the presented thesis, it was shown that migrating differentiated HL-60 cells have a nearly constant persistence length at normal (35 – 39 °C) and hyperthermic (39 – 42 °C) temperatures, regardless of their extracellular ligand environment. It could be theorized that the preservation of persistence length confers an advantage to immune cells migrating at higher temperatures, as they are able to cover more ground in search of their target independent of extracellular matrix composition. Additionally the experiments in 2D temperature gradients revealed that motile HL-60 cells could be divided into two subpopulations exhibiting "positive" (migration towards heat source) and "negative" thermotaxis (migration towards heat sink). Primary neutrophil thermotaxis has been reported [188], with two subpopulations of thermotactic cells identified. The first was capable of reversing course after the thermotactic stimulus was reversed, while the other continued migration in the same direction. However, this phenomenon has not been investigated further since its original observation in 1982. Thus, this work provides evidence for a similar behavior in two subgroups of a model cell line which may hint to a physiological relevant thermotaxis of immune cells. The findings on 2D surfaces show that neutrophil differentiated HL-60 cells can be a valuable tool for investigating immune cell thermotaxis, a complex process that is not yet well understood.

In the second part of the presented thesis, pancreatic cancer motility was investigated in the absence of each of the three Protein Kinase D isoforms. Using Crispr/Cas9 modified stable knockout pancreatic cancer cell lines (PKD1 KO, PKD2 KO and PKD3 KO), it was shown that the loss of each of the isoform had a significant impact on *in vitro* cell motility and cell biomechanical properties. Loss of PKD1, in particular, was shown to enhance cell migration

persistence and contact guidance. Additionally, for the first time, PKD1-dependent regulation of cell biomechanical properties was revealed, with significant cell softening measure in the absence of this isoform. Taken together, PKD1 KO cells were shown to exhibit signs of an invasive phenotype. On the contrary, PKD2 KO cells exhibited characteristics of epithelial, less invasive, cell phenotype, with significantly lower cell motility and enhanced cell-cell and cell-surface adherence. And lastly, it was shown for the first time that PKD3 isoform also influences pancreatic cancer behavior, as PKD3 knockout significantly reduced cell speed and cell-cytoskeletal stability.

Combined, the presented findings further support the notion that PKD enzymes govern the invasion-related migration capacity in an isoform-specific way. Furthermore, for pancreatic cancer therapeutic treatments the loss of PKD2 and PKD3 isoforms could be more beneficiary than the loss of the PKD1.

Chapter 11

Outlook

In the temperature-sensitive migration studies a model cell line was used as a substitute for blood neutrophils.

Though HL-60 cells are an accepted model for neutrophil migration, in a next step, temperature-dependent cell migration of primary human blood cells should be studied to reveal possible differences in their behavior. Furthermore, along with neutrophils, other white blood cells such as T-cells are also involved in the body's immune reaction. Each of them has various functions and exhibit different migration characteristics. It would be hence beneficial to look at the effects of elevated temperatures on all cells involved in inflammation processes.
The changes in actin dynamics and membrane fluidity could explain the ability of HL-60 cells to maintain the migration persistence length at various temperature ranges. To verify these observations, further quantitative analysis is necessary. F-actin polymerization dynamics can be measured for example by performing local FRAP (fluorescent recovery after bleaching) on actin. Membrane fluidity is customary measured using UV fluorescence polarization (FP) measurements, which measure changes in membrane-bound fluorophore mobility.
Additionally, further studies have to be done in the physiologically relevant conditions. A preliminary study of temperature gradients in 3D collagen gels was performed in this thesis, with the cells showing a tendency to migrate towards the heat source. But due to the limited time and complexity of the 3D studies, it is difficult to make any definitive arguments without further in-depth investigations.

Further research in understanding the temperature-sensitive migratory mechanisms of immune cells will pave the way to better understanding of immune cell functions during disease and injury.

In the PKD isoform-dependent pancreatic cancer cell invasion studies PDMS-based chips with microchannels were used. This assay is a versatile tool for single-cell migration studies

in a precisely confined environment. However, it does not account for *in vivo* cancer cell invasion by matrix degradation via secretion of matrix metalloproteinases (MMPs). Indeed, Wille et al. have shown pro-invasive functions of PKD2 in pancreatic cancer cells through upregulation of MMP7/9 secretion [169]. It is hence important to do further experiments in ECM gels. As an example, PKD1 KO, PKD2 KO and PKD3 KO cell spheroids can be imbedded into matrigel, and cell invasive behavior observed over time. Further studies on the mechanical properties of each of the cell lines are also necessary. In the PKD1 KO cells the possible biomechanical changes in the perinuclear region due to downregulation of intermediate filament keratin could explain the delayed "squeezing" of the nucleus when permeating 3 μm wide channels. Additionally, PKD3 KO cell mechanical properties could not be measured with the laser-based optical stretcher due to membrane bleb formation under strain. AFM indentation measurements would allow cell deformability measurements in the PKD3 KO cells as well as perinuclear region of PKD1 KO cells.

In conclusion, as Protein Kinase D inhibitors are considered to be used in pancreatic cancer therapy, it is imperative to further study all possible isoroform-mediated changes in pancreatic cancer invasive behavior. This may lead to better treatment options and higher patient survival rates.

Appendix

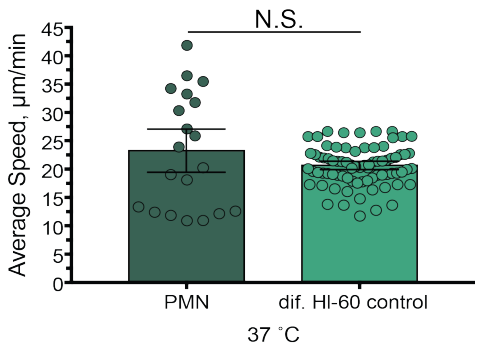

Figure A.1: Blood neutrophils and neutrophil differentiated HL-60 cells have similar migration speed. Average cell speed 95 % Confidence Intervals of PMN cells isolated from human venous blood (23.27 4.45 µm/min) and differentiated HL-60 cells (20.67 0.78 µm/min) at 37 °C. 20 and 78 cells were tracked for blood neutrophils and differentiated HL-60 cells, respectively. N.S. not significant.

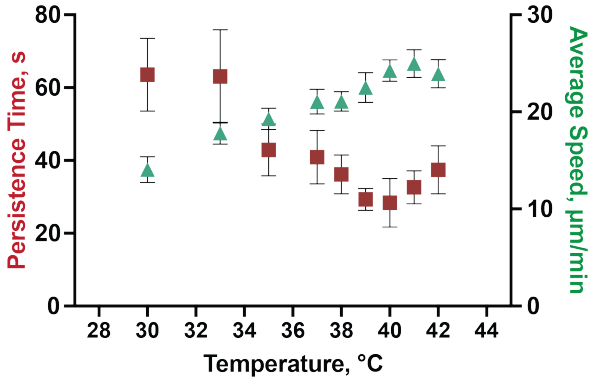

Figure A.2: Relationship between average cell speed and migration persistence time for differentiated HL-60 cells at control conditions and as a function of temperature. With increasing temperature cell average speed increases (left axis, red), but migration persistence time decreases (right axis, green).

Table A.1: **Pro- and anti-carcinogenic functions as well as expression level of PKD isoforms in major cancers.** The arrows represent up- and down-regulation respectively. Colors represent isoform function in tumorogenisis (Pro- Red, Anti-Green)

Type of cancer	PKD Isoform	Effect	Function	Pathways	Ref.
Breast	PKD1 ↓	Pro	Anti-Apoptotic	PKD1-mediated activation of NFκB in response to loss of cell-cell adhesion and oxidative stress	[163, 164]
			Proliferation	The overexpression of PKD1 promotes proliferation through MERK/ERK pathway	[165]
		Anti	Migration	Active PKD1-mediated phosphorylation and inactivation of SSH1L, leading to suppression of directed cell migration	[155]
			Invasion and EMT	PKD1 inhibits EMT by up-regulation of E-cadherin expression	[153]
				PKD1 inhibits breast cancer cell invasion by regulating MMPs	[210]
	PKD2 ↑	Pro	Anti-apoptotic	PKD2-mediated activation of NFκB in response to reactive oxygen species (ROS)	[211, 212]
			Migration	Higher levels of activated PKD2 in drug resistant MCF7 breast cancer cell line were detected. Loss of PKD2 significantly reduced cell migration.	[167]
			Drug resistance	PKD2 upregulates P-glycoprotein and mediates multi-drug resistance	[144]
	PKD3 ↑	Pro	Proliferation	Silencing PKD3 in HCC1806 and TNBC cells led to reduced tumor growth	[213, 214]
Gastric	PKD1 ↓	Anti	Proliferation and invasion	PKD1 is epigenetically silenced. Loss of PKD1 supports tumor cell migration and invasion.	[156, 162]
	PKD2 ↑	Pro	Proliferation and invasion	Upregulation of PKD2 supports tumor cell migration	[156]
Skin	PKD1 ↑ (in mice keratinocytes)	Pro	Proliferation	In mice models PKD1 promotes proliferation	[215]
			Anti-apoptosis	In mice models reduces UVB-induced apoptosis	[216]
	PKD2	Anti	Proliferation	Loss of PKD-2 resulted in enhanced keratinocyte proliferation	[217]
	PKD3	Pro	Proliferation	Loss of PKD-3 resulted in reduced proliferation, loss of clongenicity and reduced tissue regenerative ability	[217]
Prostate	PKD1 ↓ (In highly metastatic cancer cell lines)	Pro	Invasion	PKD-1-mediated Wnt5a signaling pathway	[166]
	PKD1 ↑ (In less metastatic androgen-independent cancer cell lines)	Anti	Proliferation	PKD1 mediates ERK pathway by complexing with β 3-integrin, resulting in increased MMP2 and MMP9 secretion and reduced proliferation	[158]
			Migration	PKD1 mediated E-cadherin phosphorylation resulting in increased cellular aggregation and decreased cellular motility	[157]
			Invasion and EMT	EMT suppression through PKD1-mediated Snail1 phosphorylation	[153]
			Carcinogenesis	PKD1-mediated AR downregulation	[218, 219]
	PKD2 ↑	Pro	Invasion	Regulation of NF-κB and HDAC1-mediated expression and activation of uPA and elevation of MMP9 expression	[154]
	PKD3 ↑	Pro	Migration	Inhibition of PKD3 impairs migration through silencing MMP9, IL-6, IL-8 and GROα	[160]
			Invasion	Regulation of NF-κB and HDAC1-mediated expression and activation of uPA and elevation of MMP9 expression	[154]
			Proliferation And Tumor growth	PKD-3-modulates AKT/ERK1 and 2 signaling and tumor growth	[159]
Brain (Glioblastoma) Colorectal	PKD2 ↑	Pro	Proliferation And Tumor growth	PKD-2 mediates AKT signaling via Golgi phosphoprotein 3. Loss of PKD2 impairs proliferation and tumor growth.	[220–222]

List of Figures

1.1 Cell migration modes and cell morphologies associated with them. 4
1.2 Cell tracking, mean square displacement (MSD) and directional autocorrelation analysis. 6
1.3 Subdiffusive, diffusive and superdiffusive migration modes characterized by mean square displacement (MSD) 7

3.1 Initiation, Promotion and Progression: Three steps of carcinogenesis that characterize the evolvement of normal tissue into invasive cancer 15
3.2 Cell-biological events occurring during the invasion-metastasis cascade . . . 17
3.3 Schematic representation of tumor invasion 18
3.4 Structure of Protein Kinase D 1, 2 and 3 isoforms. 19

5.1 Schematic representation of the microfluidic 2D (A) and 3D (B) temperature gradient chambers with cross sections in X and Y directions 28
5.2 3D Volume temperature gradient distribution computed by COMSOL Multiphysics. 29
5.3 Schematic representation of PDMS-based microgrooved substrates (A) and invasion chips with microchannels (B) used for pancreatic cancer cell migration studies. 30
5.4 Best fitting ellipse of a cell on a microgrooved substrate used for cell AR and alignment analysis 38
5.5 Three categories of cell-channel interactions. 39
5.6 Working principle of 3D optical stretcher. 40

6.1 Successful differentiation of HL-60 cells into neutrophil-like cells. 46
6.2 Motile fragment formation was possible in human blood neutrophils but not in differentiated HL-60 cells. 47
6.3 Representative phase contrast images of differentiated HL-60 cells at different heating conditions. 49
6.4 Temperature-dependent attachment and migration dynamics of differentiated HL-60 cells. 50
6.5 Temperature- and ECM-dependent direction correlation of differentiated HL-60 cell migration. 52
6.6 Differentiated HL-60 cell thermotaxis in response to temperature gradients in 2D microchambers. 54

6.7 Fluid shear flow of a similar magnitude to that produced by temperature gradients does not induce directed migration. 56
6.8 Differentiated HL-60 cell thermotaxis in response to temperature gradients in 3D microchambers. 57

8.1 Attachment efficiency (A) and cell proliferation (B) over 48 hours of PKD1 KO, PKD2 KO, and PKD3 KO cells 68
8.2 PKD enzymes regulate cell morphology in an isoform specific way 69
8.3 Representative immunofluorescent confocal images of E-cadherin (green) and nuclei (blue) in fixed Panc1 cells with PKD1, PKD2 and PKD3 knockouts. 70
8.4 2D Panc1 cell migration speed is dependent on the presence of PKD2 and 3 isoforms. 71
8.5 Mean square displacement (MSD) analysis of cell migration dynamics in 2D revealed strong PKD isoform dependence of the cell persistency. 72
8.6 Representative immunofluorescent images of F-actin (red) and Vinculin (green) in fixed Panc1 cells with PKD1, PKD2 and PKD3 knockouts. . . . 74
8.7 Only PKD1 knockout had effect on Panc1 cell morphology plated on microgrooved substrates. 76
8.8 PKD isoform-specific knockouts in Panc1 cells induce enhanced cell alignment on structured substrates. 77
8.9 Rose plots of cell displacement angles. 78
8.10 Cell average velocity as a function of groove dimensions and PKD isoform-specific knockout. 79
8.11 Single cell-channel interactions and confined cell average migration speed of Panc1 control, PKD 1, PKD2 and PKD3 knockout cells. 81
8.12 Representative phase contrast cell and immunofluorescently labeled nucleus images inside 3x11x150 and 10x11x150 μm^3 (WxHxL) wide channels. . . 83
8.13 PKD1 KO cells are significantly more deformable. 84

A.1 Blood neutrophils and neutrophil differentiated HL-60 cells have similar migration speed. 97
A.2 Relationship between average cell speed and migration persistence time for differentiated HL-60 cells at control conditions and as a function of temperature. 97

List of Tables

5.1 List of antibodies used for modified and non-modified Panc1 cells staining . 32

A.1 Pro- and anti-carcinogenic functions as well as expression level of PKD isoforms in major cancers 98

Bibliography

[1] Francisco Sánchez-Madrid and Miguel Angel del Pozo. “Leukocyte polarization in cell migration and immune interactions”. In: *The EMBO Journal* 18.3 (Jan. 1999), pp. 501–511.

[2] Raye Keller. “Shaping the Vertebrate Body Plan by Polarized Embryonic Cell Movements”. In: *Science* 298.5600 (Dec. 2002), pp. 1950–1954.

[3] Carole LaBonne and Marianne Bronner-Fraser. “Molecular Mechanisms of Neural Crest Formation”. In: *Annual Reviews of Cell and Developmental Biology* 15.1 (Nov. 1999), pp. 81–112.

[4] Anne J Ridley et al. “Cell Migration: Integrating Signals from Front to Back”. In: *Science* 302.5655 (Dec. 2003), pp. 1704–1709.

[5] Andrew D Luster, Ronen Alon, and Ulrich H von Andrian. “Immune cell migration in inflammation: present and future therapeutic targets”. In: *Nature Immunology* 6.12 (Dec. 2005), pp. 1182–1190.

[6] Paul Martin. “Wound Healing—Aiming for Perfect Skin Regeneration”. In: *Science* 276.5309 (Apr. 1997), pp. 75–81.

[7] Peter Friedl and Katarina Wolf. “Plasticity of cell migration: a multiscale tuning model”. In: *The Journal of Cell Biology* 188.1 (Jan. 2010), pp. 11–19.

[8] Thomas P Stossel. “The Machinery of Blood Cell Movements”. In: *Blood* 84.2 (July 1994), pp. 367–379.

[9] Peter Friedl, Stefan Borgmann, and Eva-B Bröcker. “Amoeboid leukocyte crawling through extracellular matrix: lessons from the *Dictyostelium* paradigm of cell movement: Amoeboid leukocyte crawling through extracellular matrix: lessons from the *Dictyostelium* paradigm of cell movement”. In: *Journal of Leukocyte Biology* 70.4 (Oct. 2001), pp. 491–509.

[10] Tim Lämmermann and Michael Sixt. “Mechanical modes of ‘amoeboid’ cell migration”. In: *Current Opinion in Cell Biology* 21.5 (Oct. 2009), pp. 636–644.

[11] Thomas D Pollard and Garry G Borisy. “Cellular Motility Driven by Assembly and Disassembly of Actin Filaments”. In: *Cell* 112 (Feb. 2003), pp. 453–465.

[12] Jörg Renkawitz et al. “Adaptive force transmission in amoeboid cell migration”. In: *Nature Cell Biology* 11.12 (Nov. 2009), pp. 1438–1443.

[13] Sarah Heerboth et al. “EMT and tumor metastasis”. In: *Clinical and Translational Medicine* 4.1 (Feb. 2015), p. 6.

[14] Peter Friedl and Stephanie Alexander. “Cancer Invasion and the Microenvironment: Plasticity and Reciprocity”. In: *Cell* 147.5 (Nov. 2011), pp. 992–1009.

[15] Roberto Mayor and Sandrine Etienne-Manneville. “The front and rear of collective cell migration”. In: *Scientific Reports* 17.2 (Jan. 2016), pp. 97–109.

[16] Pernille Rørth. “Collective Cell Migration”. In: *Annual Review of Cell and Developmental Biology* 25.1 (Nov. 2009), pp. 407–429.

[17] Elena Scarpa and Roberto Mayor. “Collective cell migration in development”. In: *The Journal of Cell Biology* 212.2 (Jan. 2016), pp. 143–155.

[18] Douglas A Lauffenburger and Alan F Horwitz. “Cell Migration: A Physically Integrated Molecular Process”. In: *Cell* 84.3 (Feb. 1996), pp. 359–369.

[19] Michael Murrell et al. “Forcing cells into shape: the mechanics of actomyosin contractility”. In: *Scientific Reports* 16.8 (July 2015), pp. 486–498.

[20] Stephen E Malawista, Eileen O Smith, and John P Seibyl. “Cryopreservable neutrophil surrogates: Granule-poor, motile cytoplasts from polymorphonuclear leukocytes home to inflammatory lesions in vivo”. In: *Cell Motility and the Cytoskeleton* 63.5 (2006), pp. 254–257.

[21] Stephen E Malawista and Anne de Boisfleury Chevance. “The Cytokineplast: Purified, Stable, and Functional Motile Machinery from Human Blood Polymorphonuclear Leukocytes”. In: *The Journal of Cell Biology* 95.3 (Dec. 1982), pp. 960–973.

[22] Alexander B Verkhovsky, Tatyana M Svitkina, and Gary G Borisy. “Self-polarization and directional motility of cytoplasm”. In: *Current Biology* 9.1 (Nov. 1998), pp. 11–20.

[23] Gaudenz Danuser, Jun Allard, and Alex Mogilner. “Mathematical Modeling of Eukaryotic Cell Migration: Insights Beyond Experiments”. In: *Annual Review of Cell and Developmental Biology* 29.1 (Oct. 2013), pp. 501–528.

[24] Roman Gorelik and Alexis Gautreau. “Quantitative and unbiased analysis of directional persistence in cell migration”. In: *Nature Protocols* 9.8 (July 2014), pp. 1931–1943.

[25] Ryan J Petrie, Andrew D Doyle, and Kenneth M Yamada. “Random versus directionally persistent cell migration”. In: *Nature Reviews Molecular Cell Biology* 10.8 (Aug. 2009), pp. 538–549.

[26] Matthew F Krummel, Frederic Bartumeus, and Audrey Gérard. “T cell migration, search strategies and mechanisms”. In: *Nature Reviews Immunology* 16.3 (Mar. 2016), pp. 193–201.

[27] Tajie H Harris et al. “Generalized Lévy walks and the role of chemokines in migration of effector CD8+ T cells”. In: *Letters to Nature* 486.7404 (June 2012), pp. 545–548.

[28] Liang Li, Simon F Nørrelykke, and Edward C Cox. “Persistent Cell Motion in the Absence of External Signals: A Search Strategy for Eukaryotic Cells”. In: *PLoS ONE* 3.5 (May 2008), e2093.

[29] Andy M Reynolds. “Current status and future directions of Lévy walk research.” In: *Biology Open* 7.1 (Jan. 2018), bio030106.

[30] Jean Paul Rieu et al. “Diffusion and Deformations of Single Hydra Cells in Cellular Aggregates”. In: *BMC Cancer* 79.4 (Oct. 2000), pp. 1903–1914.

[31] Richard B Dickinson and Robert T tranquillo. “Optimal Estimation of Cell Movement Indices from the Statistical Analysis of Cell Tracking Data”. In: *Bioengineering, Food an Natural Products* 39.12 (Dec. 1993), pp. 1995–2010.

[32] Alex J Loosley et al. “Describing directional cell migration with a characteristic directionality time”. In: *PLoS ONE* 10.5 (May 2015), e0127425.

[33] Adrià Sales Ramos, Andrew W Holle, and Ralf Kemkemer. “Initial contact guidance during cell spreading is contractility-independent”. In: *Soft Matter* 13.30 (2017), pp. 5158–5167.

[34] Dimitris Missirlis et al. “Substrate engagement of integrins $\alpha_5\beta_1$ and $\alpha_v\beta_3$ is necessary, but not sufficient, for high directional persistence in migration on fibronectin”. In: *Scientific Reports* 6 (Mar. 2016), p. 23258.

[35] Rachael A Ream, Julie A Theriot, and George N Somero. “Influences of thermal acclimation and acute temperature change on the motility of epithelial wound-healing cells (keratocytes) of tropical, temperate and Antarctic fish”. In: *The Journal of Experimental Biology* 206.24 (Sept. 2003), pp. 4539–4551.

[36] Andrew W Holle et al. “Intermediate filament reorganization dynamically influences cancer cell alignment and migration”. In: *Scientific Reports* 7 (Mar. 2017), p. 45152.

[37] Fei Wang. “The signaling mechanisms underlying cell polarity and chemotaxis”. In: *Cold Spring Harbor Perspectives in Biology* (Sept. 2009), a002980.

[38] Xuefeng Li and John Kolega. “Effects of direct current electric fields on cell migration and actin filament distribution in bovine vascular endothelial cells”. In: *Journal of Vascular Research* 39.5 (2002), pp. 391–404.

[39] Kohki Okabe et al. “Intracellular temperature mapping with a fluorescent polymeric thermometer and fluorescence lifetime imaging microscopy”. In: *Nature Communications* 3 (Feb. 2012), p. 705.

[40] Ronald Henry Fraser Hunter, Niels Einer-Jensen, and Torben Greve. “Presence and significance of temperature gradients among different ovarian tissues”. In: *Microscopy Research and Technique* 69.6 (June 2006), pp. 501–507.

[41] Reiko Sakaguchi, Shigeki Kiyonaka, and Yasuo Mori. “Fluorescent sensors reveal subcellular thermal changes”. In: *Current Opinion in Biotechnology* 31 (Feb. 2015), pp. 57–64.

[42] Marta Viano et al. “A thermal gradient modulates the oxidative metabolism and growth of human keratinocytes”. In: *FEBS Open Bio* 7.12 (Oct. 2017), pp. 1843–1853.

[43] Thomas A Mace et al. “Differentiation of CD8 +T cells into effector cells is enhanced by physiological range hyperthermia”. In: *Journal of Leukocyte Biology* 90.5 (Aug. 2011), pp. 951–962.

[44] Dominique Chrétien et al. “Mitochondria are physiologically maintained at close to 50 °C”. In: *PLoS Biology* 16.1 (Jan. 2018), e2003992.

[45] Steven G Kuntz and Michael B Eisen. “Drosophila Embryogenesis Scales Uniformly across Temperature in Developmentally Diverse Species”. In: *PLoS Genetics* 10.4 (Apr. 2014), e1004293.

[46] Anat Bahat, S Roy Caplan, and Michael Eisenbach. “Thermotaxis of human sperm cells in extraordinarily shallow temperature gradients over a wide range”. In: *PLoS ONE* 7.7 (July 2012), e41915.

[47] Christopher Rosin et al. “Combined effects of temperature, pressure, and co-solvents on the polymerization kinetics of actin”. In: *ChemPhysChem* 16.7 (Feb. 2015), pp. 1379–1385.

[48] Thomas R Gaborski et al. “Membrane mobility of $\beta 2$ integrins and rolling associated adhesion molecules in resting Neutrophils”. In: *Biophysical Journal* 95.10 (Nov. 2008), pp. 4934–4947.

[49] Evan Evans and David Needham. “Physical properties of surfactant bilayer membranes: thermal transitions, elasticity, rigidity, cohesion and colloidal interactions”. In: *The Journal of Physical Chemistry* 91.16 (July 1987), pp. 4219–4228.

[50] Baoyu Liu, Craig J Goergen, and Jin-Yu Shao. “Effect of temperature on tether extraction, surface protrusion, and cortical tension of human neutrophils”. In: *BMC Cancer* 93.8 (Oct. 2007), pp. 2923–2933.

[51] Sharon S Evans, Elizabeth A Repasky, and Daniel T Fisher. “Fever and the thermal regulation of immunity: the immune system feels the heat”. In: *Nature Reviews Immunology* 15.6 (May 2015), pp. 335–349.

[52] Michel Gautherie. “Thermopathology of breast cancer: Measurement and analysis of in vivo temperature and blood flow”. In: *Annals of the New York Academy of Sciences* 335.1 (June 2002), pp. 383–415.

[53] Elizabeth A Repasky, Sharon S Evans, and Mark W Dewhirst. “Temperature Matters! And Why It Should Matter to Tumor Immunologists”. In: *Cancer Immunology Research* 1.4 (Oct. 2013), pp. 210–216.

[54] Peter Wust et al. “Hyperthermia in combined treatment of cancer”. In: *The Lancet Oncology* 3.8 (Aug. 2002), pp. 487–497.

[55] Bert Hildebrandt et al. “The cellular and molecular basis of hyperthermia”. In: *Critical Reviews in Oncology/ Hematology* 43.1 (Mar. 2002), pp. 33–56.

[56] Meir Djaldetti and Hanna Bessler. “High temperature affects the phagocytic activity of human peripheral blood mononuclear cells”. In: *Scandinavian Journal of Clinical and Laboratory Investigation* 75.6 (July 2015), pp. 482–486.

[57] Allen J Rosenspire, Andrei L Kindzelskii, and Howard R Petty. “Cutting edge: Fever-associated temperatures enhance neutrophil responses to lipopolysaccharide: A potential mechanism involving cell metabolism”. In: *The Journal of Immunology* 169.10 (Nov. 2002), pp. 5396–5400.

[58] Tanya N Mayadas, Xavier Cullere, and Clifford A Lowell. “The multifaceted functions of neutrophils”. In: *Annual Review of Pathology: Mechanisms of Disease* 9 (Jan. 2014), pp. 181–218.

[59] Leonardo Olivieri Carvalho et al. “The Neutrophil Nucleus and Its Role in Neutrophilic Function”. In: *Journal of Cellular Biochemistry* 116.9 (July 2015), pp. 1831–1836.

[60] Carl Nathan. “Neutrophils and immunity: challenges and opportunities”. In: *Nature Reviews Immunology* 6.3 (Feb. 2006), pp. 173–182.

[61] Mathieu-Benoit Voisin and Sussan Nourshargh. “Neutrophil transmigration: emergence of an adhesive cascade within venular walls”. In: *Journal of Innate Immunity* 5.4 (Mar. 2013), pp. 336–347.

[62] Eduardo Fernández-Segura et al. “Shape, F-actin, and surface morphology changes during chemotactic peptide-induced polarity in human neutrophils”. In: *The Anatomical Record* 241.4 (Apr. 1995), pp. 519–528.

[63] Jingsong Xu et al. “Divergent signals and cytoskeletal assemblies regulate self-organizing polarity in neutrophils”. In: *Cell* 114.2 (July 2003), pp. 201–214.

[64] Andrew R Houk et al. “Membrane tension maintains cell polarity by confining signals to the leading edge during neutrophil migration”. In: *Cell* 148.1-2 (Jan. 2012), pp. 175–188.

[65] Eun Young Choi, Sentot Santoso, and Triantafyllos Chavakis. “Mechanisms of neutrophil transendothelial migration”. In: *Frontiers in Bioscience* 14 (Jan. 2009), p. 1596.

[66] Volker Brinkmann et al. “Neutrophil Extracellular Traps Kill Bacteria”. In: *Science* 303.5663 (Mar. 2004), pp. 1532–1535.

[67] Stephen E Malawista and Anne de Boisfleury Chevance. “Chemotaxis by human neutrophils and their cytokineplasts treated with inhibitors of nitric oxide synthase: no suppression of orientation or trajectory”. In: *Journal of Leukocyte Biology* 61.1 (Jan. 1997), pp. 58–62.

[68] Stephen E Malawista and Gretchen Van Blaricom. “Cytoplasts made from human blood polymorphonuclear leukocytes with or without heat: preservation of both motile function and respiratory burst oxidase activity.” In: *Proceedings of the National Academy of Sciences* 84.2 (Jan. 1987), pp. 454–458.

[69] Stephen E Malawista, Ruth R Montgomery, and Gretchen Van Blaricom. “Microbial killing by human neutrophil cytokineplasts: similar suppressive effects of reversible and irreversible inhibitors of nitric oxide synthase”. In: *Journal of Leukocyte Biology* 60.6 (Dec. 1996), pp. 753–757.

[70] Chang-Hoon Woo et al. “Transepithelial migration of neutrophils in response to leukotriene B4 is mediated by a reactive oxygen species-extracellular signal-regulated kinase-linked cascade”. In: *The Journal of Immunology* 170.12 (June 2003), pp. 6273–6279.

[71] Jingsong Xu et al. “Neutrophil microtubules suppress polarity and enhance directional migration”. In: *PNAS* 102.19 (May 2005), pp. 6884–6889.

[72] Kerry Wilson et al. “Mechanisms of leading edge protrusion in interstitial migration”. In: *Nature Communications* 4 (Nov. 2013), p. 2986.

[73] Pan Jian et al. “Retinoic acid induces HL-60 cell differentiation via the upregulation of miR-663”. In: *Journal of Hematology & Oncology* 4.1 (Apr. 2011), p. 20.

[74] Corrado Tarella et al. “Induction of Differentiation of HL-60 Cells by Dimethyl Sulfoxide: Evidence for a Stochastic Model Not Linked to the Cell Division Cycle1 ”. In: *Cancer Research* 42.2 (Feb. 1982), pp. 445–449.

[75] Arthur Millius and Orion D Weiner. *Live Cell Imaging*. Vol. 591. Manipulation of Neutrophil-Like HL-60 Cells for the Study of Directed Cell Migration. Totowa, NJ: Humana Press, 2010.

[76] Anna Barbara Hauert et al. “Differentiated HL-60 cells are a valid model system for the analysis of human neutrophil migration and chemotaxis”. In: *The Journal of Biochemistry and Cell Biology* 34.7 (Apr. 2002), pp. 838–854.

[77] Rebecca L Siegel, Kimberly D Miller, and Ahmedin Jemal. “Cancer statistics, 2018”. In: *CA: A Cancer Journal for Clinicians* 68.1 (Jan. 2018), pp. 7–30.

[78] Maria Syl D De La Cruz, Alisa P Young, and Mack T Ruffin. “Diagnosis and Management of Pancreatic Cancer ”. In: *Ameriacn Family Physician* 89.8 (Apr. 2014), pp. 626–632.

[79] Jun Yu et al. “Time to progression of pancreatic ductal adenocarcinoma from low-to-high tumour stages”. In: *Gut* (Oct. 2015), gutjnl–2014.

[80] Nabeel Bardeesy and Ronald A DePinho. “Pancreatic cancer biology and genetics”. In: *Nature Reviews Cancer* 2.12 (Dec. 2002), pp. 897–909.

[81] Anne Grapin-Botton. “Ductal cells of the pancreas”. In: *The International Journal of Biochemistry and Cell Biology* 37.3 (Mar. 2005), pp. 504–510.

[82] Agnieszka K Swidnicka-Siergiejko et al. “Chronic inflammation initiates multiple forms of K-Ras-independent mouse pancreatic cancer in the absence of TP53”. In: *Oncogene* 36.22 (Dec. 2016), p. 3149.

[83] Catherine Carrière et al. "Acute pancreatitis markedly accelerates pancreatic cancer progression in mice expressing oncogenic Kras". In: *Biochemical and Biophysical Research Communications* 382.3 (May 2009), pp. 561–565.

[84] Anirban Maitra and Ralph H Hruban. "Pancreatic Cancer". In: *Annual Review of Pathology: Mechanisms of Disease* 3.1 (Feb. 2008), pp. 157–188.

[85] Oliver Stobel et al. "In vivo lineage tracing defines the role of acinar-to ductal transdifferentiation in inflammatory ductal metaplasia". In: *Gastroenterology* 133.6 (Dec. 2007), pp. 1999–2009.

[86] Veronique Giroux and Anil K Rustgi. "Metaplasia: tissue injury adaptation and a precursor to the dysplasia–cancer sequence". In: *Scientific Reports* 17.10 (Sept. 2017), pp. 594–604.

[87] John P Morris, Sam C Wang, and Matthias Hebrok. "KRAS, Hedgehog, Wnt and the twisted developmental biology of pancreatic ductal adenocarcinoma". In: *Scientific Reports* 10.10 (Sept. 2010), pp. 683–695.

[88] Kyoichi Takaori et al. "Pancreatic Intraepithelial Neoplasia". In: *Pancreas* 28.3 (Apr. 2004), pp. 257–262.

[89] Sylwia Jančík et al. "Clinical Relevance of KRAS in Human Cancers". In: *Journal of Biomedicine and Biotechnology* (June 2010), p. 2010.

[90] Daniel Zeitouni et al. "KRAS Mutant Pancreatic Cancer: No Lone Path to an Effective Treatment". In: *Cancers* 8.4 (Apr. 2016), p. 45.

[91] Sunil R Hingorani et al. "Preinvasive and invasive ductal pancreatic cancer and its early detection in the mouse". In: *Cancer Cell* 4.6 (Dec. 2003), pp. 437–450.

[92] F McCormick. "KRAS as a Therapeutic Target". In: *Clinical Cancer Research* 21.8 (Apr. 2015), pp. 1797–1801.

[93] Gunther Zimmermann et al. "Small molecule inhibition of the KRAS-PDEδ interaction impairs oncogenic KRAS signalling". In: *Letters to Nature* 497.7451 (May 2013), pp. 638–642.

[94] Asad Umar, Barbara K Dunn, and Peter Greenwald. "Future directions in cancer prevention". In: *Nature Reviews Cancer* 12.12 (Nov. 2012), pp. 835–848.

[95] M J Thun et al. "The global burden of cancer: priorities for prevention". In: *Carcinogenesis* 31.1 (Jan. 2010), pp. 100–110.

[96] P Vineis, A Schatzkin, and J D Potter. "Models of carcinogenesis: an overview". In: *Carcinogenesis* 31.10 (Oct. 2010), pp. 1703–1709.

[97] Roy M Bremnes et al. “The Role of Tumor Stroma in Cancer Progression and Prognosis: Emphasis on Carcinoma-Associated Fibroblasts and Non-small Cell Lung Cancer”. In: *JTO Acquisition* 6.1 (Dec. 2010), pp. 209–217.

[98] Mei Rosa Ng and Joan S Brugge. “A Stiff Blow from the Stroma: Collagen Crosslinking Drives Tumor Progression”. In: *Cancer Cell* 16.6 (Dec. 2009), pp. 455–457.

[99] Pengfei Lu, Valerie M Weaver, and Zena Werb. “The extracellular matrix: A dynamic niche in cancer progression”. In: *The Journal of Cell Biology* 196.4 (Feb. 2012), pp. 395–406.

[100] Andrew G Clark and Danijela Matic Vignjevic. “Modes of cancer cell invasion and the role of the microenvironment”. In: *Current Opinion in Cell Biology* 36 (Oct. 2015), pp. 13–22.

[101] Gao-Feng Xiong and Ren Xu. “Function of cancer cell-derived extracellular matrix in tumor progression”. In: *Journal of Cancer Metastasis and Treatment* 2.9 (Sept. 2016), pp. 357–8.

[102] Raghu Kalluri and Michael Zeisberg. “Fibroblasts in cancer”. In: *Nature Reviews Cancer* 6.5 (Mar. 2006), pp. 392–401.

[103] Irene Acerbi et al. “Human breast cancer invasion and aggression correlates with ECM stiffening and immune cell infiltration”. In: *Integrative Biology* 7.10 (2015), pp. 1120–1134.

[104] Andrew W Holle, Jennifer L Young, and Joachim P Spatz. “In vitro cancer cell–ECM interactions inform in vivo cancer treatment”. In: *Advanced Drug Delivery Reviews* 97.C (Feb. 2016), pp. 270–279.

[105] Carmen Guerra et al. “Pancreatitis-Induced Inflammation Contributes to Pancreatic Cancer by Inhibiting Oncogene-Induced Senescence”. In: *Cancer Cell* 19.6 (June 2011), pp. 728–739.

[106] Paolo P Provenzano et al. “Collagen reorganization at the tumor-stromal interface facilitates local invasion”. In: *BMC Medicine* 4.1 (Dec. 2006), p. 38.

[107] Mikala Egeblad, Morten G Rasch, and Valerie M Weaver. “Dynamic interplay between the collagen scaffold and tumor evolution”. In: *Current Opinion in Cell Biology* 22.5 (Oct. 2010), pp. 697–706.

[108] Matthew W Conklin et al. “Aligned Collagen Is a Prognostic Signature for Survival in Human Breast Carcinoma”. In: *AJPA* 178.3 (Mar. 2011), pp. 1221–1232.

[109] Patrick Mehlen and Alain Puisieux. “Metastasis: a question of life or death”. In: *Nature Reviews Cancer* 6.6 (June 2006), pp. 449–458.

[110] Scott Valastyan and Robert A Weinberg. "Tumor Metastasis: Molecular Insights and Evolving Paradigms". In: *Cell* 147.2 (Oct. 2011), pp. 275–292.

[111] Bruce R Zetter. "ANGIOGENESIS AND TUMOR METASTASIS". In: *Annual review of medicine* 49.1 (Feb. 1998), pp. 407–424.

[112] Christoph A Klein. "Parallel progression of primary tumours and metastases". In: *Nature Reviews Cancer* 9.4 (Apr. 2009), p. 302.

[113] Liling Wan, Klaus Pantel, and Yibin Kang. "Tumor metastasis: moving new biological insights into the clinic". In: *Nature Medicine* 19.11 (Nov. 2013), pp. 1450–1464.

[114] Andrew D Rhim et al. "EMT and Dissemination Precede Pancreatic Tumor Formation". In: *Cell* 148.1 (Jan. 2012), pp. 349–361.

[115] Franziska van Zijl, Georg Krupitza, and Wolfgang Mikulits. "Initial steps of metastasis: Cell invasion and endothelial transmigration". In: *Mutation Research-Reviews in Mutation Research* 728.1-2 (Aug. 2011), pp. 23–34.

[116] Hae-Yun Jung, Laurent Fattet, and Jing Yang. "Molecular Pathways: Linking Tumor Microenvironment to Epithelial-Mesenchymal Transition in Metastasis". In: *Clinical Cancer Research* 21.5 (Mar. 2015), pp. 962–968.

[117] Silvia Giampieri et al. "Localized and reversible TGFβ signalling switches breast cancer cells from cohesive to single cell motility". In: *Nature Cell Biology* 11.11 (Oct. 2009), pp. 1087–1096.

[118] Jeff H Tsai and Jing Yang. "Epithelial-mesenchymal plasticity in carcinoma metastasis". In: *Genes & Development* 27.20 (Oct. 2013), pp. 2192–2206.

[119] Nicola Gaianigo, Davide Melisi, and Carmine Carbone. "EMT and Treatment Resistance in Pancreatic Cancer". In: *Cancers* 9.12 (Dec. 2017), pp. 122–17.

[120] Nicole M Aiello et al. "Upholding a role for EMT in pancreatic cancer metastasis". In: *Scientific Reports* 547.7661 (July 2017), E7.

[121] Hin Ching Lo and Xiang H F Zhang. "EMT in Metastasis: Finding the Right Balance". In: *Developmental Cell* 45.6 (June 2018), pp. 663–665.

[122] Wei Shen et al. "TGF-ß in pancreatic cancer initiation and progression: two sides of the same coin". In: *Cell & Bioscience* 7.1 (Aug. 2017), p. 39.

[123] Joseph W O'Connor and Esther W Gomez. "Biomechanics of TGFβ-induced epithelial-mesenchymal transition: implications for fibrosis and cancer". In: *Clinical and translational medicine* 3.1 (2014), p. 23.

[124] Michael Zeisberg and Eric G Neilson. “Biomarkers for epithelial-mesenchymal transitions.” In: *Journal of Clinical Investigation* 119.6 (June 2009), pp. 1429–1437.

[125] Marion J Bussemakers et al. “Decreased Expression of E-Cadherin in the Progression of Rat Prostatic Cancer”. In: *Cancer Research* 52.10 (Sept. 2006), pp. 2916–2922.

[126] Young-Eun Joo et al. “Expression of E-cadherin, alpha-and beta-catenins in patients with pancreatic adenocarcinoma”. In: *Pancreatology* 2.2 (Jan. 2002), pp. 129–137.

[127] Massimo Pignatelli et al. “Loss of Membranous E-cadherin Expression in Pancreatic Cancer: Correlation with Lymph Node Metastasis, High Grade, and Advanced Stage”. In: *Journal of Pathology* 174.4 (Sept. 1994), pp. 243–248.

[128] Nelson R Alexander et al. “Extracellular Matrix Rigidity Promotes Invadopodia Activity”. In: *Current Biology* 18.17 (Sept. 2008), pp. 1295–1299.

[129] Aron Parekh and Alissa M Weaver. “Regulation of invadopodia by mechanical signaling”. In: *Experimental cell research* 343.1 (2016), pp. 89–95.

[130] Matthew J Paszek et al. “Tensional homeostasis and the malignant phenotype”. In: *Cancer Cell* 8.3 (Sept. 2005), pp. 241–254.

[131] Michele A Wozniak et al. “ROCK-generated contractility regulates breast epithelial cell differentiation in response to the physical properties of a three-dimensional collagen matrix”. In: *The Journal of Cell Biology* 163.3 (Nov. 2003), pp. 583–595.

[132] Kozaburo Hayashi and Mayumi Iwata. “Stiffness of cancer cells measured with an AFM indentation method”. In: *Journal of the Mechanical Behavior of Biomedical Materials* 49 (Sept. 2015), pp. 105–111.

[133] Małgorzata Lekka et al. “Cancer cell recognition–mechanical phenotype”. In: *Micron* 43.12 (2012), pp. 1259–1266.

[134] Sarah E Cross et al. “Nanomechanical analysis of cells from cancer patients”. In: *Nature Nanotechnology* 2.12 (Dec. 2007), pp. 780–783.

[135] Vinay Swaminathan et al. “Mechanical stiffness grades metastatic potential in patient tumor cells and in cancer cell lines.” In: *Cancer Research* 71.15 (Aug. 2011), pp. 5075–5080.

[136] Subra Suresh. “Biomechanics and biophysics of cancer cells”. In: *Acta Biomaterialia* 3.4 (July 2007), pp. 413–438.

[137] Ivan Stamenkovic. “Matrix metalloproteinases in tumor invasion and metastasis ”. In: *Seminars in Cancer Biology* 10.6 (Apr. 2000), pp. 415–433.

[138] Tony Hunter. “Protein Kinases and Phosphatases: Review The Yin and Yang of Protein Phosphorylation and Signaling”. In: *Cell* 80.2 (Jan. 1995), pp. 225–236.

[139] Georgios Giamas et al. “Protein kinases as targets for cancer treatment”. In: *Pharmacogenomics* 8.8 (Aug. 2007), pp. 1005–1016.

[140] Peng Wu, Thomas E Nielsen, and Mads H Clausen. “Small-molecule kinase inhibitors: an analysis of FDA-approved drugs”. In: *Drug Discovery Today* 21.1 (Jan. 2016), pp. 5–10.

[141] Khushwant S Bhullar et al. “Kinase-targeted cancer therapies: progress, challenges and future directions”. In: 17.1 (Dec. 2018), p. 48.

[142] Tim Eiseler et al. “Protein Kinase D Controls Actin Polymerization and Cell Motility through Phosphorylation of Cortactin”. In: *Journal of Biological Chemistry* 285.24 (May 2010), pp. 18672–18683.

[143] Geou-Yarh Liou et al. “Protein kinase D1 drives pancreatic acinar cell reprogramming and progression to intraepithelial neoplasia”. In: *Nature Communications* 6 (Feb. 2015), p. 6200.

[144] Jiao Chen et al. “PKD2 mediates multi-drug resistance in breast cancer cells through modulation of P-glycoprotein expression”. In: *Cancer Letters* 300.1 (Nov. 2010), pp. 48–56.

[145] Nisha Durand, Sahra Borges, and Peter Storz. “Protein Kinase D Enzymes as Regulators of EMT and Cancer Cell Invasion”. In: *Journal of Clinical Medicine* 5.2 (Feb. 2016), p. 20.

[146] Enrique Rozengurt. “Protein Kinase D Signaling: Multiple Biological Functions in Health and Disease”. In: *Physiology* 26.1 (Feb. 2011), pp. 23–33.

[147] Min Ren et al. “Protein Kinase D Is an Essential Regulator of C. elegans Innate Immunity”. In: *Immunity* 30.4 (Apr. 2009), pp. 521–532.

[148] Grzegorz Sumara et al. “Regulation of PKD by the MAPK p38δ in Insulin Secretion and Glucose Homeostasis”. In: *Cell* 136.2 (Jan. 2009), pp. 235–248.

[149] Ellen Dirkx et al. “Protein kinase D increases maximal Ca 2+-activated tension of cardiomyocyte contraction by phosphorylation of cMyBP-C-Ser 315”. In: *American Journal of Physiology-Heart and Circulatory Physiology* 303.3 (Aug. 2012), H323–H331.

[150] Osvaldo Rey, Jingzhen Yuan, and Enrique Rozengurt. "Intracellular redistribution of protein kinase D2 in response to G-protein-coupled receptor agonists". In: *Biochemical and Biophysical Research Communications* 302.4 (Mar. 2003), pp. 817–824.

[151] Osvaldo Rey et al. "Protein Kinase C_ν/Protein Kinase D3 Nuclear Localization, Catalytic Activation, and Intracellular Redistribution in Response to G Protein-coupled Receptor Agonists". In: *Journal of Biological Chemistry* 278.26 (June 2003), pp. 23773–23785.

[152] Adhiraj Roy et al. "Protein kinase D signaling in cancer: A friend or foe?" In: *BBA - Reviews on Cancer* 1868.1 (Aug. 2017), pp. 283–294.

[153] Cheng Du et al. "Protein Kinase D1 Suppresses Epithelial-to-Mesenchymal Transition through Phosphorylation of Snail". In: *Cancer Research* 70.20 (Oct. 2010), pp. 7810–7819.

[154] Zhipeng Zou et al. "PKD2 and PKD3 promote prostate cancer cell invasion by modulating NF- B- and HDAC1-mediated expression and activation of uPA". In: *Journal of Cell Science* 125.20 (Dec. 2012), pp. 4800–4811.

[155] Tim Eiseler et al. "Protein kinase D1 regulates cofilin-mediated F-actin reorganization and cell motility through slingshot". In: *Nature Cell Biology* 11.5 (Mar. 2009), pp. 545–556.

[156] M Yu Shabelnik et al. "Differential Expression of PKD1 and PKD2 in Gastric Cancer and Analysis of PKD1 and PKD2 Function in the Model System". In: *Experimental Oncology* 33.4 (July 2011), pp. 206–211.

[157] Meena Jaggi et al. "E-Cadherin Phosphorylation by Protein Kinase D1/Protein Kinase CM is Associated with Altered Cellular Aggregation and Motility in Prostate Cancer". In: *American Association for Cancer Research* 65.2 (Jan. 2005), pp. 483–492.

[158] Helal Uddin M Biswas et al. "Protein Kinase D1 Inhibits Cell Proliferation through Matrix Metalloproteinase-2 and Matrix Metalloproteinase-9 Secretion in Prostate Cancer". In: *Cancer Research* 70.5 (Feb. 2010), pp. 2095–2104.

[159] Jun Chen et al. "Protein Kinase D3 (PKD3) Contributes to Prostate Cancer Cell Growth and Survival Through a PKC /PKD3 Pathway Downstream of Akt and ERK 1/2". In: *Cancer Research* 68.10 (May 2008), pp. 3844–3853.

[160] Courtney R LaValle et al. "Inducible silencing of protein kinase D3 inhibits secretion of tumor-promoting factors in prostate cancer." In: *Molecular Cancer Therapeutics* 11.7 (July 2012), pp. 1389–1399.

[161] Nisha Durand, Sahra Borges, and Peter Storz. “Functional and therapeutic significance of protein kinase D enzymes in invasive breast cancer”. In: *Cellular and Molecular Life Sciences* 72.22 (Aug. 2015), pp. 4369–4382.

[162] Mirang Kim et al. “Epigenetic inactivation of protein kinase D1 in gastric cancer and its role in gastric cancer cell migration and invasion”. In: *Carcinogenesis* 29.3 (Oct. 2007), pp. 629–637.

[163] Catherine F Cowell et al. “Loss of cell-cell contacts induces NF-κB via RhoA-mediated activation of protein kinase D1”. In: *Journal of Cellular Biochemistry* 106.4 (Mar. 2009), pp. 714–728.

[164] Heike Döppler and Peter Storz. “A Novel Tyrosine Phosphorylation Site in Protein Kinase D Contributes to Oxidative Stress-mediated Activation”. In: *The Journal of Biological Chemistry* 282.44 (Oct. 2007), pp. 31873–31881.

[165] Manale Karam et al. “Protein kinase D1 stimulates proliferation and enhances tumorigenesis of MCF-7 human breast cancer cells through a MEK/ERK-dependent signaling pathway”. In: *Experimental cell research* 318.5 (2012), pp. 558–569.

[166] Hide Yamamoto et al. “Wnt5a signaling is involved in the aggressiveness of prostate cancer and expression of metalloproteinase”. In: *Oncogene* 29.14 (Jan. 2010), pp. 2036–2046.

[167] Aktan Alpsoy and Ufuk Gündüz. “Protein kinase D2 silencing reduced motility of doxorubicin-resistant MCF7 cells”. In: *Tumor Biology* 36.6 (Jan. 2015), pp. 4417–4426.

[168] Geou-Yarh Liou et al. “Mutant KRas-Induced Mitochondrial Oxidative Stress in Acinar Cells Upregulates EGFR Signaling to Drive Formation of Pancreatic Precancerous Lesions”. In: *Cell Reports* 14.10 (Mar. 2016), pp. 2325–2336.

[169] Christoph Wille et al. “Protein kinase D2 induces invasion of pancreatic cancer cells by regulating matrix metalloproteinases”. In: *Molecular Biology of the Cell* 25.3 (Feb. 2014), pp. 324–336.

[170] Tim Eiseler et al. “Protein Kinase D1 Mediates Anchorage-dependent and -independent Growth of Tumor Cells via the Zinc Finger Transcription Factor Snail1”. In: *Journal of Biological Chemistry* 287.39 (Sept. 2012), pp. 32367–32380.

[171] Kevin A Maupin et al. “Glycogene Expression Alterations Associated with Pancreatic Cancer Epithelial-Mesenchymal Transition in Complementary Model Systems”. In: *PLoS ONE* 5.9 (Sept. 2010), e13002.

[172] Huadong Pei et al. “FKBP51 Affects Cancer Cell Response to Chemotherapy by Negatively Regulating Akt”. In: *Cancer Cell* 16.3 (Sept. 2009), pp. 259–266.

[173] Tim Eiseler et al. “Protein Kinase D2 Assembles a Multiprotein Complex at the Trans-Golgi Network to Regulate Matrix Metalloproteinase Secretion”. In: *Journal of Biological Chemistry* 291.1 (Jan. 2016), pp. 462–477.

[174] Sunyoung Lee et al. “Processing of VEGF-A by matrix metalloproteinases regulates bioavailability and vascular patterning in tumors”. In: *The Journal of Cell Biology* 169.4 (May 2005), pp. 681–691.

[175] Claudio G Rolli et al. “Impact of Tumor Cell Cytoskeleton Organization on Invasiveness and Migration: A Microchannel-Based Approach”. In: *PLoS ONE* 5.1 (Jan. 2010), e8726.

[176] Adrià Sales Ramos, Catherine Picart, and Ralf Kemkemer. “Age-dependent migratory behavior of human endothelial cells revealed by substrate microtopography”. In: *Experimental Cell Research* (Oct. 2018), pp. 1–11.

[177] Sarit K Das et al. “A microfluidic platform for studying the effects of small temperature gradients in an incubator environment”. In: *Biomicrofluidics* 2.3 (Sept. 2008), p. 034106.

[178] Yoojin Shin et al. “Microfluidic assay for simultaneous culture of multiple cell types on surfaces or within hydrogels”. In: *Nature Protocols* 7.7 (June 2012), pp. 1247–1259.

[179] Johannes Schindelin et al. “Fiji: an open-source platform for biological-image analysis”. In: *Nature Methods* 9.7 (July 2012), pp. 676–682.

[180] Jochen Guck et al. “The Optical Stretcher: A Novel Laser Tool to Micromanipulate Cells”. In: *BMC Cancer* 81.2 (Aug. 2001), pp. 767–784.

[181] Franziska Lautenschläger et al. “The regulatory role of cell mechanics for migration of differentiating myeloid cells”. In: *PNAS* 106.37 (Sept. 2009), pp. 115696–115701.

[182] Fernando Erra Díaz et al. “Fever-range hyperthermia improves the anti-apoptotic effect induced by low pH on human neutrophils promoting a proangiogenic profile”. In: *Cell Death & Disease* 7.10 (Oct. 2016), e2437.

[183] Edward G Hayman et al. “Vitronectin - a major cell attachment-promoting protein in fetal bovine serum”. In: 160.2 (Oct. 1985), pp. 245–248.

[184] Sean P Palecek et al. “Integrin–ligand binding properties govern cell migration speed through cell–substratum adhesiveness”. In: *Letters to Nature* 385.6616 (Feb. 1997), p. 537.

[185] Kenneth C Ingham et al. “Thermal stability of human plasma fibronectin and its constituent domains”. In: *The Journal of Biological Chemistry* 259.19 (Oct. 1984), pp. 11901–11907.

[186] Paolo Maiuri et al. “Actin Flows Mediate a Universal Coupling between Cell Speed and Cell Persistence”. In: *Cell* 161.2 (Apr. 2015), pp. 374–386.

[187] Margaret F Ware, Alan Wells, and Douglas A Lauffenburger. “Epidermal growth factor alters fibroblast migration speed and directional persistence reciprocally and in a matrix-dependent manner”. In: *Journal of Cell Science* 111.16 (Aug. 1998), pp. 2423–2432.

[188] T K Fu et al. “Philothermal and chemotactic locomotion of leukocytes. Methods and results”. In: *Cell Biophysics* 4 (Jan. 1982), pp. 77–95.

[189] Alan Wells, Clayton Yates, and Christopher R Shepard. “E-cadherin as an indicator of mesenchymal to epithelial reverting transitions during the metastatic seeding of disseminated carcinomas”. In: *Clinical & Experimental Metastasis* 25.6 (July 2008), pp. 621–628.

[190] Katie Palen et al. “E-cadherin re-expression shows *in vivo* evidence for mesenchymal to epithelial transition in clonal metastatic breast tumor cells”. In: *Oncotarget* 7.28 (May 2016), pp. 43363–43375.

[191] Lola Rahib et al. “Projecting cancer incidence and deaths to 2030: the unexpected burden of thyroid, liver, and pancreas cancers in the United States.” In: *Cancer Research* 74.11 (June 2014), pp. 2913–2921.

[192] A Ponti et al. “Two Distinct Actin Networks Drive the Protrusion of Migrating Cells”. In: *Science* 305.5691 (Sept. 2004), pp. 1782–1786.

[193] Jochen Guck et al. “Optical Deformability as an Inherent Cell Marker for Testing Malignant Transformation and Metastatic Competence”. In: *BMC Cancer* 88.5 (May 2005), pp. 3689–3698.

[194] Alperen N Ketene et al. “The effects of cancer progression on the viscoelasticity of ovarian cell cytoskeleton structures”. In: *Nanomedicine: Nanotechnology, Biology, and Medicine* 8.1 (Jan. 2012), pp. 93–102.

[195] Daniel A Fletcher and R Dyche Mullins. “Cell mechanics and the cytoskeleton”. In: *Letters to Nature* 463.7280 (Jan. 2010), pp. 485–492.

[196] Torsten W Remmerbach et al. “Oral Cancer Diagnosis by Mechanical Phenotyping”. In: *Cancer Research* 69.5 (Feb. 2009), pp. 1728–1732.

[197] Nadine Walter et al. “Elastic moduli of living epithelial pancreatic cancer cells and their skeletonized keratin intermediate filament network”. In: *Biointerphases* 6.2 (June 2011), pp. 79–85.

[198] Pierre A Coulombe and Pauline Wong. “Cytoplasmic intermediate filaments revealed as dynamic and multipurpose scaffolds”. In: *Nature Cell Biology* 6.8 (Aug. 2004), pp. 699–706.

[199] Michael Beil et al. “Sphingosylphosphorylcholine regulates keratin network architecture and visco-elastic properties of human cancer cells”. In: *Nature Cell Biology* 5.9 (Aug. 2003), pp. 803–811.

[200] Hara Polioudaki et al. “Variable expression levels of keratin and vimentin reveal differential EMT status of circulating tumor cells and correlation with clinical characteristics and outcome of patients with metastatic breast cancer”. In: *BMC Cancer* 15.1 (Dec. 2015), p. 339.

[201] Kristin Seltmanna et al. “Keratins significantly contribute to cell stiffness and impact invasive behavior”. In: *Proceedings of the National Academy of Sciences* 110.46 (Nov. 2013), pp. 18507–18512.

[202] Celine M Denais et al. “Nuclear envelope rupture and repair during cancer cell migration”. In: *Science* 352.6283 (Apr. 2016), pp. 353–358.

[203] Lena A Lautscham et al. “Migration in Confined 3D Environments Is Determined by a Combination of Adhesiveness, Nuclear Volume, Contractility, and Cell Stiffness”. In: *BMC Cancer* 109.5 (Sept. 2015), pp. 900–913.

[204] Isabelle Dupin, Yasuhisa Sakamoto, and Sandrine Etienne-Manneville. “Cytoplasmic intermediate filaments mediate actin-driven positioning of the nucleus”. In: *Journal of Cell Science* 124.6 (Mar. 2011), pp. 865–872.

[205] Antoine Fruleux and Rhoda J Hawkins. “Physical role for the nucleus in cell migration”. In: *Journal of Physics: Condensed Matter* 28.36 (July 2016), pp. 363002–12.

[206] Guillaume Charras and Erik Sahai. “Physical influences of the extracellular environment on cell migration”. In: *Scientific Reports* 15.12 (Oct. 2014), pp. 813–824.

[207] Nisha Durand et al. “Protein Kinase D1 regulates focal adhesion dynamics and cell adhesion through Phosphatidylinositol-4-phosphate 5-kinase type-l γ”. In: *Scientific Reports* 6 (Oct. 2016), p. 35963.

[208] Jean-Yves Tinevez et al. “Role of cortical tension in bleb growth”. In: *Proceedings of the National Academy of Sciences* 106.44 (Nov. 2009), pp. 18581–18586.

[209] Godwin A Ponuwei. "Unmasking Plasma Membrane Blebbing". In: *Journal of Biomedical Sciences and Applications* 1.2:6 (Nov. 2017), pp. 1–10.

[210] Tim Eiseler et al. "Protein kinase D1 regulates matrix metalloproteinase expression and inhibits breast cancer cell invasion". In: *Breast Cancer Reasearch* 11.1 (June 2009), R13.

[211] Peter Storz, Heike Döppler, and Alex Toker. "Protein Kinase Cδ selectively regulates Protein Kinase D-dependent activation of NF- κB in oxidative stress signaling". In: *Molecular and Cellular Biology* 24.7 (Mar. 2004), pp. 2614–2626.

[212] Peter Storz, Heike Döppler, and Alex Toker. "Protein Kinase D Mediates Mitochondrion-to-Nucleus Signaling and Detoxification from Mitochondrial Reactive Oxygen Species". In: *Molecular and Cellular Biology* 25.19 (Sept. 2005), pp. 8520–8530.

[213] Qin Hao et al. "Protein Kinases D2 and D3 Are Novel Growth Regulators in HCC1806 Triple-negative Breast Cancer Cells". In: *Anticancer Research* 33.2 (Feb. 2013), pp. 393–399.

[214] Bettina Huck et al. "Elevated Protein Kinase D3 (PKD3) Expression Supports Proliferation of Triple-negative Breast Cancer Cells and Contributes to mTORC1-S6K1 Pathway Activation". In: *The Journal of Biological Chemistry* 289.6 (Feb. 2014), pp. 3138–3147.

[215] Mohammad Rashel, Ninche Alston, and Soosan Ghazizadeh. "Protein Kinase D1 Has a Key Role in Wound Healing and Skin Carcinogenesis". In: *Journal of Investigative Dermatology* 134.4 (Nov. 2014), pp. 902–909.

[216] Senthil N Arun et al. "Ultraviolet B irradiation and activation of protein kinase D in primary mouse epidermal keratinocytes". In: *Oncogene* 30.13 (Dec. 2010), pp. 1586–1596.

[217] Vladislav Ryvkin et al. "Opposing Growth Regulatory Roles of Protein Kinase D Isoforms in Human Keratinocytes". In: *Journal of Biological Chemistry* 290.17 (Apr. 2015), pp. 11199–11208.

[218] Sazzad Hassan et al. "Heat shock protein 27 mediates repression of androgen receptor function by protein kinase D1 in prostate cancer cells". In: *Oncogene* 28.49 (Sept. 2009), pp. 4386–4396.

[219] Paul Mak et al. "Protein kinase D1 (PKD1) influences androgen receptor (AR) function in prostate cancer cells". In: *Biochemical and Biophysical Research Communications* 373.4 (Sept. 2008), pp. 618–623.

[220] Eva Bernhart et al. “Silencing of protein kinase D2 induces glioma cell senescence via p53-dependent and -independent pathways”. In: *Neuro-Oncology* 16.7 (Jan. 2014), pp. 933–945.

[221] Xiuping Zhou et al. “Protein kinase D2 promotes the proliferation of glioma cells by regulating Golgi phosphoprotein 3”. In: *Cancer Letters* 355.1 (Dec. 2014), pp. 121–129.

[222] Ninel Azoitei et al. “Protein kinase D2 is a novel regulator of glioblastoma growth and tumor formation”. In: *Neuro-Oncology* 13.7 (July 2011), pp. 710–724.

List of Publications

Galina Khachaturyan, Andrew W Holle, Christoph Frey, Tim Eiseler, Stephan Paschke, Alexandre Micoulet, Joachim P Spatz, Ralf Kemkemer, *Temperature-sensitive migration dynamics in neutrophil-differentiated HL-60 cells*, Scientific Reports, in submission.

Galina Khachaturyan, Andrew W Holle, Tim Eiseler, Thomas Seuferlein, Joachim P Spatz, Ralf Kemkemer, *Protein Kinase D isoforms alter mechanosensitive cancer migration*, in preparation, to be submitted, 2019

Acknowledgement

I would like to start my acknowledgment by expressing my deepest gratitude to Prof. Joachim P. Spatz, for the amazing opportunity to do my PhD research in the Max Planck Institute and especially in his group.

Next, I would like to sincerely thank Professor Reiner Dahint for kindly accepting to review my work and to be a part of the examination committee.

This thesis would not have been possible without the help and constant guidance of my supervisor Prof. Ralf Kemkemer. I am immensely grateful for his support and encouragements throughout my work.

I would also like to thank Andrew Holle for his supervision during the last two years. I learnt a lot of important and particularly useful set of skills. Working with him made the last years of my PhD so much more enjoyable. Also a big thank you goes to Jennifer Young, for always supporting me and helping me whenever I had any questions or doubts.

I thank our collaboration partners Dr. Tim Eiseler and Dr. Christoph Wille from Thomas Seufferlein's laboratory at the University Clinic Ulm for sharing their research with me.

A special thank you goes to the current Stuttgart members of our group, especially Kerstin Göpfrich and Sadaf Paschapour for always helping me when needed.

I also appreciate the help of all the technicians of Spatz group, in particular Christine Mollenhauer and Henriette Reis.

One of the perks of a PhD life is meeting wonderful people and making friends from all over the world. And, although due to the nature of the scientific world, the time we spend together is often shorter than wanted, good fiends manage to support you from afar. So I am saying a very warm thank you to Adria Sales Ramos, Elham Sharifikolouei and my "muse" at the Hochschule Reutlingen, Kiriaki Athanasopulu, with whom I started this journey and who were always there for me.

Last, but not least comes my family. Without their loving support and constant encouragements I wouldn't be able to reach where I am today.

Eidesstattliche Versicherung gemäß § 8 der Promotionsordnung der Naturwissenschaftlich-Mathematischen Gesamtfakultät der Universität Heidelberg

1. Bei der eingereichten Dissertation zu dem Thema **The role of Protein Kinase D signaling and the thermal microenvironment on single cell migration** handelt es sich um meine eigenständig erbrachte Leistung.
2. Ich habe nur die angegebenen Quellen und Hilfsmittel benutzt und mich keiner unzulässigen Hilfe Dritter bedient. Insbesondere habe ich wörtlich oder sinngemäß aus anderen Werken übernommene Inhalte als solche kenntlich gemacht.
3. Die Arbeit oder Teile davon habe ich bislang nicht an einer Hochschule des In-oder Auslandes als Bestandteil einer Prüfungs- oder Qualifikationsleistung vorgelegt.
4. Die Richtigkeit der vorstehenden Erklärung bestätige ich.
5. Die Bedeutung der eidesstattlichen Versicherung und die strafrechtlichen Folgen einer unrichtigen oder unvollständigen eidesstattlichen Versicherung sind mir bekannt.

Ich versichere an Eides statt, dass ich nach bestem Wissen die reine Wahrheit erklärt und nichts verschwiegen habe.

_____ _____

Ort und Datum Unterschrift